New Approaches to the Synthesis of Porous and/or High Surface Area Transition Metal Oxides

Dissertation

Zur Erlangung des akademischen Grades
eines Doktors der Naturwissenschaften (Dr. rer. nat.)
im Fach Chemie der Fakultät für Biologie, Chemie und Geowissenschaften
der Universität Bayreuth

vorgelegt von

Ram Sai Yelamanchili

aus Indien

Bayreuth, 2008

Die vorliegende Arbeit wurde in der Zeit von April 2005 bis August 2008 am Lehrstuhl für Anorganische Chemie I der Universität Bayreuth durchgeführt.

Vollständiger Abdruck der von der Fakultät für Biologie, Chemie und Geowissenschaften der Universität Bayreuth zur Erlangung des akademischen Grades eines Doktors der Naturwissenschaften genehmigten Dissertation.

Dissertation eingereicht am: 05.09.2008
Zulassung durch die Promotionskommission: 10.10.2008
Wissenschaftliches Kolloquium:

Amtierender Dekan: Prof. Dr. Axel H. E. Müller

Prüfungsausschuss:
Prof. Dr. J. Breu (Erstgutachter)
Prof. Dr. M. Ballauff (Zweitgutachter)
Prof. Dr. A. Müller
Prof. Dr. H. Keppler

Acknowledgements

A journey, be in personal or professional life, is easier when you travel together. Many people have accompanied, contributed their time and knowledge to my research career. It is a pleasant opportunity for me to express my gratitude for all of them. First, I would like to express my sincere appreciation to my supervisor, Prof. Dr. Josef Breu, for his intelligence, insight, constructive suggestions, generosity, and for guiding me through entire doctoral research work at the Inorganic Chemistry I, Universität Bayreuth.

More so, I am indebted for encouragement and invaluable suggestions to my graduation committee members, Prof. Dr. Hans Keppler, Prof. Dr. Gerd Müller. I am acknowledging my obligations to the Oxide Materials International Graduate School, and Elitenetzwerk Bayern (ENB) program for funding my research projects. I am thankful to Prof. Dr. Axel H. E. Müller and Prof. Dr. Matthias Ballauff, University of Bayreuth, for accepting the collaborations, and their valuable time. I am very thankful to Prof. Dr. Ulrich Wiesner, Cornell University, USA for accepting collaboration, hosting me in his department, and his valuable suggestions. I am also thankful to Mr. Andreas Walther, Dr. Yan Lu, Mr. Bolisetty Sreenath, University of Bayreuth, and Dr. Marleen Kamperman, Cornell University, for collaborations, their valuable time and interesting discussions. I offer my special thanks to all the colleagues, technical and administrative staff of the Inorganic Chemistry I and BGI for the assistances, encouragements and support.

It gives me great pleasure to thank my parents, brother and my wife for their love, unfailing support, tremendous patience, trust and encouragement they have shown in their own way during my long period of career.

I remain

Ram Sai Yelamanchili

Bayreuth, September 2008

Table of Contents

Chapter 1
Introduction

1.1 Nanomaterials and Nanoscience

We all know from reality that good things come in small packages. Therefore, technologies in the twenty first century emphasize the miniaturization of devices into the nanometer range while their ultimate performance is concomitantly enhanced. This raises many issues regarding new materials for achieving specific functionality and selectivity. Thus, recently there is a tremendous excitement in the study of fundamental properties of nanoscale materials, their organization to form superstructures and applications. The unit of nanometer derives its prefix nano from a Greek word meaning dwarf or extremely small. One nanometer spans 3-5 atoms lined up in a row. The nanoscale is not just the middle ground between molecular and macroscopic but also a dimension that is specifically geared to the gathering, processing, and transmission of chemical-based information [1-2]. Nanoscience refers to a field of applied science and technology whose theme is the control of matter on the atomic and molecular scale, generally 100 nanometers or smaller [1,3-4]. It also involves the fabrication of devices or materials that lie within the nano size range.

Although widespread interest in nanomaterials is recent, the concept was raised over 50 years ago. In a classic talk given on December 29th 1959 at the annual meeting of the American Physical Society at the Caltech entitled ‘There´s Plenty of Room at the Bottom’ Richard Feynman said [2], “*The principles of physics, as far as I can see, do not speak against the possibility of maneuvering things atom by atom. It is not an attempt to violate any laws; it is something, in principle, that can be done; but in practice, it has not been done because we are too big.*” Over the past decade, nanomaterials have been the subject of enormous interest. Nanomaterials are already an integral part of today's data storage media, semiconductor manufacturing, biomedical research, emerging memory, computing, optical, and sensing devices [4-10]. Nanoparticles, nanowires, nanotubes, and

nanoscale films along with nanofabrication technologies will allow for continued advancements in a wide range of applications [1,5-8,11-22]. A greater understanding of the manipulation of matter at the nanoscale has led to a number of advances in materials science, ranging from the development of novel optical and electronic properties and the formation of high strength materials, which mimic nature, all the way to stimuli-responsive materials applicable to a range of applications [6-17].

What makes the nanomaterials so different? Their extremely small size featured by nanomaterials is of the same scale as the critical size for physical phenomena. This leads to size dependant effects of the electronic structures (quantum dot effects). Additionally, surfaces and interfaces are also important in explaining nanomaterial behavior. Nanomaterials characteristically exhibit physical and chemical properties different from the bulk materials, because of their having at least one spatial dimension in the size range of 1±100 nm. For example, in bulk materials only a relatively small percentage of atoms will be at or near a surface or interface whereas in nanomaterials, the small volume ensures that many atoms, perhaps half or more in some cases, will be near or at interfaces. When the materials are nanoscopic, surface dependant properties such as free energy, and reactivity can be quite different from material properties of the bulk [13-15].

1.2 What is Mesoscience and why?

If we have nano, what is meso? It is well known that different materials properties, defined by physicochemical underlying principles, scale with the physical size with distinct length scales in the meso region. Meso is not directly related to a length scale, but to a principle of operation. It is in-between molecular and solid-state chemistry, in-between a molecular and a continuum approach, in-between covalent chemistry and micromechanical techniques [12-13]. Therefore, meso can mean different things. For instance, in case of porous materials the International Union of Pure and Applied Chemistry (IUPAC) has classified materials into three different classes, microporous < 2 nm, mesoporous 2 - 50 nm, macroporous > 50 nm [14,23-25]. These designations strictly

refer to the pore sizes and not the dimensions of the material between pores. In this context, pore length scales are set by a convention and the mesoscale is clearly intermediate between that of the micro and macro scale. In soft matter science, again mesophases are ubiquitous and involved in a scale of complexity when utilized as structure directing templates for making mesostructured forms of matter. In this context, meso extends over a wider size range, 2 - 500 nm [12,13,16]. The nano-size is just a side aspect where as a mesophase is classified by its order and its mode of self-organization. Manipulation and control of chemical structures on the mesoscale has recently developed to a very promising and aesthetically appealing area of chemistry.

Mesoscience can be defined as the controlled generation of objects with characteristic features on the mesoscale with chemical reactions and principles. It is not just classical covalent chemistry to be employed on mesostructures but also involves routes and chemical strategies especially designed to be effective in the nano- and micro- range. Mesoscience bridges the world of molecules connected by molecular bonds and the chemical engineering of micron-sized structures [12]. In general, chemistry is the art of manipulating bonds, interactions, arrangements of atoms, groups, components in a controlled and reproducible fashion. However, in terms of mesoscience chemists want to control size, shape, surface area, and curvature for mesocomponents such as hybrids, and porous systems. Additionally, mutual arrangement, morphology and order are something more specific for the mesoscience. Mesoscience can engineer a completely disordered state to a partially ordered enroute to a completely ordered state of matter. Through mesoscience it is possible to design various chemical and physical strategies to arrange the morphology of matter to finely divided particulate, fiber, film, monolith, sphere, superlattice and patterned forms [12-19].

Synthetic hybrid materials, in which organic and inorganic components are integrated by means of self-assembly approaches, are also beginning to reveal certain advantages when fashioned at the mesoscale [13]. Hybrid structures of this type are interesting as their properties can significantly exceed those of its component parts.

1.3 Synthesis approaches: Bottom-up and Top-down

Top-down and bottom-up are the two approaches used for assembling/structuring materials and devices on nano and mesoscale. Bottom-up approaches attempt to have smaller components arrange themselves into more complex assemblies, while top-down approaches try to create nanoscale devices by using larger, externally-controlled components [3]. Alignment of nanoparticle building blocks into ordered superstructures by bottom-up approaches is one of the key topics of modern colloid and materials chemistry [4,15]. In this area, much can be learned from the processes of biomineralization, which lead to well defined organic–inorganic hybrid materials with superior materials properties, complex morphologies and hierarchical order spanning different length scales [13]. Through bottom-up approaches, controlled self-organization of nanoparticles can lead to new materials with attractive properties.

Bottom-up approaches use the chemical properties of single molecules to cause single-molecule components to automatically arrange themselves into some useful conformation. These approaches utilize the concepts of molecular self-assembly and/or molecular recognition. The top-down approach, in contrast, often uses the traditional workshop or microfabrication methods where externally-controlled tools are used to cut, mill and shape materials into the desired shape and order [3,25-29]. Micropatterning techniques, such as photolithography and ink-jet printing belong to this category [27,29]. In brief, bottom-up approaches should be able to produce devices in parallel and much cheaper than top-down methods, but could potentially be overwhelmed as the size and complexity of the desired assembly increases.

1.4 Types of templates: Endo and Exo templates

Materials with pores and/or high surface area are of interest, academically and industrially, to many scientific disciplines. Such materials can be prepared using templating pathways. Templating approaches can offer a high degree of control over

structural and textural properties of materials. Generally, templates can be categorized into two types, endo- and exo- templates [3,27,29]. When molecular or supramolecular units are added to the synthesis mixture, these units are occluded in the growing solid and leave a pore system after their removal. These kinds of templates are called “endotemplates”. Alternatively, materials with structural pores can be used as scaffolds in which another solid is created. After removal of the scaffold, a porous or finely divided material remains, depending on the connectivity in the scaffold. Such materials are called “exotemplates”. In some processes, it is possible to create one-to-one replica of the template. This replication process can be so perfect to justify the use of the term “nanocasting” to describe this process [21].

It is necessary to understand the templating procedures and its consequences in detail. The ability to template at the micro, meso, and macro scale in a wide variety of materials has resulted in the discovery of fascinating porous and/or high surface area materials. Judicious choice of the templating procedure can offer unprecedented control of the structure and texture on length scales between nanometers and micrometers. High surface area materials are possible by structuring materials on the nanometer level. Whether the solid is ordered or disordered is of limited importance with respect to high surface areas [3]. High surface area materials may be crystalline, they may be ordered on a mesoscopic length scale, but amorphous on the atomic length scale, or they may be fully disordered. Porous materials with controlled porosity, well-defined textures and morphologies are expected to function as improved-performance stationary phases for separation processes [23-34]. Porous materials with mesoscopic dimensions also offer advantages as mesocuvettes and mesoreactors, for example as hosts for the synthesis and stabilization of semiconductor clusters whose size dependent properties only appear at the mesoscale [12]. However, it must be noted that a periodic pore structure has in general no specific advantage over disordered and in many applications, periodic pore structures are by principle coupled to serious disadvantages, such as low surface area [3]. An important class of structures directing agents or templates used for the synthesis of porous and/or high surface area materials is the organics such as surfactants and block copolymers.

1.5 Organics as structure directing agents and templates

In presence of organics such as surfactants and block copolymers, combined principles of self-assembly, polymer, colloidal and inorganic chemistries were used to synthesize materials with various functionalities and properties [15,16,35-37]. This is because these organic materials self-assemble into a variety of nano- and mesostructures with well-defined shape and size resulting in the discovery of fascinating hybrid materials (Figure 1). For example, in a simple binary system of water-surfactant, surfactant molecules manifest themselves as very active (in respect to self-assembly) components that realize variable supramolecular structures as function of increasing concentrations [16,36]. While at low concentrations isolated molecules are present and with increasing concentrations molecules aggregate together to form micelles of different structures. As the concentration continues to increase, hexagonal, lamellar and cubic phases appear. The particular phase present in a surfactant aqueous solution at a given concentration depends not only on the concentrations but also on the nature of the surfactant itself like the length of the hydrophobic carbon chain, hydrophilic head group, and counter ion. Even the environmental parameters like pH, temperature, the ionic strength, and other additives can influence the phase formation [37]. However, two main limitations exist for surfactant-templated synthetic procedures: (a) typical wall thickness obtained is in the range of 8–13 A˚, which is a serious limitation regarding structural stability in catalysis; (b) limited pore size offered by molecular surfactants [26]. Block copolymers exhibit a similar self-assembly behaviour like surfactants. Amphiphilic block copolymers therefore belong to an important family of surfactants, widely used in detergency, emulsifying, coating, thickening, etc [26]. The self-assembly characteristics of these block copolymers permit to control the superstructure, to vary the typical length scales and to add specific functions.

The use of amphiphilic block copolymers with higher molecular weights can be expected to yield materials with large pores, with potentially thicker walls and correspondingly enhanced hydrothermal stabilities [26]. Block copolymers are indeed interesting as

supramolecular templates as they are capable to impart larger pores and thicker walls. Block copolymers have been increasingly used to organize mesostructured composite solids, because the architectures of the amphiphilic block copolymers can be rationally adjusted to control the interactions between the inorganic and organic species, the self-assembly, and especially the processibility than with low molecular weight surfactants [22,26,34,35].

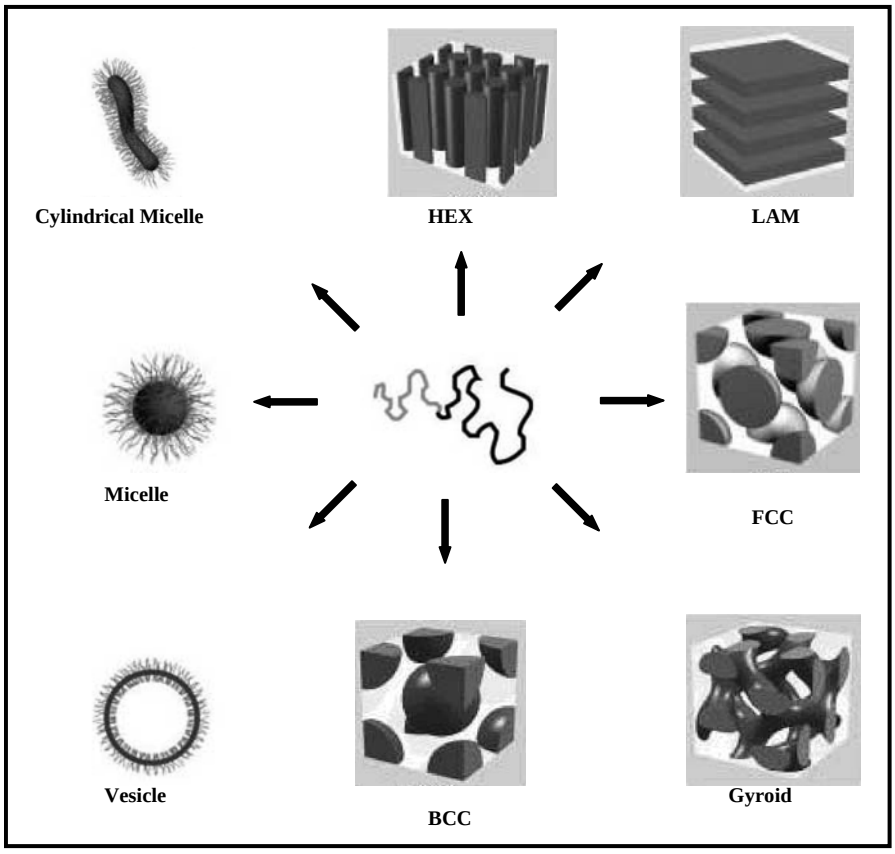

Figure 1. Schematic representation of the nano and mesostructures that can be obtained with organics such as block copolymers under various reaction conditions [reproduced from ref. 36].

1.6 General problems

The use of surfactants and block copolymers as structure directing agents and/or templates has resulted in the discovery of fascinating silica molecular sieves such as MCM-41, and SBA-15 [22-27]. These materials, which possess a regular hexagonal array of uniform pore openings, aroused a worldwide resurgence in the research field of porous and/or high surface area materials. There has been a great deal of interest in synthesizing transition-metal oxide analogues of these materials, because transition metal oxides have variable oxidation states and populated d-bands, which are lacking in aluminium and silicon oxides [22,25,28]. However, the synthesis procedures developed for MCM-41 and SBA-15 works well only for silica related systems under established reaction conditions. Control of the synthesis process becomes very difficult with even minor changes in the reaction system. This is the reason, why only few mesoporous materials are reported which have been synthesized applying templating with surfactants or high molecular weight block copolymers. Even in case of well-studied SBA-15 slight alteration of reaction conditions will lead to the collapse of the mesostructure [38]. In the case of SBA-15 like materials, if any particular functionality has to be achieved then necessary changes should be done only after the rigid silica mesostructure is formed in the solution. Nevertheless, once the rigid silica mesostructure is formed, it does not offer much space for synthesizing the materials with different functionalities. In brief, these methods cannot be readily used for other systems such as transition metal oxides [37].

This is because there are two major problems involved in the synthesis of porous and/or high surface area transition metal oxides. Firstly, the very quick formation of insoluble inorganic oxide oligomer species [25]. As a result, the interactions with the template may be rendered insufficient to form the desired structures. Secondly, the drastic change in behavior of block copolymers with the addition/presence of inorganic precursors [35-38]. It is very difficult to predict the phase behavior of the block copolymers with changes in reaction conditions. The synthesis process of transition metal oxide materials involves the control of pH, condensation, reaction temperature, aging temperature, time, etc. Hence,

the use of routine approaches with commercial block copolymers does not offer much flexibility for the synthesis of porous and/or high surface area materials with desired morphologies. Therefore, there is a substantial need to search for new approaches that offer flexibility in terms of reaction conditions and can be readily applied for different metal oxide systems.

1.7 Objectives of this thesis

We hypothesize and thereby explore the applicability of new approaches to the synthesis of porous and/or high surface area materials, particularly transition metal oxides. The ability to manipulate and control chemical structures on the mesoscale is greatly enhanced when taking advantage of an electrostatic interaction of inorganic building blocks and organic templates. This not only prevents phase segregation reliably but also allows to apply larger building blocks like oligomers and even colloids to be structured on the mesoscale. The structure directing process is of course complex and involves a number of interactions and bonds that need to be controlled [12]. But supramolecular assembly of charged precursors (oligomeries and colloids) over the oppositely charged templates by the strong Coulomb interactions gives a great deal of control. The supramolecular assembly of charged colloids on the mesoscale for instance only requires the optimization of the surface potentials of the colloid. It is our aim to explore the applicability of charged soft templates (block copolymers) for the synthesis of porous and/or high surface area transition metal oxides by using charged metal oxide oligomers or colloids as inorganic precursors instead of very reactive molecular alkoxide precursors. The discrete and charged metal oxide clusters (e.g. polyoxometalates) represent local minima in respect to the formation of extended oxide structures through condensation. Moreover, the problems related with the micelle stability could be overcome by freezing the dynamics through crosslinking. Another approach is to prepare composite films through evaporation induced self-assembly (EISA) by carefully choosing the block copolymers compositions and fractions.

1.8 References

[1] J. H. Fendler, *Membrane Mimetic Chemistry Approach to Advanced Materials*; Springer-Verlag : Berlin, **1992**.

[2] R. P. Feynman, in *Engineering and Science* magazine, California Institute of Technology vol. XXIII, **1960**, no. 5.

[3] F. Schüth, *Angew. Chem.* **2003**, *115*, 3730; *Angew. Chem. Int. Ed.* **2003**, *42*, 3604.

[4] M. Templin, A. Franck, A. Du Chesne, H. Leist, Y. Zhang, R. Ulrich, V. Schädler, U. Wiesner, *Science* **1997**, *278*, 1795.

[5] A. Henglein, *Top. Curr. Chem.* **1988,** *143*, 113.

[6] M. A. El-Sayed, *Acc.Chem.Res.* **2001,** *34*, 257.

[7] A. P. Alivisatos, *Science* **1996,** *271*, 933.

[8] T. Ahmadi, Z. L. Wang, T. C. Green, A. Henglein, M. A. El-Sayed, *Science* **1996,** *272*, 1924.

[9] H. Weller, *Angew.Chem.Int.Ed.Engl.* **1998,** *37*, 1658.

[10] Y. Wang, *Acc.Chem.Res.* **1991,** *24*, 133.

[11] S. A. Davis, M. Breulmann, K. H. Rhodes, B. Zhang and S. Mann, *Chem. Mater.* **2001**, *13*, 3218.

[12] M. Antonietti, G. A. Ozin, *Chem. Eur. J.* **2004**, *10*, 28.

[13] H. Cölfen, S. Mann, *Angew. Chem. Int. Ed.* **2003**, *42*, 2350.

[14] F. Hoffmann, M. Cornelius, J. Morell, M. Fröba, *Angew. Chem.* **2006**, *118*, 3290; *Angew. Chem. Int. Ed.* **2006**, *45*, 3216.

[15] A. C. Finnefrock, R. Ulrich, A. D. Chesne, C. C. Honeker, K. Schumacher, K. K. Unger, S. M. Gruner, U. Wiesner, *Angew. Chem.* **2001**, *113*, 1247; *Angew. Chem. Int. Ed.* **2001**, *40*, 1207.

[16] S. Förster, *Top. Curr. Chem.* **2003**, *226*, 1.

[17] C. J. Brinker, Y. Lu, A. Sellinger, H. Fan, *Adv. Mater.* **1999**, *11*, 579.

[18] J. Lee, M. C. Orilall, S. C. Warren, M. Kamperman, F. J. Disalvo, U. Wiesner, *Nature Mater.* **2008**, *7*, 222.

[19] S. C. Warren, L. C. Messina, L. S. Slaughter, M. Kamperman, Q. Zhou, S. M. Gruner, F. J. Disalvo, U. Wiesner, *Science* **2008**, *320*, 1748.

[20] Q. Huo, D. I. Margolese, U. Ciesla, P. Feng, T. E. Gier, P. Sieger, R. Leon, P. M. Petroff, F. Schüth, G. D. Stucky, *Nature* **1994**, *368*, 317.

[21] F. Schüth, W. Schmidt, *Adv. Mater.* **2002**, *14*, 629.

[22] P. Yang, T. Deng, D. Zhao, P. Feng, D. Pine, B. F. Chmelka, G. M. Whitesides, G. D. Stucky, *Science* **1998**, *282*, 2244.

[23] J. S. Beck, C. Vartuli, W. J. Roth, M. E. Leonowicz, C. T Kresge, K. D. Schmitt, C. T-W. Chu, D. H. Olson, E. W. Sheppard, S. B. McCullen, J. B. Higgins, J. L. Schlenker, *J. Am. Chem. Soc*. **1992**, *114*, 10834.

[24] C. T. Kresge, M. E. Leonowicz,; W. J. Roth, J. C. Vartulli, J. S. Beck, *Nature* **1992**, *359*, 710.

[25] D. M. Antonelli, J. Y. Ying, *Angew. Chem. Int. Ed. Engl.* **1996**, *35*, 426.

[26] G. J. D. A. A. Soler-lllia, C. Sanchez, B. Lebeau, J. Patarin, *Chem. Rev.* **2002**, *102*, 4093.

[27] T. J. Barton, L. M. Bull, W. G. Klemperer, D. A. Loy, B. McEnaney, M. Misono, P. A. Monson, G. Pez, G. W. Scherer, J. C. Vartuli, O. M. Yaghi, *Chem. Mater.* **1999**, *11*, 2633.

[28] J. Y. Ying, C. P. Mehnert, M. S. Wong, *Angew. Chem. Int. Ed.* **1999**, *38*, 56.

[29] X. S. Zhao, G. Q. Lu, and G. J. Millar, *Ind. Eng. Chem. Res.* **1996**, *35*, 2075.

[30] D. Zhao, J. Feng, Q. Huo, N. Melosh, G. H. Frederickson, B. F. Chmelka, G. D. Stucky, *Science* **1998**, *279*, 548.

[31] P. T. Tanev, T. J. Pinnavaia, *Science* **1996**, *271*, 1267.

[32] S. Oliver, A. Kuperman, N. Coombs, A. Lough, G. A. Ozin, *Nature* **1995**, *378*, 47.

[33] P. Yang, D. Zhao, D. Margolese, B. Chmelka, G. D. Stucky, *Nature* **1998**, *396*, 152.

[34] G. J. D. A. A. Soler-lllia, E. L. Crepaldi, D. Grosso, C. Sanchez, *Current opinion in Colloid and Interface Science* **2003**, *8*, 109.

[35] G. Wanka, H. Hoffmann, W. Ulbricht, *Macromolecules* **1994**, *27*, 4145.

[36] S. Forster, T. Plantenberg, *Angew. Chem. Int. Ed.* **2002**, *41*, 689.

[37] R. S. Yelamanchili, A. Walther, A. H. E. Müller, J. Breu, *Chem. Commun.* **2008**, 489.

[38] S. Ruthstein, J. Schmidt, E. Kesselman, Y. Talmon, D. Goldfarb, *J. Am. Chem. Soc*. **2006,** *128,* 3366.

Chapter 2
Synopsis

Bottom-up approaches to achieve miniaturization goals use the uniform nanoscopic supramolecular structures that result from organized macromolecule packing, the so-called 'self-assembly' process [1-5]. As mentioned in the introduction, organic materials have the ability to self-assemble into a variety of nanostructures with well-defined shape and size. An important class of organics used for the synthesis of porous and/or high surface area materials is the class of amphiphilic block copolymers. Block copolymers consist of two or more chemically different polymer blocks which are covalently linked together to form a complex macromolecule [1-3,6]. If the constituents of polymers are immiscible, microphase separation is induced on a scale that is related to the size of the copolymer chains. Because of the chemical immiscibility of the covalently linked segmental chains, block copolymers tend to self-assemble into a variety of well-ordered nanostructures with almost continuously tunable resolution from several to hundreds of nanometers [2-4,7-25]. Depending on the segmental interactions, the polymer molecular weight, and the volumetric composition, different microdomain structures are formed with typical length scales in the range between 5 and 100 nm.

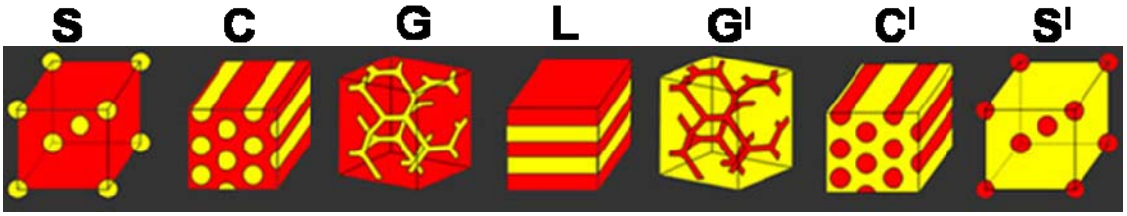

Figure 2. Thermodynamic equilibrium morphologies in a typical AB diblock copolymer depending on the volume fraction of component A (φA). S: spheres, arranged in a body centered cubic lattice; C: cylinders, arranged on a hexagonal lattice; G: gyroid, bicontinuous double-gyroid phase; L: lamella structure (reproduced from ref. 1).

Diblock copolymers which have blocks of comparable volume fractions exhibit a lamella structure [2,7]. Upon decreasing or increasing the volume fraction of one block gyroid,

cylindrical, and spherical microdomains are formed (Figure 2). Through various templating processes and approaches using these block copolymer structures, functional nanostructures can be generated. The self-assembly characteristics of these block copolymers permit to control the superstructure, to vary the typical length scales and to add specific functions. Indeed, the properties of block copolymers can be continuously tuned by adjusting the solvent composition, molecular weight or polymer architecture [14]. Two main processes can be recognized in the formation of hybrid mesophases using these block copolymers. Firstly, creation of an organized texture due to the self-assembly properties of the block copolymers and secondly, formation of an inorganic network [2,4]. The former process results in a microphase separation that divides the space in to two domains, hydrophilic and hydrophobic. The inorganic components are placed in one of the spatially separated parts of these nanoheterogeneous systems. Condensation reactions will give rise to an extended inorganic network. Three fundamental interactions will control the final supramolecular structure; block copolymer–block copolymer, inorganic–inorganic and block copolymer–inorganic. These interactions take place in each of the microsegregated phases, or at the inorganic-template hybrid interface (HI) [2,5-7,17-22]. The solvent will also take part in mesophase formation.

However, these self-assembled block copolymer nanostructures are very sensitive to the reaction conditions such as pH, temperature, solvent, ionic strength and so on [2,26-29]. The stability of the self-assembled nanostructures is especially important for the synthesis of materials that ask for changes in reaction conditions. The synthesis procedures developed for silica systems such as MCM-41 and SBA-15 works well only for other silica related systems under established reaction conditions [2-4,9-14,17-28]. The cooperative self-assembling process of surfactant and inorganic precursor is very sensitive to reaction conditions [17,29]. In case of SBA-15, the micrographs from cryo-TEM revealed that spheroid micelles form during the first 10 min and they evolve into thread like micelles within 20-25 min, which become longer and straighter with time. After 40 min, bundles with the dimensions similar to those found in the final material appeared, although there was no sign of a hexagonal arrangement up to 40 min. The 2 h

samples showed some areas of hexagonal ordered structures, which become very clear at 2 h 50 min [29]. Even slight modifications of this process will affect the cooperative self-assembly and hence lead to different/unexpected mesostructures. This imposes severe restrictions when trying to extend the concept beyond silica-based materials [19,20,25]. This is the main reason, why only few porous and/or high surface area transition metal oxides are reported which have been synthesized applying surfactants or high molecular weight block copolymers. Especially, transition metal oxides are difficult to be cast into thermally stable porous and/or high surface area oxides, because controlling fast hydrolysis rates of metal alkoxide precursors, the subsequent condensation reaction, and the ripening of the oxohydroxide gels would ask for more flexibility in reaction conditions [30-40]. Hence, there is a substantial need to develop new approaches that offer flexibility in terms of reaction conditions and can be readily applied for different metal oxide systems.

Therefore, we are exploring new approaches to overcome these problems. Firstly, instead of dynamic polymer micelles we use rigid polymeric templates in the synthesis of porous and/or high surface area metal oxides. Rigidity could be achieved through cross-linking the non-continuous phase in the block copolymer [41]. In addition, we use charged polymers as templates. This is because strong coulomb interactions between template and oxide systems can lead to the formation of desired and stable hybrid materials. Secondly, instead of very reactive alkoxide precursors we explore polyoxometalates as comparatively stable secondary building units. These polyoxometalates represent local minima in respect to the formation of extended oxide structures through condensation [30]. Besides, Keggin-type polyoxometalates (Keggin POM), discrete transition metal oxide clusters, exhibit fascinating properties and applications due to their high ion conductivity, electron density, rapid and reversible oxidative-reductive processes [30-40]. But, low surface areas of Keggin POMs limits the accessibility to the active sites and limit their efficiency and applications. Keggin POMs with high surface areas and controllable nanostructures are of interest in a variety of applications such as high performance catalysts.

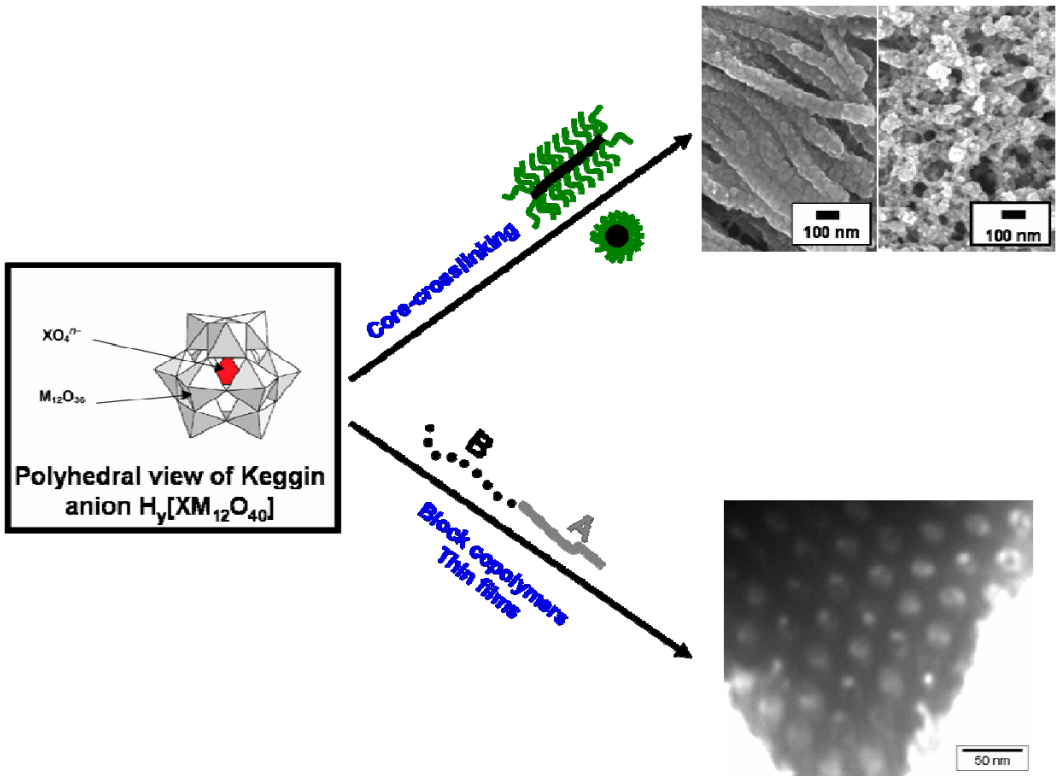

Scheme 1. Overview of our approaches to the synthesis of porous and/or high surface area metal oxides using different cationic polymer templates and anionic oxide precursors. Strong coulomb interactions between cationic templates and anionic oxide precursors drive composite formation.

Following the above principles, we have designed new approaches to achieve Keggin POMs with high surface areas. High surface areas could be achieved by synthesizing Keggin POM framework composite materials with discrete nanostructures, and/or Keggin POM framework porous materials. Discrete nanostructures are possible through charged soft templates. In the first approach, crosslinking of non-continuous phase of the block copolymers will freeze the dynamics of polymer nanostructures. Resultant self-assembled polymeric nanostructures are stable and resistant to changes in reaction conditions. In these systems, cationic PB-P2VP block copolymer nanostructures were used to graft anionic Keggin POMs (Scheme 1).

The second approach we followed was the evaporation-induced self-assembly (EISA) process. Brinker and co-workers pionereed this approach to encompass the synthesis methods leading to ordered hybrid mesophases from dilute solutions [18,19]. EISA can be considered a liquid crystalline template based method. Starting from solutions below the critical micellar concentration, permits one to obtain thin films or gels with excellent homogeneity. This method is particularly interesting to work with non-silica systems, where condensation has to be thoroughly controlled [2,7,18]. Following the principles of EISA, we have developed a new synthesis route for the synthesis of hexagonally ordered mesoporous keggin POM framework using an amphiphilic diblock copolymer. The underlying principles of our approach are as follows. Firstly, keggin POM itself is used as inorganic precursors so that keggin POM units (diameter of keggin POM is ca. 1.2 nm) act as nanobuilding blocks which in respect to further condensation are already in a local minimum. Secondly, an amphiphilic diblock copolymer, poly(isoprene-b-dimethylaminoethylmethacrylate) (PI-b-PDMAEMA), is used as a structure directing agent that contains a hydrophilic PDMAEMA block and an sp^2 hybridized carbon containing hydrophobic PI block [19]. When neutral polymer solution in tetrahydrofuran (THF) is added to the keggin POM (which is a heteropolyacid) solution in THF, the amine units in the PDMAEMA will be protonated. Thus, formation of the inorganic-organic composite is driven by strong coulombic interactions between the protonated amine and keggin POM anions. In addition, when heat-treated under an inert environment, the PI block containing sp^2 carbons will be converted to an amorphous carbon material. This in situ generated carbon acts as a rigid support to mesostructured keggin POM walls and prevents structure collapse during heat treatment. Further calcinations in air will finally remove amorphous carbon and mesoporous hexagonally ordered structures could be obtained.

In contrast to the above approaches where cationic organic templates and anionic oxide precursors were used for the composite formation, we also tested the composite formation using anionic templates and cationic oxide precursors (Scheme 2). As expected, this approach also leads to the formation of well-defined stable crystalline

composites. Herein, we presented a new approach to the direct synthesis of crystalline polymer-titania composites with well-defined crystalline forms through mesoscale supramolecular assembly of crystalline titania colloids over spherical polyelectrolyte brush (SPB) particles [6,42]. The supramolecular assembly of charged colloids achieved through the strong coulombic interactions between the anionic SPB colloids and cationic crystalline titania colloids. The strong coulomb interactions between anionic polymer chains and cationic crystalline titania colloids, whose surfaces are naked and therefore reactive, are the key factors in this approach for the organic-inorganic crystalline composite formation.

Step A:

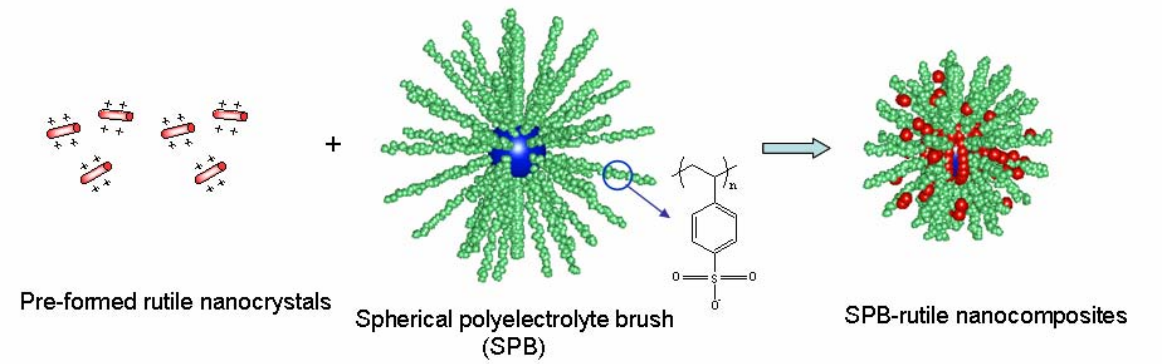

Step B:

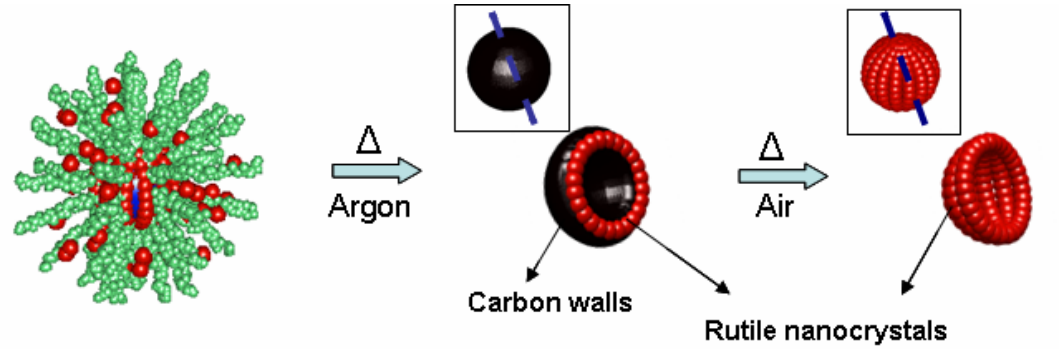

Scheme 2. Step A: Synthesis of rutile composites using cationic rutile colloids and anionic SPB. Step B: Formation of porous rutile balls by two-step calcination. Heat treatment under argon and further calcination in air will lead to porous rutile balls with mesoporous crystalline walls.

Briefly, this thesis includes four publications/manuscripts, which are presented in the appendix. Firstly, dynamics of the polymeric nanostructures were frozen by cross-linking the non-continuous phase of the block copolymers. These core-crosslinked block copolymer nanorods were used as templates for the synthesis of Keggin POM nanostructures by grafting $[SiMo_{12}O_{40}]^{4-}$ Keggin ions over the template. Developed polymer-Keggin POM nanostructures showed high surface areas with well dispersion of Keggin POMs over polymer rods. This synthesis strategy was extended with spherical micelles with different charge and metal contaning Keggin POMs. Interestingly, spherical polymer-Keggin POM nanocomposites exhibit much higher surface areas than their worm-like composite counterparts. These developed hybrid Keggin POM nanostructures are expected to be useful in several catalysis applications. The developed hybrid Keggin POM materials are amorphous. However, by controlled annealing experiments they may be crystallized into corresponding metal oxide phases. We have studied the calcinations conditions where amorphous Keggin POM hybrids were first converted to corresponding amorphous metal oxides through loss of phosphate ligands present in the hybrids. Later, these amorphous metal oxides were calcined to crystallize into corresponding metal oxide phases.

In another approach, the principles of EISA technique were followed to synthesize hexagonally ordered Keggin POM framework mesostructured films using PI-PDMAEMA block copolymers. Stepwise calcination of 1:4 (polymer:Keggin POM) films under inert argon atmosphere followed by a second calcination under air lead to hexagonally ordered Keggin POM framework mesoporous materials. To the best of our knowledge, these are the first hexagonally ordered mesoporous oxides with Keggin POM framework.

Composite materials with crystalline metal oxide framework and corresponding thermally stable porous materials, particularly crystalline TiO_2, have immense potential for applications in various fields. Evolution of rutile and anatase nanocrystals at low temperatures was studied using different inorganic acids. We have developed modified

routes to the synthesis of well-defined rutile and anatase nanocrystals under aqueous conditions. These nanocrystals are stabilized by anionic inorganic ligands such as chloride, sulphate and exhibit positively charged surfaces. In general, supramolecular assembly of charged colloids can be directed over the oppositely charged templates by the strong coulombic interactions. This kind of supramolecular assembly of charged colloids on the mesoscale can be achieved by optimization of the surface potential of the colloidals. We have studied the pH vs zetapotential properties of the crystalline colloids and polymer brush particles. Using this information charged titania nanocrystals were mesoscopically structured onto anionic spherical polyelectrolyte brushes through strong coulomb interactions. In general, majority of the reports required heat treatment to achieve the crystalinity. However, this mesoscopic supramolecular apparoach allows us the direct synthesis of crystalline oxide composites. Following these principles, we have reported a direct facile, low temperature approach to synthesize TiO_2 composites with well-defined crystalline forms using spherical polyelectrolyte brushes as templates. It is worth to note that in this system anionic template and cationic oxide precursors were used where as in our former approaches cationic templates and anionic oxide precursors were used.

References

[1] S. Forster, T. Plantenberg, *Angew. Chem. Int. Ed.* **2002**, *41,* 689.

[2] G. J. D. A. A. Soler-lllia, E. L. Crepaldi, D. Grosso, C. Sanchez, *Current opinion in Colloid and Interface Science* **2003**, *8*, 109.

[3] G. Wanka, H. Hoffmann, W. Ulbricht; *Macromolecules* **1994**, *27*, 4145.

[4] G. J. D. A. A. Soler-lllia, C. Sanchez, B. Lebeau, J. Patarin, *Chem. Rev.* **2002**, *102*, 4093.

[5] S. Förster, *Top. Curr. Chem.* **2003**, *226*, 1.

[6] M. Ballauff, *Prog. Polym. Sci.* **2007**, *32*, 1135.

[7] M. Templin, A. Franck, A. Du Chesne, H. Leist, Y. Zhang, R. Ulrich, V. Schädler, U. Wiesner, *Science* **1997**, *278*, 1795.

[8] S. A. Davis, M. Breulmann, K. H. Rhodes, B. Zhang and S. Mann, *Chem. Mater.* **2001**, *13*, 3218.

[9] J. S. Beck, C. Vartuli, W. J. Roth, M. E. Leonowicz, C. T Kresge, K. D. Schmitt, C. T-W. Chu, D. H. Olson, E. W. Sheppard, S. B. McCullen, J. B. Higgins, J. L. Schlenker, *J. Am. Chem. Soc*. **1992**, *114*, 10834.

[10] C. T. Kresge, M. E. Leonowicz, W. J. Roth, J. C. Vartulli, J. S. Beck, *Nature* **1992**, *359*, 710.

[11] M. Antonietti, G. A. Ozin, *Chem. Eur. J.* **2004**, *10*, 28.

[12] D. M. Antonelli, J. Y. Ying, *Angew. Chem. Int. Ed. Engl.* **1996**, *35*, 426.

[13] H. Cölfen, S. Mann, *Angew. Chem. Int. Ed.* **2003**, *42*, 2350.

[14] F. Schüth, *Angew. Chem.* **2003**, *115*, 3730; *Angew. Chem. Int. Ed.* **2003**, *42*, 3604.

[15] Q. Huo, D. I. Margolese, U. Ciesla, P. Feng, T. E. Gier, P. Sieger, R. Leon, P. M. Petroff, F. Schüth, G. D. Stucky, *Nature* **1994**, *368*, 317.

[16] J. Y. Ying, C. P. Mehnert, M. S. Wong, *Angew. Chem. Int. Ed.* **1999**, *38*, 56.

[17] C. Finnefrock, R. Ulrich, A. D. Chesne, C. C. Honeker, K. Schumacher, K. K. Unger, S. M. Gruner, U. Wiesner, *Angew. Chem.* **2001**, *113*, 1247; *Angew. Chem. Int. Ed.* **2001**, *40*, 1207.

[18] C. J. Brinker, Y. Lu, A. Sellinger, H. Fan, *Adv. Mater.* **1999**, *11*, 579.

[19] J. Lee, M. C. Orilall, S. C. Warren, M. Kamperman, F. J. Disalvo, U. Wiesner, *Nature Mater.* **2008**, *7*, 222.

[20] S. C. Warren, L. C. Messina, L. S. Slaughter, M. Kamperman, Q. Zhou, S. M. Gruner, F. J. Disalvo, U. Wiesner, *Science* **2008**, *320*, 1748.

[21] F. Schüth, W. Schmidt, *Adv. Mater.* **2002**, *14*, 629.

[22] P. Yang, T. Deng, D. Zhao, P. Feng, D. Pine, B. F. Chmelka, G. M. Whitesides, G. D. Stucky, *Science* **1998**, *282*, 2244.

[23] T. J. Barton, L. M. Bull, W. G. Klemperer, D. A. Loy, B. McEnaney, M. Misono, P. A. Monson, G. Pez, G. W. Scherer, J. C. Vartuli, O. M. Yaghi, *Chem. Mater.* **1999**, *11*, 2633.

[24] X. S. Zhao, G. Q. Lu, and G. J. Millar, *Ind. Eng. Chem. Res.* **1996**, *35,* 2075.

[25] D. Zhao, J. Feng, Q. Huo, N. Melosh, G. H. Frederickson, B. F. Chmelka, G. D. Stucky, *Science* **1998**, *279*, 548.

[26] P. T. Tanev, T. J. Pinnavaia, *Science* **1996**, *271*, 1267.

[27] S. Oliver, A. Kuperman, N. Coombs, A. Lough, G. A. Ozin, *Nature* **1995**, *378*, 47.

[28] P. Yang, D. Zhao, D. Margolese, B. Chmelka, G. D. Stucky, *Nature* **1998**, *396*, 152.

[29] S. Ruthstein, J. Schmidt, E. Kesselman, Y. Talmon, D. Goldfarb, *J. Am. Chem. Soc*. **2006,** *128,* 3366.

[30] M. T. Pope and A. Müller, *Polyoxometalate Chemistry From Topology via Self-Assembly to Applications*, Kluwer Academic Publishers, Netherlands, **2001**.

[31] J. B. Moffat, in *Metal-Oxygen Clusters - The Surface and Catalytic Properties of Heteropoly Oxometalates*, Kluwer Academic / Plenum Publishers, New York, **2001**.

[32] K. Okamoto, S. Uchida, T. Ito, N. Mizuno, *J. Am. Chem. Soc.* **2007**, *129*, 7378.

[33] K. Nomiya, H. Murasaki, M. Miwa, *Polyhedron* **1986**, *5*, 1031.

[34] D. E. Katsolulis, *Chem. Rev.* **1998**, *98*, 359.

[35] R. S. Yelamanchili, A. Walther, A. H. E. Müller, J. Breu, *Chem. Commun.* **2008**, 489.

[36] A. Taguchi, T. Abe, M. Iwamoto, *Adv. Mater.* **1998**, *10*, 667.

[37] A. Stein, M. Fendorf, T. P. Jarvie, K. T. Mueller, A. J. Benesi, T. E. Mallouk, *Chem. Mater.* **1995**, *7*, 304.

[38] G. G. Janauer, A. Dobley, J. Guo, P. Zavalij, M. S. Whittingham, *Chem. Mater.* **1996**, *8*, 2096.

[39] H. Yun, M. Kuwabara, H. Zhou, I. Honma, *Thin Solid Films* **2007**, *515*, 2842.

[40] G. Maayan, R. Popovitz-Biro, R. Neumann, *J. Am. Chem. Soc.* **2006**, *128*, 4968.

[41] R. K. O'Reilly, C. J. Hawker. K. L. Wooley, *Chem. Soc. Rev.* **2006**, *35*, 1068.

[42] Y. Mei, Y. Lu, F. Polzer, M. Drechsler, M. Ballauff, *Chem. Mater.* **2007**, *19*, 1062.

Chapter 3

Summary

We have explored the applicability of hypothesized approaches to the synthesis of porous and/or high surface area transition metal oxides. In addition, applicability and advantage of charged templates where strong Coulomb interactions favour the supramolecular arrangements/assembly were studied. The problems related with the dynamics of polymeric nanostructures for the synthesis of predesigned mesostructures could be avoided by crosslinking micelles, strictly speaking non-continuous phase in the bulk structure. Thereby, we presented a new approach for the grafting of Keggin POMs around the core-crosslinked PB-P2VP worm-like polymer templates (A 1 and 2). The produced POM-1 exhibits high dispersion, improved surface area and is thus expected to be useful in catalytic, electrochemical and biotechnology related applications. The general applicability of the method to other Keggin POMs and spherical polymer nanostructures were studied. Developed Keggin POMs-1 to 6 showed high dispersion of Keggin POM and surface areas. To the best of our knowledge, our approaches lead to Keggin POM nanocomposites with the highest surface areas reported todate. As-synthesized Keggin POM nanocomposites are amorphous. We have studied the removal of polymer template and crystallization of hybrid to corresponding metal oxides through step-wise calcinations under argon followed by air.

We have presented another approach to the synthesis of high surface area and mesoporous keggin POM framework materials using amphiphilic PI-PDMAEMA block copolymers (A 3). The calcined mesoporous materials exhibit Keggin POM hexagonal pore structure with high keggin POM dispersion, improved surface area. These developed materials are expected to be useful in catalytic applications. A fundamental principle involved in this method is that an attractive interaction between the organic block copolymer and the keggin POM precursors is obtained via Coulombic interactions through in situ quaternization (protonation) of PDMAEMA part, which also ensure the formation of a homogeneous hybrid material without any macrophase separation. Further,

step-wise calcinations under argon and air lead to evolution of mesoporous keggin POM material. To the best of our knowledge, this is the first hexagonally ordered mesoporous Keggin POM framework material.

We have presented a low-temperature, non-hydrothermal synthesis route to rutile nanocrystals. Both rutile and anatase nanocrystals exhibit positive surface charges. In contrary to the above approaches where polymer templates are cationic and inorganic precursors are anionic, in this case, inorganic nanocrystals are cationic and polymer templates are anionic. In this approach, we have demonstrated that crystalline TiO_2 nanocomposites with well-defined crystalline form could be directly synthesized at temperatures as low as 40 ^oC by mesostructuring the positively charged crystalline titania colloids over anionic spherical polyelectrolyte brush particles under aqueous conditions. Stepwise calcinations first under argon followed with a second calcination in air lead to the complete removal of polymer template without collapse and hollow porous spheres with crystalline framework are obtained. Porosity and surface areas increased dramatically after stepwise calcinations. Moreover, the porous rutile nanomaterials are photocatalytically active. We proved that our hypothesis to the synthesis of crystalline TiO_2 nanocomposites with well-defined crystalline form and morphologie is feasible.

Zusammenfassung

Im Mittelpunkt dieser Dissertation stehen Synthese und Charakterisierung poröser Materialien mit hoher spezifischer Oberfläche. Untersucht wurde dabei auch die Übertragbarkeit theoretischer Überlegungen auf die Synthese dieser Substanzen. Insbesondere sollten die Vorzüge geladener Template dargelegt werden, welche durch ihre starken Coulomb-Wechselwirkungen supramolekulare Strukturen ausbilden können und somit vorteilhaft zur Synthese der Materialien genutzt werden können. Ein während der Synthese von porösen Materialien oft auftretendes Problem ist die Dynamik der Polymer-Nanostrukturen bei der Ausbildung der für einen Templatmechanismus notwendigen Mesostrukturen. Die hier verwendete Templatgenerierung umgeht dieses Problem, indem eine Vernetzung der Micellen untereinander als strukturfixierendes Element eingeführt wird. Es wird eine neue Synthesemethode gezeigt, mit der Keggin-Polyoxometallate (Keggin-POM) unter Verwendung des Polymertemplats PB-P2VP dargestellt werden können. Das Templat PB-P2VP liegt in einer wurmartigen Morphologie vor und bietet die gewünschte Vernetzung zwischen den Micellen. Das mit dieser Methode synthetisierte POM-1 zeigt eine hohe Dispersion und eine große Oberfläche. Diese Vorteile begründen ihr Potential für die Anwendung in der Katalyse, Elektrochemie oder Biochemie. Nachfolgend wurde die Übertragbarkeit dieser Synthesemethode auf andere Keggin-POM untersucht (A 1 und 2). Die daraus resultierenden Keggin-POM-1 bis -6 zeigten ebenfalls die hohe Dispersion und große Oberflächen. Die hier vorgestellte Synthesemethode liefert Keggin-POM-Nanocomposite, deren Oberfläche über den bis dato publizierten liegt.

Weiterhin wird eine Synthesemethode für mesoporöse Keggin-POM-Materialien mit großer Oberfläche vorgestellt, welche sich amphiphiler PI-PDMAEMA-Blockpolymere bedient. Das nach Calcinierung erhaltene mesoporöse Material zeigt eine hexagonale Porenstruktur aus Keggin-POM, hohe Dispersion der Keggin-POM und hohe Oberflächenwerte (A 3). Die Anwendung dieser Materialien kann in der Katalyse gesehen werden. Die Besonderheit dieser Synthesemethode liegt in der Coulomb-

Wechselwirkung zwischen dem organischen Block-Copolymer und der Keggin-POM-Anion. Die Ladung am organischen Block-Copolymer wird in situ durch Quarternisierung (Protonierung) des PDMAEMA-Teils generiert, was eine Phasenseparation verhindert und damit die Ausbildung eines homogenen Hybridmaterials begünstigt. Das mesoporöse Keggin-POM-Material wird im nachfolgenden Schritt durch Calcinieren an Luft bzw. Argon erzeugt. Nach unserem Wissen stellt dieses Produkt das erste hexagonal geordnete mesoporöse Keggin-POM-Material dar.

Zusätzlich wird eine Synthese von Rutil-Nanokristallen bei niedriger Temperatur und unter nicht-hydrothermalen Bedingungen vorgestellt. Rutil-Nanokristalle weisen bei niedrigem pH ein positives Zetapotential auf. Im Gegensatz zu den in A 1-3 beschriebenen Synthesen, bei denen die Polymertemplate kationisch und die inorganischen Vorstufen anionisch geladen sind, liegen in dieser Synthese dagegen die Polymertemplate anionisch und die inorganischen Vorstufen kationisch geladen vor. Es konnte gezeigt werden, dass hochkristalline TiO_2-Nanopartikel unter wässrigen Bedingungen selbst bei niedrigen Temperaturen (40 °C) erzeugt werden können. Als Templat wurden dabei sphärische Polyelektrolyt-Partikel verwendet. Durch die Calcinierung unter Argon und anschließend unter Luft konnte das Polymertemplat vollständig und ohne Zerstörung der anorganischen Struktur oder Morphologie entfernt werden. Als Produkt wurden hohle Kugeln mit porösen Wänden, die einen hohem Grad an Kristallinität aufweisen, erhalten. Sowohl die Porosität als auch die Oberfläche steigt mit jedem Calcinierungsschritt dramatisch an. Bei den Eigenschaften dieser Rutil-Nanomaterialien konnte die photokatalytische Aktivität belegt werden.

List of publications

The following publications are enclosed in this PhD thesis:

- Yelamanchili, R. S., Walther, A., Müller, A. H. E., Breu, J., ´´Core-crosslinked block copolymer nanorods as templates for grafting $[SiMo_{12}O_{40}]^{4-}$ Keggin ions`` *Chem. Commun.* **2008**, 489.
- Yelamanchili, R. S., Walther, A., Lunkenbein, T., Müller, A. H. E., Breu, J., "Synthesis of high surface area Keggin-type polyoxometalates using core-crosslinked block copolymer nanorods and nanospheres" is to be submitted to *Langmuir*.
- Yelamanchili, R. S., Kamperman, M., Kiya, Y., Lee, Abruna, H. D., J., Breu, J., Wiesner, U., "Hexagonally Ordered Mesoporous Keggin Polyoxometalates" is to be submitted to *Nature Mater.*
- Yelamanchili, R. S., Lu, Y., Lunkenbein, T., Miyajima, N., Yan, L., Ballauff, M., Breu, J., "Shaping colloidal rutile into thermally stable and porous mesoscopic titania-balls" has been submitted to *Small.*

The following publications have been additionally published within the scope of my PhD thesis:

- Walther, A., Goldmann, A. S., Yelamanchili, R. S., Drechsler, M., Schmalz, H., Eisenberg, A., Müller, A. H. E., ´´ Multiple Morphologies, Phase Transitions, and Cross-Linking of Crew-Cut Aggregates of Polybutadiene-*block*-poly(2-vinylpyridine) Diblock Copolymers`` *Macromolecules* **2008**, *41*, 3254.
- Lu, Y., Hoffmann, M., Yelamanchili, R. S., Terrenoire, A., Schrinner, M., Drechsler, M., Möller, M., Breu, J., Ballauff, M., ´´ Well-defined crystalline TiO2 nanoparticles generated by a templated synthesis at room temperature`` *J. Mater. Chem.* **2008**, submitted

Individual Contribution to Joint Publications

The publications/manuscripts, which are presented in the appendix, were obtained in cooperation with other co-workers in different departments. My contributions to each publication are specified below.

Appendix A1

This work has been published with the title "**Core-crosslinked block copolymer nanorods as templates for grafting $[SiMo_{12}O_{40}]^{4-}$ Keggin ions**" by Yelamanchili, R. S., Walther, A., Müller, A. H. E., Breu, J., in *Chem. Commun.* 489-491 (2008).

- I have performed all the composite synthesis experiments and characterization.
- A. Walther, from Macromolecular Chemistry II, synthesized and crosslinked worm-like PB-P2VP block copolymers.
- J. Breu and A. H. E. Mueller contributed to the discussion.

Appendix A2

This work with the title "**Synthesis of high surface area Keggin-type polyoxometalates using core-crosslinked block copolymer nanorods and nanospheres**" by Yelamanchili, R. S., Lunkenbein, T., Walther, A., Müller, A. H. E., Breu, J., is to be submitted to *Langmuir*.

- I have performed all the composite synthesis experiments, characterization, calcinations and crystallization studies.
- T. Lunkenbein, a diploma student, did some synthesis experiments under my supervision.
- A. Walther, from Macromolecular Chemistry II, synthesized and crosslinked worm-like/spherical PB-P2VP block copolymers.
- J. Breu and A. H. E. Mueller contributed to the discussion.

Appendix A3

This work with the title "**Hexagonally Ordered Mesoporous Keggin-type Polyoxometalates**" by Yelamanchili, R. S., Kamperman, M., Kiya, Y., Lee, Abruna, H. D., J., Breu, J., Wiesner, U., is to be submitted to *Nature Mater.*.

- I have performed all the composite film synthesis experiments, calcinations, and characterization.
- M. Kamperman from Department of Materials Science and Engineering, Cornell University synthesized PI-PDMAEMA block copolymer, performed SAXS and some TEM measurements.
- Y. Kiya from Department of Chemistry and Chemical Biology, Cornell University performed cyclic voltagram experiments.
- J. Breu, J. Lee, H. D. Abruna and U. Wiesner contributed to the discussion.

Appendix A4

This work with the title "Shaping colloidal rutile into thermally stable and porous mesoscopic titania-balls" by Yelamanchili, R. S., Lu, Y., Lunkenbein, T., Miyajima, N., Yan, L., Ballauff, M., Breu, J., has been submitted to *Small.*

- I have performed all the composite film synthesis experiments, calcinations, and characterization using PXRD, FESEM, TEM and N_2 sorption measurements.
- Y. Lu from Physical Chemistry I synthesized polyelectrolyte brush and did FESEM, TEM measurements.
- T. Lunkenbein, a diploma student, did some synthesis experiments under my supervision.
- N. Miyajima performed HRTEM measurements.
- L. Yan prepared the scheme.
- J. Breu, and M. Ballauff contributed to the discussion.

Personal details

Name: Mr. Ram Sai Yelamanchili

Address: Sterntallering-12, 95447 Bayreuth, Germany

Date of Birth: 20th January, 1980

Nationality: Indian

Place of Birth: Khanapuram, India

Sex: Male

Marital status: Married

Education

06/1989-05/1995: Secondary School in Mathematics, Natural Sciences, English Jawahar Navodaya Vidyalayam, Paleru, India

06/1995-05/1997: Higher Secondary School in Mathematics, Physics, Chemistry Scholars junior college, Khammam, India

06/1997-05/2000: Bachelor of Science Degree in Mathematics, Physics and Chemistry, Kakatiya University, India

07/2000-05/2002: Master of Science Degree in Chemistry, Indian Institute of Technology (IIT), Chennai, India

Scientific background

07/2003-02/2005: Research assistant at University of Bielefeld, Germany

04/2005-Present: Doctorate in Natural Sciences at University of Bayreuth, Germany

10/2007-12/2007: Visiting Scientist: Cornell fuel cell institute and Department of Materials Science & Engineering, Cornell University, USA

Erklärung

Hiermit versichere ich, die vorliegende Arbeit selbstständig verfasst und keine anderen als die von mir angegebenen Quellen und Hilfsmittel benutzt zu haben.

Ferner erkläre ich, dass ich weder an der Universität Bayreuth, noch an einer anderen Hochschule versucht habe, eine Dissertation einzureichen, oder mich einer Promotionsprüfung zu unterziehen.

Ram Sai Yelamanchili
Bayreuth

Appendix Publications

The following publications/manuscripts are included as part of thesis

- **A 1** Core-crosslinked block copolymer nanorods as templates for grafting $[SiMo_{12}O_{40}]^{4-}$ Keggin ions
- **A 2** Synthesis of high surface area Keggin-type polyoxometalates using core-crosslinked block copolymer nanorods and nanospheres
- **A 3** Hexagonally ordered mesoporous Keggin-type polyoxometalates
- **A 4** Shaping colloidal rutile into thermally stable and porous mesoscopic titania-balls

A 1 Core-crosslinked block copolymer nanorods as templates for grafting $[SiMo_{12}O_{40}]^{4-}$ Keggin ions

This work has been published with the title "**Core-crosslinked block copolymer nanorods as templates for grafting $[SiMo_{12}O_{40}]^{4-}$ Keggin ions**" by Yelamanchili, R. S., Walther, A., Müller, A. H. E., Breu, J., in *Chem. Commun.* 489-491 (2008).

Core-crosslinked block copolymer nanorods as templates for grafting $[SiMo_{12}O_{40}]^{4-}$ Keggin ions†‡

Ram Sai Yelamanchili,[a] Andreas Walther,[b] Axel H. E. Müller*[b] and Josef Breu*[a]

Received (in Cambridge, UK) 18th September 2007, Accepted 22nd November 2007
First published as an Advance Article on the web 7th December 2007
DOI: 10.1039/b714435k

Core-crosslinked PB-P2VP block copolymer nanorods are used as templates for the synthesis of Keggin-type heteropolyoxometalate (POM) nanostructures by grafting $[SiMo_{12}O_{40}]^{4-}$ Keggin ions on the template.

The organic template-directed synthesis of inorganic materials has attracted world wide attention due to the ability of organics to self-assemble into a variety of micelle nanostructures with well-defined shape and size.[1–3] An important class of organic templates used for the synthesis of materials is the amphiphilic block copolymers.[4] However, block copolymer micelles are very sensitive to the reaction conditions. Change in pH, temperature, solvent, or ionic strength can lead to micelle transformation or disintegration. For example, when polybutadiene-block-poly(2-vinylpyridine) (PB-P2VP) with 80% PB is dissolved in THF, worm-like micelles are formed in solution. Addition of water or protonation leads to a micelle transformation thus leading to undesired changes in the template morphology (see ESI‡). Hence, the use of polymeric micelles to synthesize inorganic materials with desired morphologies is not always possible due to the dynamic nature of micelles. The micelle stability is especially important for the synthesis of materials which ask for changes in reaction conditions.

In this communication, we present a novel synthesis strategy for the development of inorganic nanostructures using core-crosslinked stable polymer templates. Scheme 1 summarizes this novel approach for the synthesis of desired inorganic nanostructures.

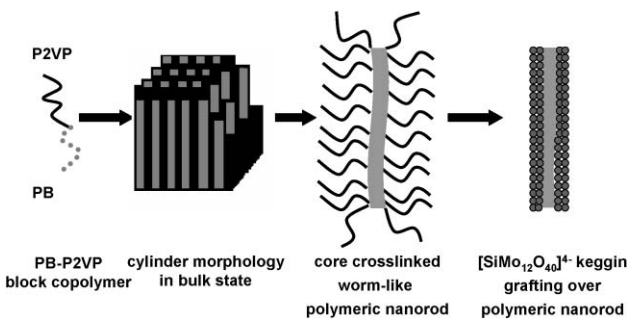

Scheme 1 Synthesis of $[SiMo_{12}O_{40}]^{4-}$ Keggin nanostructures using core-crosslinked PB-P2VP worm-like polymer template and $H_4[SiMo_{12}O_{40}]$.

[a]*Department of Inorganic Chemistry I, University of Bayreuth, 95447, Bayreuth, Germany. E-mail: josef.breu@uni-bayreuth.de; Fax: +49 921552788; Tel: +49 921552530*
[b]*Department of Macromolecular Chemistry II, University of Bayreuth, 95447, Bayreuth, Germany. E-mail: axel.mueller@uni-bayreuth.de; Fax: +49 921553393; Tel: +49 921553399*
† Dedicated to Professor H.-P. Böhm on the occasion of his 80th birthday.
‡ Electronic supplementary information (ESI) available: Experimental details, TEM, SEM, and XRD. See DOI: 10.1039/b714435k

Firstly, a block copolymer is synthesized which microphase-separates into a well-defined cylindrical bulk structure. Generally, adjusting the volume fractions and molecular weight of the block copolymer allows a facile tunability of the dimensions and shapes of the desired polymeric template. Secondly, it is possible to freeze the dynamics of the polymeric nanostructures by crosslinking the core, shell or even the surface.[5] In the present study, the core of the micelles is crosslinked and the resultant polymeric micelles are stable and resistant to changes in reaction conditions. Thirdly, protonation or quaternization can be performed at controllable rate to achieve charge matching between the polymer template and inorganic complexes. Fourthly, anionic inorganic precursors are grafted on the charged template and the inorganic/organic nanocomposite will precipitate. Please note, that when using an acidic inorganic precursor, quaternization of polymer template and grafting of the corresponding anion take place simultaneously.

Keggin-type heteropolyoxometalates (POM) were chosen as inorganic precursors due to the following reasons. Polyoxometalates (POM), the discrete metal-oxygen cluster compounds mainly of transition metals, exhibit fascinating properties and applications.[6] The properties of the POMs, particularly of the Keggin-type, depend mainly on the nature of the counter cation and the composition of the POM anion.[7] POMs with high surface areas and controllable nanostructures are of interest in a variety of applications such as high performance catalysts (acid and redox), sensor devices and electrodes (due to their high ion conductivity, electron density, rapid and reversible oxidative-reductive processes).[7,8] But, POMs present relatively small surface areas, the surface area of commercial $H_4SiMo_{12}O_{40}$ is 4 $m^2\ g^{-1}$, which hinders accessibility to the active sites and as a result the applications of POMs are limited.[7] Hence, there is a great demand to develop POM materials with high surface area.

The efficiency of the POMs can be increased by two approaches. (1) using high surface area solids as supports to disperse POM and (2) developing composite materials with POMs as building blocks. Mesoporous silica materials like MCM-41 or SBA-15 have very high surface area (*ca.* 800–1000 $m^2\ g^{-1}$) and these materials were used as supports for the dispersion of POM.[9,10] There are also reports using carbon, silica gel, titanium gel, aluminium, *etc.* as solid supports for the dispersion of POM.[11] Even though, the accessible surface area for POMs can be increased by these methods, limitations rely on low POM loading, leaching of the active sites into the reaction medium and pore blocking in porous supports. Another approach involves the synthesis of POM nanocomposites using organic surfactants or polymers.[12,13] However, the accessible surface area is lower and the organic templates need to be removed to allow free access to the POM

active sites but the hybrid structures tend to collapse during the template removal.[12] Neumann and co-workers used polymeric micelles to synthesize POM nanoparticles and observed improved catalytic activities for the developed POM nanostructures.[14] All together, these results indicate that the synthesis of chemically and physically well defined, discrete POM nanostructures with a highly accessible surface area is of great interest. But the synthesis of POM nanostructures requires the control of various reaction parameters like pH, temperature, ionic strength, *etc*. Hence, the templating micelles should be stable and resistant to changes in the reaction parameters.

To prove our concept, a well-defined PB-P2VP block copolymer with 30 wt % PB and a molecular weight of 2.0×10^5 g mol^{-1} was synthesized by anionic polymerization (see ESI‡). The weight fractions are chosen in such a way that it forms a cylindrical morphology in the bulk state with PB-cylinders embedded in a P2VP matrix. The unsaturated PB-cores were crosslinked using a commercial photointiator to lock the cylindrical structure. The core-crosslinked cylinders exhibit worm-like morphologies when dissolved in THF or acetone. The block copolymer nanostructures were characterized using scanning electron microscopy (SEM), transmission electron microscopy (TEM), energy dispersive X-ray analysis (EDX), and Fourier transform infrared (FTIR) measurements.

The TEM images of the core-crosslinked PB-P2VP worm-like polymer template are shown in Fig. 1. The core-corona structure of the worm-like polymer template is revealed due to the different electron penetrability of the PB core and P2VP corona. The diameter of the PB core is approximately 40 nm and the P2VP corona extends *ca.* 35 nm around the PB-core. The total diameter of the worm-like polymeric rods is *ca.* 110 nm. As sonication is necessary for the dissolution of the crosslinked PB-P2VP template, worm-like polymer rods with different lengths are observed. Fig. 2 shows the SEM image of worm-like polymer rods, where the smooth surface of the polymer cylinders can be observed.

The Keggin-type POM nanostructures can be synthesized by adding the PB-P2VP worm-like polymer solution to the $H_4SiMo_{12}O_{40}$ (POM) solution. Experimental details are provided in the ESI.‡ When neutral polymer rods in THF are added to the POM solution (which is a heteropolyacid) the 2-vinylpyridine units in the arms will be protonated, while the POM-anions are simultaneously grafted onto the template. Thus formation of the inorganic–organic nanocomposites is driven by strong Coulombic interactions between the 2-vinylpyridinium arms of the core-crosslinked PB-P2VP worm-like micelles and the inorganic POM anions. The polymer–POM nanocomposite is referred hereafter as POM-1. The produced POM-1 was characterized using SEM, EDX, TEM, FTIR, X-ray diffraction (XRD) and N_2 sorption measurements.

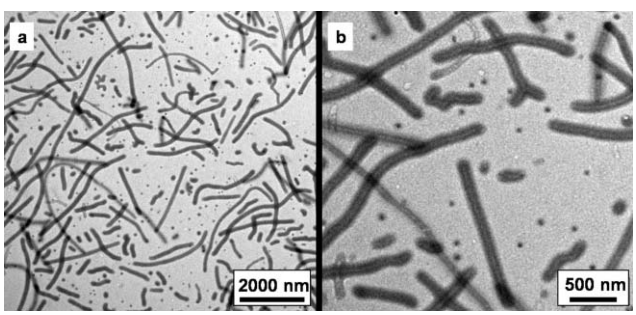

Fig. 1 TEM images of the core-crosslinked PB-P2VP worm-like polymer template at different magnifications.

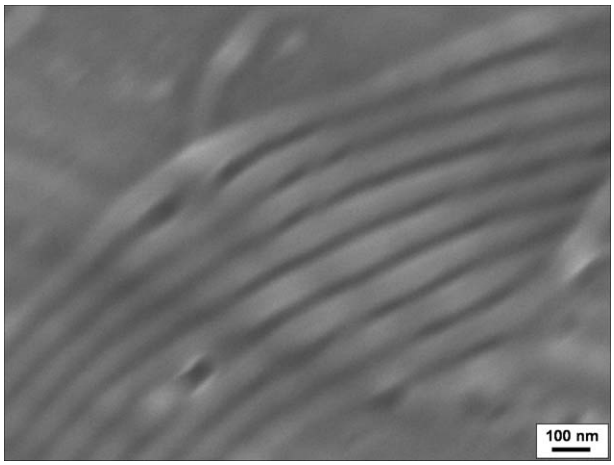

Fig. 2 SEM image of the core-crosslinked PB-P2VP worm-like polymer template.

The formation of POM-1 can be directly observed by SEM and TEM. In comparison to the pure polymer nanorods (Fig. 2), the surface of the POM-1 is rough (Fig. 3). The surface roughness of the POM-1 is due to the grafting of $[SiMo_{12}O_{40}]^{4-}$ Keggin around the polymer template. The selected area EDX spectrum clearly shows the presence of Si, Mo and C and confirms the grafting of $[SiMo_{12}O_{40}]^{4-}$ Keggin around the template. The surface roughness due to the presence of $[SiMo_{12}O_{40}]^{4-}$ Keggin POM around the polymer template becomes also obvious when comparing the TEM images of the pure polymer template (Fig. 1) with POM-1 (Fig. 4). The interaction of the inorganic $[SiMo_{12}O_{40}]^{4-}$ Keggin POM with the P2VP block of the core-crosslinked PB-P2VP worm-like polymer template also changed the dimensions of the resultant composite nanostructures. In the absence of the $[SiMo_{12}O_{40}]^{4-}$ Keggin POM anions, the P2VP corona of the core-crosslinked PB-P2VP worm-like polymer rods is stretched (*ca.* 35 nm around the core). Addition of $[SiMo_{12}O_{40}]^{4-}$ Keggin POM

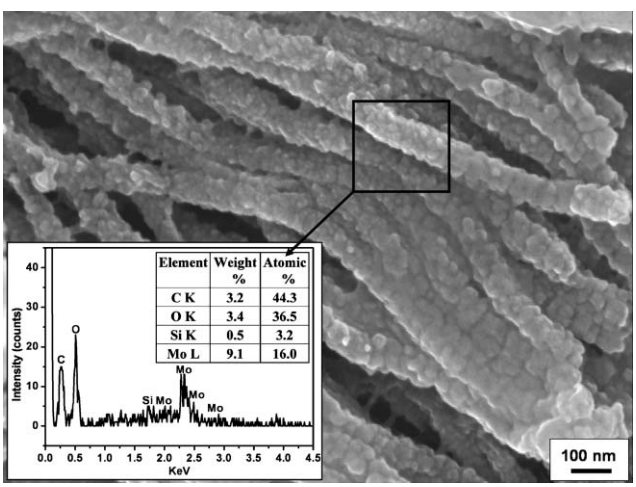

Fig. 3 SEM image of the $[SiMo_{12}O_{40}]^{4-}$ Keggin POM grafted onto core-crosslinked PB-P2VP worm-like polymer template (inset: EDX spectrum).

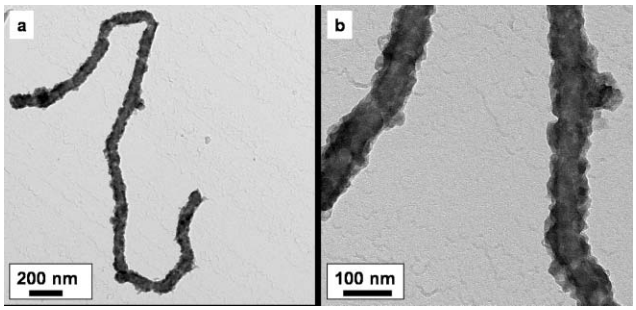

Fig. 4 TEM images of the $[SiMo_{12}O_{40}]^{4-}$ Keggin POM-grafted onto core-crosslinked PB-P2VP worm-like polymer template at different magnifications.

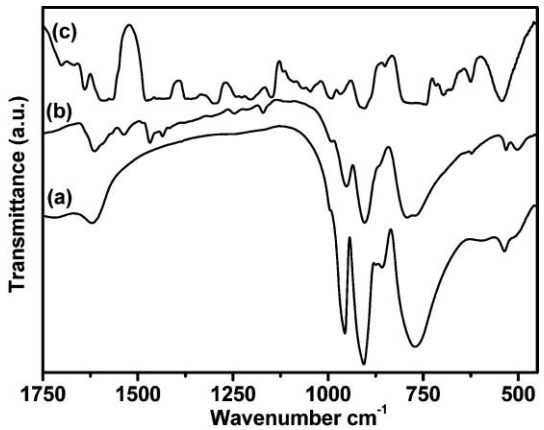

Fig. 5 FTIR spectra of the (a) pure $H_4[SiMo_{12}O_{40}]$ Keggin POM, (b) POM-1 and (c) core-crosslinked PB-P2VP worm-like polymer template.

caused the complexation of the 2-vinylpyridine units in the arms with the Keggin anions and as a result the P2VP corona shrinks from initial *ca.* 35 nm to *ca.* 15–20 nm. The $[SiMo_{12}O_{40}]^{4-}$ Keggin POM-grafted worm-like polymer rods exhibit overall diameters in the range of *ca*. 60–65 nm, significantly smaller than the initial pure worm-like polymer rod.

The grafting of $[SiMo_{12}O_{40}]^{4-}$ Keggin POM over wormlike polymer rods was further verified by FTIR analysis. FTIR spectra of the pure $H_4SiMo_{12}O_{40}$ Keggin POM, POM-1 and core-crosslinked polymer rod template are shown in Fig. 5. It has been widely reported that the Keggin-type heteropolyoxometalates show four characteristic bands, which are the fingerprint of the Keggin structure.[15] There are four kinds of oxygen atoms in $H_4SiMo_{12}O_{40}$ (O_a—oxygen in SiO_4 tetrahedra, O_d—terminal oxygen atom to Mo, O_b—corner sharing oxygen and O_c—edge sharing oxygen) and these characteristic bands were observed at ν_{as} (Mo–O_d) −952 cm^{-1}, ν_{as} (Mo–O_b–Mo) −794 cm^{-1}, ν_{as} (Mo–O_c–Mo) −864 cm^{-1} and ν_{as} (Si–O_a) −902 cm^{-1}. The FTIR spectrum of the POM-1 corresponds well to the superposition of the spectra of the pure Keggin type heteropolyoxometalates and PB-P2VP polymer rod template which is clear evidence that the Keggin structure stayed intact when being grafted onto the worm-like polymer rods.

In addition, wide-angle powder XRD patterns of the pure $H_4[SiMo_{12}O_{40}]$ Keggin POM, core-crosslinked worm-like polymer template and POM-1 were recorded (see ESI‡). In contrast to the pure $H_4[SiMo_{12}O_{40}]$ Keggin POM, XRD patterns of POM-1 do not show any characteristic peaks for $H_4[SiMo_{12}O_{40}]$. This amorpous nature is an indication of the very high degree of dispersion of Keggin POM in the polymer matrix.[10d] The N_2 sorption measurements of POM-1 show that the developed Keggin POM nanostructures have a 37 $m^2\ g^{-1}$ surface area, whereas the commercially available POM ($H_4SiMo_{12}O_{40}$) only has a 4 $m^2\ g^{-1}$ surface area.

In conclusion, we presented a novel approach for the grafting of Keggin-type heteropolyoxometalates around the core-crosslinked PB-P2VP worm-like polymer templates. The produced POM-1 exhibit high dispersion, improved surface area and are thus expected to be useful in catalytic, electrochemical and biotechnology related applications. An investigation of the properties of the POM-1 is ongoing together with steps aimed at the synthesis of other metal oxide nanostructures. The method appears to be generally applicable. For instance, $[PMo_{12}O_{40}]^{3-}$ Keggin-type POM nanostructures can be synthesized following the same procedure (see ESI‡).

This project is supported by Elite Network Bavaria (ENB). R. S. Y. and A. W. would like to acknowledge Elite Network Bavaria for a fellowship. We would like to thank Dr Holger Schmalz and Dr Markus Drechsler for their help with uncrosslinked polymer synthesis and cryo-TEM measurements, respectively.

Notes and references

1 F. Schüth, *Angew. Chem., Int. Ed.*, 2003, **42**, 3604.
2 R. Ulrich, A. D. Chesne, M. Templin and U. Wiesner, *Adv. Mater.*, 1999, **11**, 141.
3 S. A. Davis, M. Breulmann, K. H. Rhodes, B. Zhang and S. Mann, *Chem. Mater.*, 2001, **13**, 3218.
4 S. Förster, *Top. Curr. Chem.*, 2003, **226**, 1–28.
5 R. K. O'Reilly, C. J. Hawker and K. L. Wooley, *Chem. Soc. Rev.*, 2006, **35**, 1068.
6 M. T. Pope and A. Müller, *Polyoxometalate Chemistry From Topology via Self-Assembly to Applications*, Kluwer Academic Publishers, Netherlands, 2001.
7 J. B. Moffat, in *Metal-Oxygen Clusters - The Surface and Catalytic Properties of Heteropoly Oxometalates*, Kluwer Academic/Plenum Publishers, New York, 2001.
8 (*a*) K. Okamoto, S. Uchida, T. Ito and N. Mizuno, *J. Am. Chem. Soc.*, 2007, **129**, 7378; (*b*) K. Nomiya, H. Murasaki and M. Miwa, *Polyhedron*, 1986, **5**, 1031; (*c*) D. E. Katsolulis, *Chem. Rev.*, 1998, **98**, 359.
9 (*a*) C. T. Kresge, M. E. Leonowicz, W. J. Roth, J. C. Vartuli and J. S. Beck, *Nature*, 1992, **359**, 710; (*b*) T. Blasco, A. Corma, A. Martinez and P. Martinez-Escolano, *J. Catal.*, 1998, **177**, 306.
10 (*a*) D. Zhao, J. Feng, Q. Huo, N. Melosh, G. H. Fredrickson, B. F. Chmelka and G. D. Stucky, *Science*, 1998, **279**, 548; (*b*) S.-Y. Yu, L.-P. Wang, B. Chen, Y.-Y. Gu, H.-M. Ding and Y.-K. Shan, *Chem.–Eur. J.*, 2005, **11**, 3894; (*c*) C. Shi, R. Wang, G. Zhu, S. Qiu and J. Long, *Eur. J. Inorg. Chem.*, 2005, **2005**, 4801; (*d*) L. Yang, Y. Qi, X. Yuan, J. Shen and J. Kim, *J. Mol. Catal. A: Chem.*, 2005, **229**, 199.
11 P. M. Rao, A. Wolfson, S. Kababya, S. Vega and M. V. Landau, *J. Catal.*, 2005, **232**, 210.
12 (*a*) A. Taguchi, T. Abe and M. Iwamoto, *Adv. Mater.*, 1998, **10**, 667; (*b*) A. Stein, M. Fendorf, T. P. Jarvie, K. T. Mueller, A. J. Benesi and T. E. Mallouk, *Chem. Mater.*, 1995, **7**, 304; (*c*) G. G. Janauer, A. Dobley, J. Guo, P. Zavalij and M. S. Whittingham, *Chem. Mater.*, 1996, **8**, 2096.
13 H. Yun, M. Kuwabara, H. Zhou and I. Honma, *Thin Solid Films*, 2007, **515**, 2842.
14 G. Maayan, R. Popovitz-Biro and R. Neumann, *J. Am. Chem. Soc.*, 2006, **128**, 4968.
15 C. Rocchiccioli-Deltcheff, M. Fournier, R. Frank and R. Thouvenot, *Inorg. Chem.*, 1983, **22**, 207.

Supplementary Material (ESI) for Chemical Communications

Supporting Information

Core-crosslinked block copolymer nanorods as templates for grafting $[SiMo_{12}O_{40}]^{4-}$ keggin ions

Ram Sai Yelamanchili,[a] Andreas Walther,[b] Axel H. E. Müller[b] and Josef Breu *[a]

Experimental section:

Synthesis of polymer and crosslinking reactions: The synthesis of the polybutadiene-*block*-poly(2-vinylpyridine) diblock copolymers (PB-P2VP) was accomplished via sequential living anionic polymerization. Butadiene polymerization was initiated with sec-BuLi at -70°C, and butadiene was allowed to polymerize at -10°C for 8 h. After subsequent cooling to -70°C, 2-vinylpyridine was added to the reaction mixture. After 1h reaction time the polymerization was terminated with degassed methanol, and the product precipitated in a water/methanol mixture. According to NMR and GPC, coupled to a multi-angle laser light scattering detector, the polymer synthesized is $PB_{30}P2VP_{70}^{200}$. The subscript numbers denote the mass fraction in percent, and the superscripts give the number-average molecular weight in kg/mol. For crosslinking of the block copolymer in the bulk state, a 10 wt% solution of PB-P2VP in THF was allowed to evaporate slowly in the presence of 40 wt% of Lucirin TPO, corresponding to the amount of polymer. After complete evaporation of the solvent and film annealing, the films were crosslinked on a UV lamp (cut-off < 350 nm) for 2 – 6 hours. Subsequently, soxhlet extraction was performed in THF and the insoluble product underwent ultrasonication in a THF dispersion in order to obtain soluble PB-P2VP core-crosslinked cylinders.

Synthesis of $[SiMo_{12}O_{40}]^{4-}$ keggin-type POM nanostructures: The template directed synthesis of the polyoxometalate nanostructures was carried out at room temperature. The core-crosslinked PB-P2VP polymer solution in THF (0.5 wt%) (colour less) was added to 10 mL of 10^{-2} M $H_4[SiMo_{12}O_{40}]$ in THF (yellow solution due to yellow colour of the $H_4[SiMo_{12}O_{40}]$) with continuous stirring for 6h. With the addition of polymer solution, a coloured precipitate was produced while the yellow colour of the POM solution starts fading. The yellow precipitate was formed by grafting coloured $[SiMo_{12}O_{40}]^{4-}$ on the polymer template. When the solution reached the neutralization point the yellow colour

of the solution had disappeared completely due to complete grafting of the coloured $H_4[SiMo_{12}O_{40}]$ on the polymer template. The resultant precipitate was allowed to age in the reaction mixture for 12 h. Finally, the precipitate was washed 3 times with deionized water and kept at 100°C for 12h to dry.

$[PMo_{12}O_{40}]^{3-}$ keggin-type POM nanostructures were synthesized following the same procedure while using $H_3[PMo_{12}O_{40}]$ .xH_2O as keggin source.

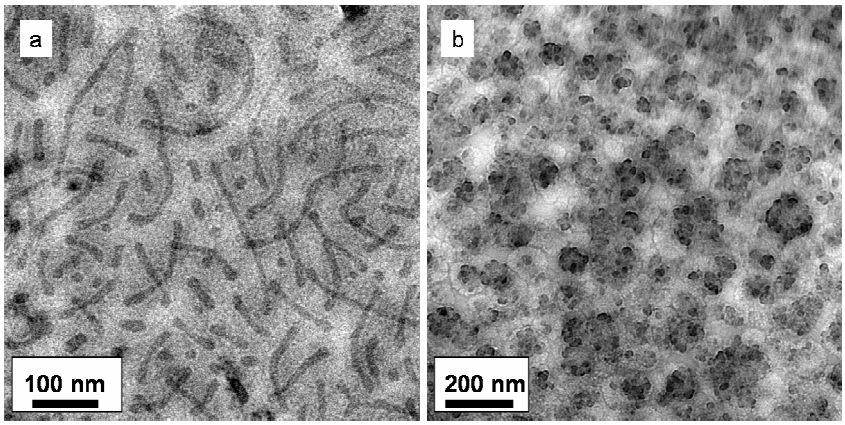

Fig. S1. Cryo-TEM images of the (a) 1 wt% of PB_{80}-$P2VP_{20}$ (64,900 g/mol) in THF wormlike micelles without core crosslinking, (b) 1 wt% of PB_{80}-$P2VP_{20}$ (64,900 g/mol) in THF acidified with 2M HCl.

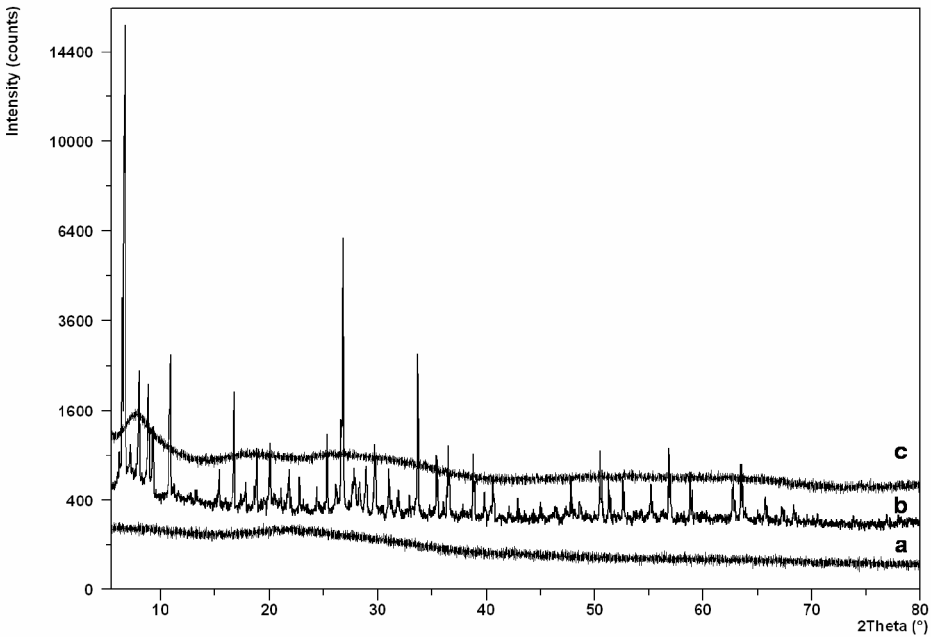

Fig. S2. Powder X-ray diffraction patterns of (a) core-crosslinked PB-P2VP polymeric nanorod template (b) pure $H_4[SiMo_{12}O_{40}]$ and (c) POM-1

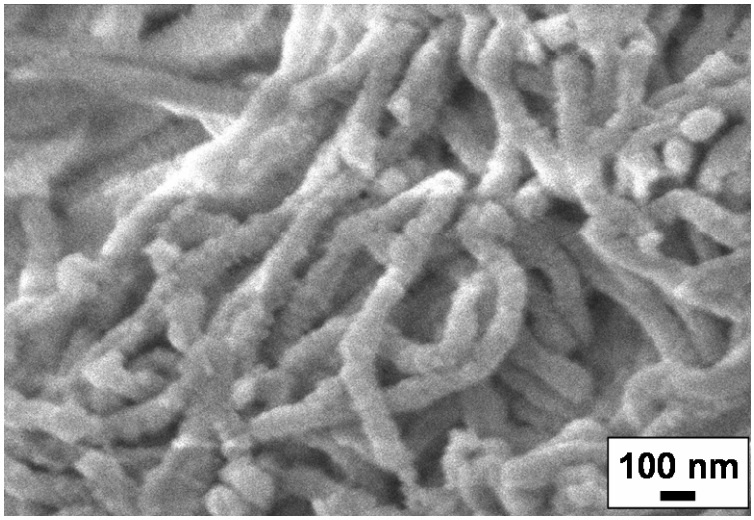

Fig. S3 SEM image of the $[PMo_{12}O_{40}]^{3-}$ keggin POM grafted over core-crosslinked PB-P2VP worm-like polymer template

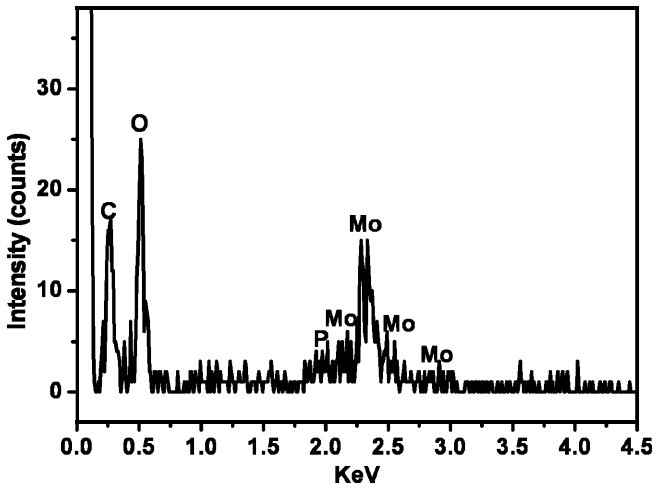

Fig. S4 EDX spectrun of the $[PMo_{12}O_{40}]^{3-}$ keggin POM grafted over core-crosslinked PB-P2VP worm-like polymer template

A 2 Synthesis of high surface area Keggin-type polyoxometalates using core-crosslinked block copolymer nanorods and nanospheres

This work with the title "**Synthesis of high surface area Keggin-type polyoxometalates using core-crosslinked block copolymer nanorods and nanospheres**" by Yelamanchili, R. S., Lunkenbein, T., Walther, A., Müller, A. H. E., Breu, J., is to be submitted to *Langmuir*.

Synthesis of high surface area Keggin-type polyoxometalate nanocomposites using core-crosslinked block copolymer nanorods and nanospheres

Ram Sai Yelamanchili[1], Thomas Lunkenbein[1], Andreas Walther[2], Axel H. E. Mueller[2] and Josef Breu[1*]*

[1]Anorganische Chemie I, University of Bayreuth, 95440 Bayreuth, Germany

[2]Macromolecular Chemie II, University of Bayreuth, 95447 Bayreuth, Germany

* Corresponding Authors: axel.mueller@uni-bayreuth.de, josef.breu@uni-bayreuth.de

Abstract

The organic template-directed synthesis of organic-inorganic nanocomposites has attracted world wide attention due to the ability of organics to self-assemble into a variety of micelle nanostructures with well-defined shape and size. But the polymer micelles are very sensitive to the reaction conditions such as pH, temperature, solvent, ionic strength. Any tiny change in the reaction system may lead to micelle transformation into other supramolecular structures. Hence, the use of polymeric micelles to synthesize organic-inorganic nanocomposites with pre-designed morphologies is not always possible due to this dynamic nature of micelles. Herein, we present a new strategy to synthesize pre-designed organic-inorganic hybrid nanocomposites using diblock copolymers with unsaturated cores (polybutadiene-poly(2-vinylpyridine), PB-P2VP). The non-continuous phase of the bulk structure is crosslinked to freeze the dynamics and the resultant polymeric nanostructures are stable and resistant to changes in reaction conditions. Moreover, the block copolymers used carry ionizable coronas. Therefore the composite formation can be driven by electrostatic interactions between soft template and inorganic precursor. Consequently, these core-crosslinked PB-P2VP block copolymer nanorods and nanospheres are ideal templates for mesostructuring Keggin-type heteropolyoxometalates (Keggin POM). Homogenous nanocomposites are reliably formed by grafting different Keggin POM anions on the protonated, cationic soft template. The as-synthesized amorphous Keggin POM nanocomposites exhibit high surface areas and are expected to be useful in catalytic applications.

KEYWORDS: Block copolymers, Crosslinking, Nanocomposites, Nanostructures, Polyoxometalates

Introduction

Synthesis of organic-inorganic nanocomposites using organic templates has attracted world wide attention due to the ability of organics to self-assemble into a variety of nanostructures with well-defined shape and size.[1-4]. In particular, block copolymers allow easy control of organic-inorganic hybrid morphology down to the nanometer scale.[4;5]. Since macroscopic properties crucially depend on both composition and morphology, properties can thus be tailored by combining principles of self-assembly, polymer, colloidal, and inorganic chemistries resulting in nanocomposites with a variety of functionalities and properties.[4-7] However, the dynamics observed between different micelle structures, represents major obstacle with the use of these supramolecular soft templates. Polymer micelles are very sensitive to the reaction conditions. Change in pH, temperature, solvent, ionic strength can lead to micelle transformation.[8;9] Consequently, in many cases the conditions required for the formation of the desired template structure do not match with those requirements for the controlled condensation/assembly of the inorganic precursors around the template.

For instance, Keggin-type heteropolyoxometalates (Keggin POM), the discrete metal-oxygen cluster compounds mainly of transition metals, exhibit fascinating properties and applications.[10-15] The properties of the POMs, particularly of the Keggin-type, depend mainly on the nature of the counter cation and the composition of the Keggin POM anion.[10-12] Due to their high ion conductivity, electron density, rapid and reversible oxidative-reductive processes Keggin POMs are of interest in variety of technological applications such as high performance catalysts, sensor devices and electrodes.[11-15] Commercial Keggin POMs present relatively small surface areas. The surface area of commercial Keggin POMs such as $H_3PMo_{12}O_{40}$.$6H_2O$ is 3 m^2g^{-1} and $H_4SiMo_{12}O_{40}$.$6H_2O$ is 4 m^2g^{-1}. Due to these small surface areas accessibility to the active sites is minimum and as a result the applications of Keggin POMs are limited.[10;11] For many of these applications, it would therefore be highly desirable to increase the surface area of these compounds by shaping them into a mesostructured morphology

Until now, the surface area of the Keggin POMs was increased following two approaches. Firstly,

Mesoporous silica materials like MCM-41, SBA-15 with high surface areas (ca. 800–1000 m^2g^{-1}) were used as supports for the dispersion of Keggin POM.[16-23] There are also reports using carbon, silica gel, titanium gel, aluminosilicate, etc, as solid supports for Keggin POM.[23-26] Among many other factors, the activity of supported Keggin POMs depends crucially on the strength of interaction with the surface sites. For instance, with aluminosilicate supports, both the number and the average acid strength of the Brönsted acid sites of the Keggin POMs decrease.[16] In brief, while the accessible surface area for Keggin POMs may indeed be increased by these high surface area supports, limitations rely on low Keggin POM loading, leaching of the active sites into the reaction medium and detrimental interactions with the supports.

Secondly, Keggin POM nanocomposites have been synthesized using organic surfactants or polymers as soft templates. [11;23-28] While nanocomposites with a variety of two dimensional and three dimensional mesostructures were accessible,[24-26] the surface area could not be increased significantly because the templates could not be removed without concomitant collapse of the mesoscopic morphologies. While the above reports use neutral acids as inorganic precursors, Neumann and co-workers used the anions in combination with spherical micelles of cationic surfactant. Unfortunately he did not report surface areas, but observed improved catalytic activities might be an indication for higher surface areas.[29] This in turn might suggest that high surface area materials might be accessible by taking advantage of coulombic interactions between inorganic precursor and soft template. It is this hypothesis that initiated our investigations.

Earlier, we have reported the synthesis of PB-P2VP/$[SiMo_{12}O_{40}]^{4-}$ nanocomposites (PB-P2VP = polybutadiene-poly(2-vinylpyridine)).using core-crosslinked PB-P2VP block copolymer nanorods as templates.[8] In the present report, the expansion of the synthesis strategy to different Keggin POMs and spherical polymer systems is discussed. Keggin POMs with different charge and metal centers were used to study the general applicability of this approach. In addition, we studied the influence of calcinations on morphology and surface area. Scheme 1 summarizes our approach for the synthesis of pre-designed Keggin POM nanostructures. Firstly, a block copolymer is synthesized which microphase-

separates into a well-defined cylindrical or spherical bulk structure. Generally, adjusting the volume fractions and molecular weight of the block copolymer allows a facile tunability of the dimensions and shapes of the desired polymeric template. Secondly, the dynamics of the polymeric nanostructures are frozen by crosslinking the core.[8;30] Thereby nanostructures are obtained that are stable and resistant to changes in reaction conditions such as different pH and solvent conditions. Thirdly, the pyridine moieties in the corona are basic enough to be protonated in situ upon addition of the Keggin POMs which are heteropoly acids. Fourthly, by this quaternization a strong Coulomb interaction between the cationic soft template and the anionic inorganic precursors is triggered and the organic-inorganic nanocomposite will precipitate.

Scheme 1. Synthesis of Keggin POM nanocomposites using core-crosslinked PB-P2VP polymer templates of different structure and Keggin POM.

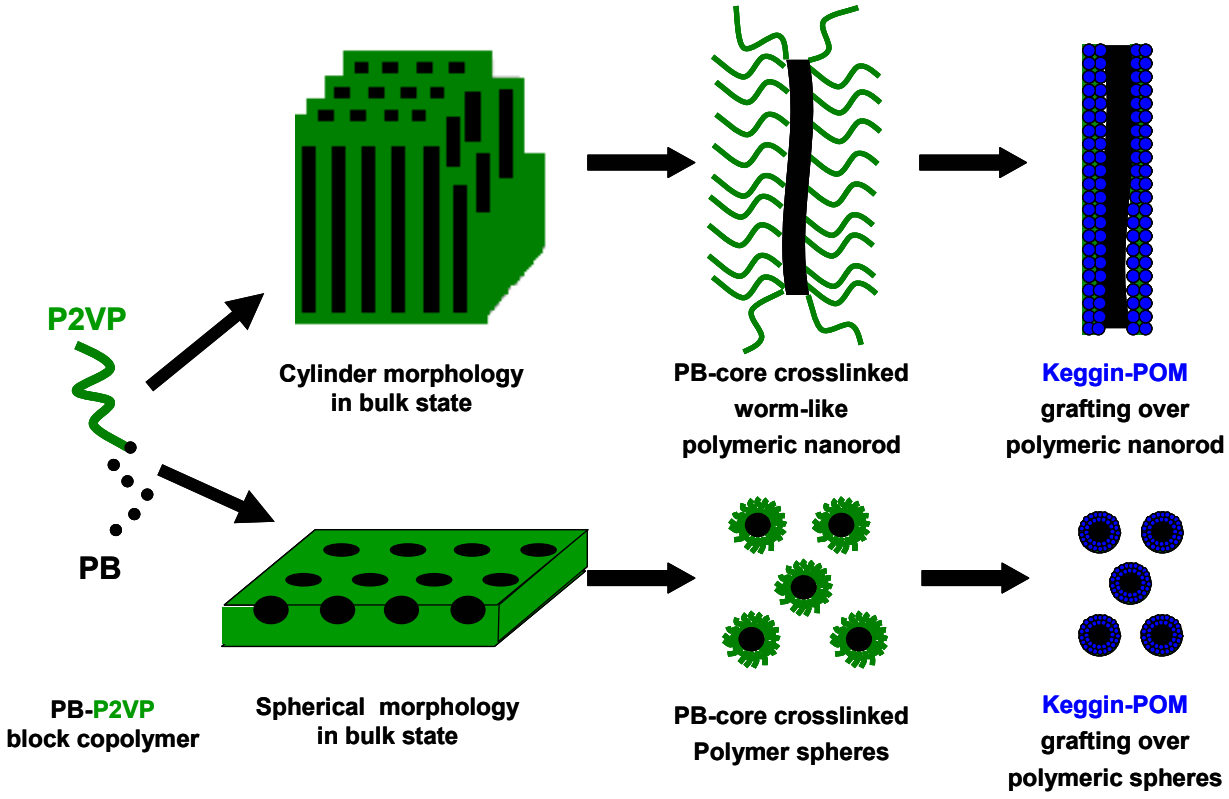

Experimental Section

Synthesis of polymer templates. A well-defined PB-P2VP block copolymer with 30 wt-% PB and a molecular weight of 2.0×10^5 g/mol was synthesized by anionic polymerization. The synthesis of the polybutadiene-poly(2-vinylpyridine) diblock copolymers (PB-P2VP) was accomplished via sequential living anionic polymerization. Butadiene polymerization was initiated with sec-BuLi at -70°C, and butadiene was allowed to polymerize at -10°C for 8 h. After subsequent cooling to -70°C, 2-vinylpyridine was added to the reaction mixture. After 1h reaction time, the polymerization was terminated with degassed methanol, and the product precipitated in a water/methanol mixture. According to NMR and GPC, coupled to a multi-angle laser light scattering detector, the polymer synthesized is $PB_{30}P2VP_{70}^{200}$. The subscript numbers denote the mass fraction in percent, and the superscripts give the number-average molecular weight in kg/mol. For crosslinking of the block copolymer in the bulk state, a 10 wt% solution of PB-P2VP in THF was allowed to evaporate slowly in the presence of 40 wt% of Lucirin TPO, corresponding to the amount of polymer. After complete evaporation of the solvent and film annealing, the films were crosslinked on a UV lamp (cut-off < 350 nm) for 2 – 6 hours. Subsequently, soxhlet extraction was performed in THF and the insoluble product underwent ultrasonication in THF dispersion in order to obtain soluble PB-P2VP core-crosslinked cylinders. The weight fractions are chosen in such a way that it form a cylindrical morphology in the bulk state with PB-cylinders embedded in a P2VP matrix. The unsaturated PB-cores were crosslinked using a commercial photointiator to lock the cylindrical structure. The core-crosslinked cylinders exhibit worm-like morphologies when dissolved in THF or acetone.

Synthesis of Keggin POM nanocomposites. The core-crosslinked PB-P2VP, worm-like or spherical, polymer solution in THF (0.5 wt%) was added to 10 mL of 10^{-2} M Keggin POM (e.g.; $H_4SiMo_{12}O_{40}.6H_2O$) in THF with continuous stirring for 6h. With the addition of polymer solution to Keggin POM solution, coloured precipitates produced. When the basic PB-P2VP polymer solutions were added to the Keggin POM (which is a heteropolyacid) solution, some of the P2VP units are protonated. Thus, in the

case of P2VP strong Coulomb interactions with the Keggin POM anions provide an additional driving force for organic-inorganic composite formation. In this way coloured precipitates were produced by grafting coloured Keggin POMs over the polymer templates. When the neutralization point was reached the colour of the Keggin POM solution had disappeared completely due to the complete grafting of the Keggin POMs over the polymer template. The resultant precipitate aged in the reaction mixture for 12 h. The precipitate was washed 3 times with deionized water and kept for overnight drying at 100^{o}C. The polymer-Keggin POM nanocomposites are referred hereafter as Keggin POM-X (see Table 1 for labels).

Instruments and measurements: Field-emission scanning electron microscopy (FESEM) was performed using a LEO Gemini microscope equipped with a field emission cathode. Transmission electron microscopy (TEM) was performed on a Zeiss CEM 902 microscope at an accelerating voltage of 80 kV. Samples for TEM analysis were prepared by sonicating the samples in ethanol for 2 min followed by depositing one drop on a holey carbon film supported by a copper grid using a Pasteur pipette. Fourier transform infrared (FTIR) spectroscopy data was collected on a Brucker IFS66V using KBr pellets. Before the measurements, samples were heated to 100 ^{o}C for 12 hours and KBr pellets were pressed. Powder X-ray diffraction (PXRD) measurement was performed at 25 °C on a Panalytical XPERT-PRO diffractometer in reflection mode using Cu K_{α} radiation. Nitrogen physisorption was conducted at 77 K on a Quantachrome Autosorb 1 instrument. Prior to the measurements, the samples were degassed at 373 K for 24 h. Ambient-temperature. All calcinations were done step-wise in a tube furnace, first under argon atmosphere with step-wise heating (200 ^{o}C – 5 h, and 375 ^{o}C – 12 h), followed with a second calcination in air with step-wise heating (200 ^{o}C – 2 h, and 300 ^{o}C – 5 h) at 3 ^{o}C min^{-1} heating and cooling rate.

Results and Discussion

Polymer Templates. As outlined in the the introduction, bi- and tri-block-copolymers are meanwhile well established as structure- directing agents for preparing mesostructured organic-inorganic composite materials. With established neutral templates like Pluoronic 123, the final morphology is determined by the cooperative self-organization of the organic template and the molecular inorganic precursor into three-dimensionally structured arrays which is driven by van der Waals-, multipole-multipole-interactions, and hydrogen bonding. The synthesis of Keggin POM nanostructures with pre-designed morphology and composition would be greatly corroborated by the flexibility in reaction conditions offered by stable polymer nanostructures. Unlike dynamic templates like Pluronic 123, rigid templates, as used in this study, are resistant to changes in reaction parameters like pH, temperature, ionic strength, etc. Furthermore, Coulomb interactions between quaternized P2VP chains of the polymer templates and anionic Keggin POMs are the key factors for the robust formation of polymer Keggin POM composites. The rigid, core-crosslinked worm-like and spherical polymer nanostructures were examined by transmission electron microscopy (TEM). Images are shown in Fig. 1. The core-corona structure of the polymer templates are revealed due to the different electron penetrability of the PB core and P2VP corona. In case of the worm-like polymer template, the diameter of the PB core is approximately 40 nm and the P2VP corona extends ca. 35 nm around the PB-core (Fig. 1a). The total diameter of the worm-like polymeric rods is ca. 110 nm. As sonication is necessary for the dissolution of the core-crosslinked PB-P2VP template, worm-like polymer rods may break during this treatment and different lengths are observed. In case of spherical polymer templates (Fig. 1b), the total diameter of the spheres is ca. 30 nm. Fig. 2 shows the FESEM image of worm-like polymer rods at different magnification, where the smooth surface of the polymer cylinders can be observed. Efforts to record FESEM images of core-crosslinked spherical polymer templates were not successful due to the small size and resolution limits of the microscope.

Polymer-Keggin POM nanocomposites. In an earlier report, we have proved the applicability of our

novel approach by grafting $[SiMo_{12}O_{40}]^{4-}$ ions on core-crosslinked PB-P2VP block copolymer nanorods. The resultant Keggin POM nanocomposites showed high surface areas and good dispersion of the Keggin POM over polymer nanorods. Similarly, in this report the polymer-Keggin POM nanocomposites are synthesized by adding the PB-P2VP polymer template solution (worm-like or spherical) to different Keggin POM solutions (e.g., $H_3PMo_{12}O_{40}$), also in THF. When neutral polymer templates (worm-like or spherical) in THF are added to the Keggin POM solution (which is a heteropolyacid) the 2-vinylpyridine units in the template arms will be protonated. The anionic POMs then assemble driven by strong Coulomb interactions between the cationic 2-vinylpyridinium arms. The polymer-Keggin POM nanocomposites are labeled as Keggin POM-X (see Table 1). The polymer-Keggin POM nanocomposites were characterized using field emission scanning electron microscopy (FESEM), transmission electron microscopy (TEM), powder X-ray diffraction (PXRD), N_2 sorption measurements, and Fourier transform infrared (FTIR) measurements.

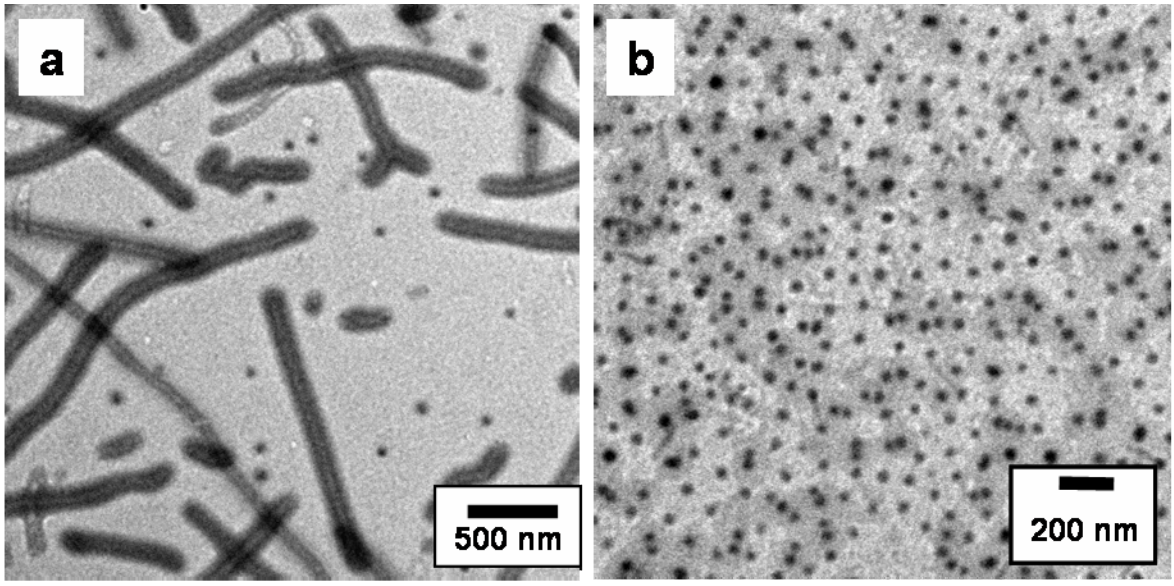

Figure 1. TEM images of the core-crosslinked PB-P2VP worm-like and spherical polymer templates.

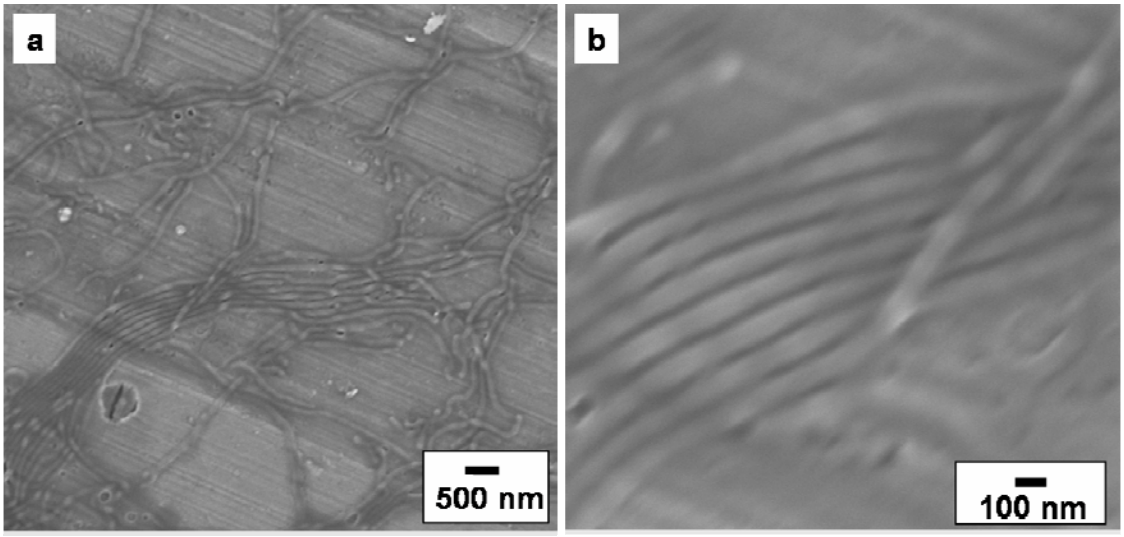

Figure 2. FESEM images of the core-crosslinked PB-P2VP worm-like polymer template at different magnifications.

Worm-like polymer-Keggin POM nanocomposites. Addition of core-crosslinked polymer templates to different metal centered Keggin POMs, as observed before, resulted Keggin POM grafted polymer-Keggin POM nanocomposites. FESEM images of worm-like polymer-Keggin POM nanocomposites, Keggin POM-1, 2, and 3 are shown in Fig. 3 (a, b, and c). In comparison to the pure core-crosslinked polymer nanorods (Fig. 2), the surface of the Keggin POM-1, 2, and 3 is rough (Fig. 3). The surface roughness of the Keggin POM-1, 2, and 3 is due to the grafting of Keggin POM anions around the core-crosslinked polymer template. Please note, that the length of core-crosslinked polymer nanorod templates, as expected, does not influence the composite formation. The Coulomb interactions renders the assembly very robust. When core-crosslinked polymer nanorods are dispersed in THF solution by prolonged stirring instead of sonication the length of the nanorods as observed in the bulk is preserved in the solution. When these very long nanorods were added to Keggin POM solution, Keggin POM composites with a interesting microstructure are obtained. Bundles of these very long rod-like composite structures are textured similar to a filter pad. (see ESI Fig. S1). TEM images of Keggin POM-1 and 2 are shown in Fig. 4 (a and b). The surface roughness of the worm-like polymer template due to the precipitation of Keggin POM anions around the rigid cationic template are also obvious when comparing the TEM images of the pure polymer template (Fig. 1a) with Keggin POM-1 and 2 (Fig. 4 a

and b). HRTEM images (Fig. 4 c and d). of the composites suggest that Keggin POMs are indeed homogenously assembled around the template as would be expected for a composite formation mechanism based on homogeneous Coulomb interactions.

Table 1. Properties of the polymer-Keggin POMs nanocomposites.

Sample	composite composition	surface area[a] (m^2g^{-1})
	commercial Keggin POMs	
$H_4SiMo_{12}O_{40}$.$6H_2O$		4
$H_3PMo_{12}O_{40}$ $6H_2O$		3
$H_3PW_{12}O_{40}$.$6H_2O$		4
	worm-like polymer-Keggin POM composites	
Keggin POM-1	worm-like PB-P2VP + $H_4SiMo_{12}O_{40}$.$6H_2O$	39
Keggin POM-2	worm-like PB-P2VP + $H_3PMo_{12}O_{40}$ $6H_2O$	34
Keggin POM-3	worm-like PB-P2VP + $H_3PW_{12}O_{40}$.$6H_2O$	36
	spherical polymer-Keggin POM composites	
Keggin POM-4	spherical PB-P2VP + $H_4SiMo_{12}O_{40}$.$6H_2O$	49
Keggin POM-5	spherical PB-P2VP + $H_3PMo_{12}O_{40}$ $6H_2O$	58
Keggin POM-6	spherical PB-P2VP + $H_3PW_{12}O_{40}$.$6H_2O$	54

[a] 5 point BET

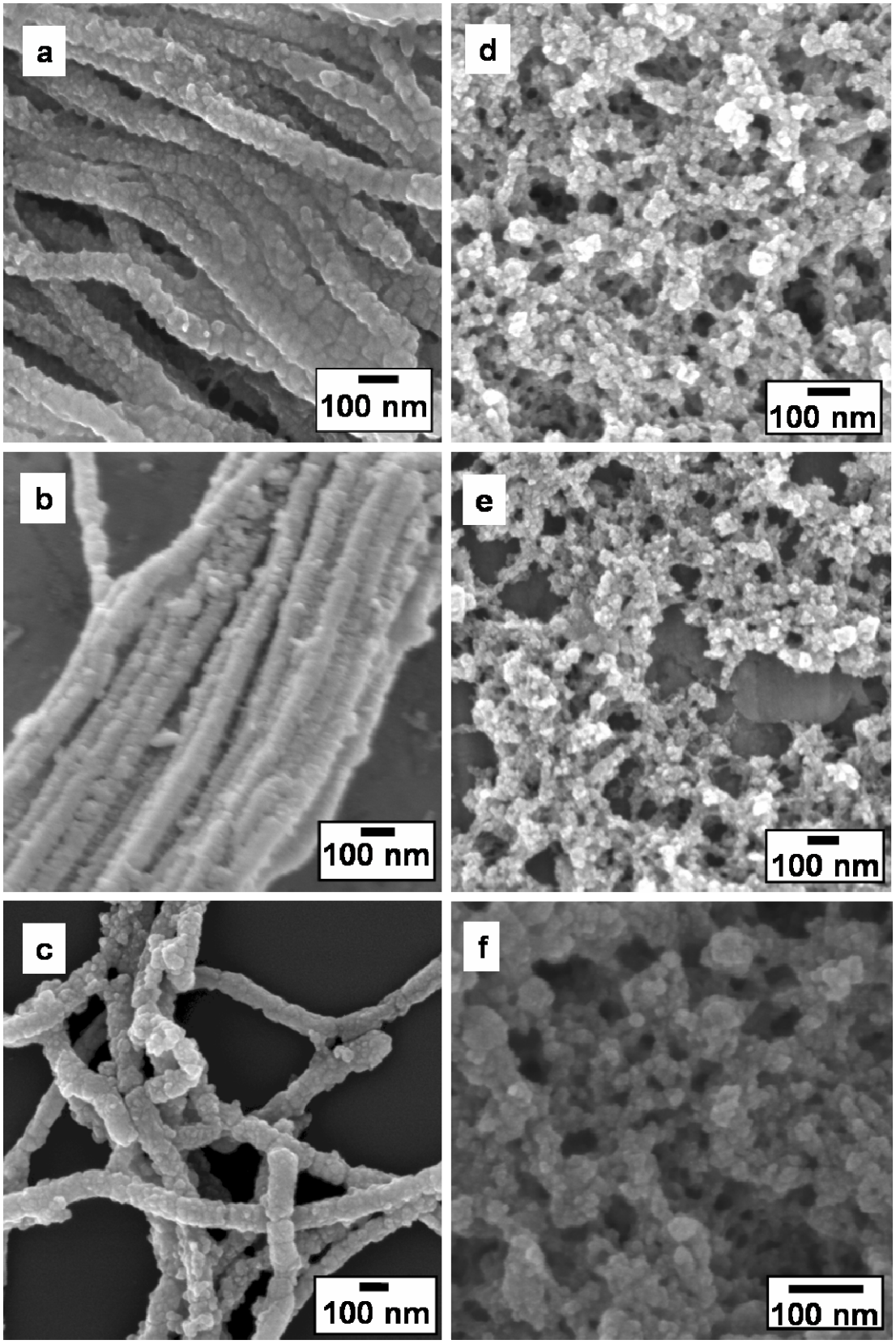

Figure 3. FESEM images of (a) Keggin POM-1, (b) Keggin POM-2, (c) Keggin POM-3, (d) Keggin POM-4, (e) Keggin POM-5, and (f) Keggin POM-6.

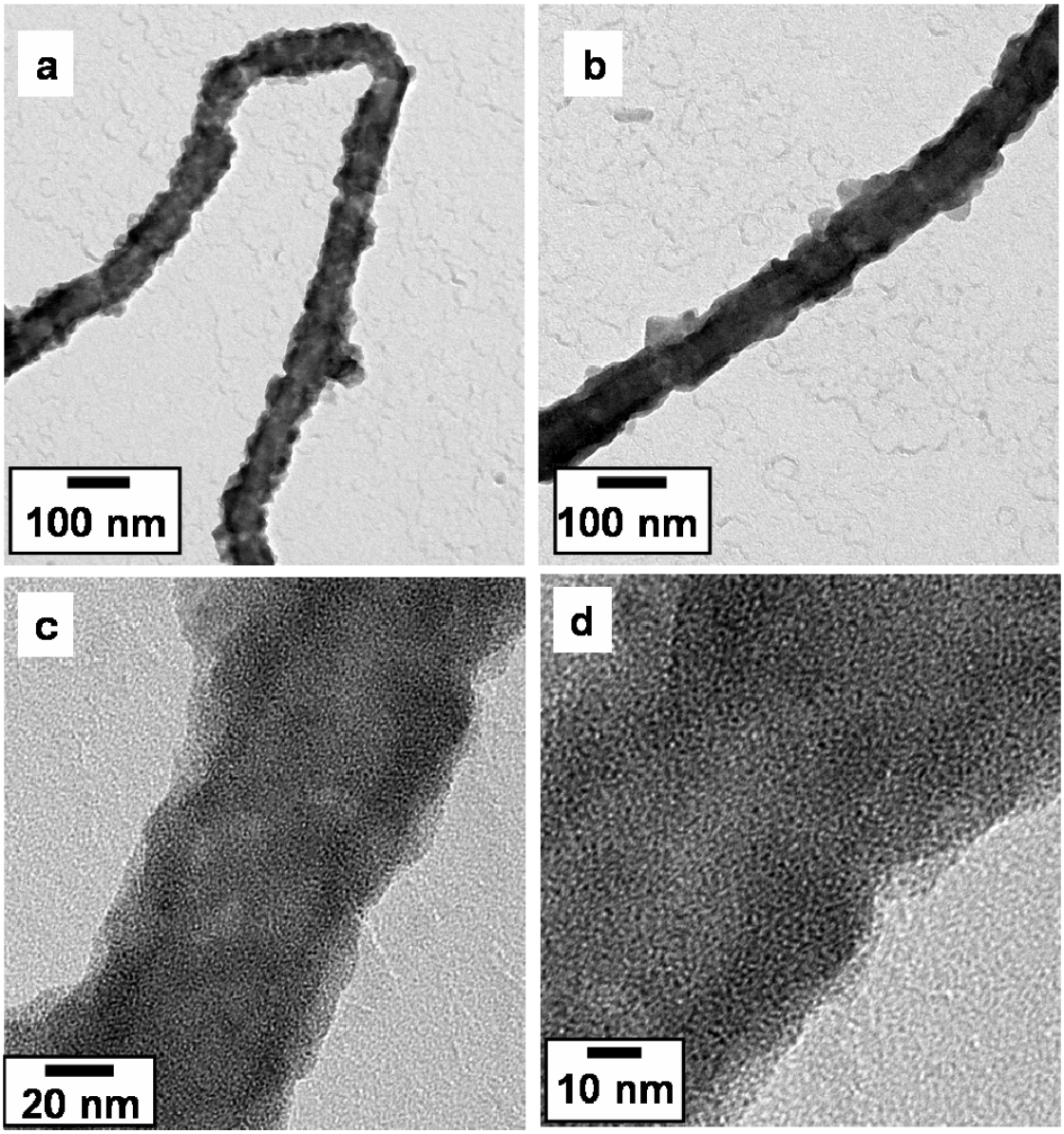

Figure 4. TEM and HRTEM images of the (a and c) Keggin POM-1 and (b and d) Keggin POM-2.

In addition, wide-angle powder XRD patterns of the commercial Keggin POMs and Keggin POM-1, 2, and 3 were recorded (see ESI Fig. S2). In contrast to the commercial Keggin POMs, XRD patterns of Keggin POM-Xs do not show any characteristic peaks for crystalline Keggin POMs, which is also an indication of very high dispersion of Keggin POMs in the polymer matrix. The grafting of Keggin POM anions over polymer templates was further verified by FTIR analysis. FTIR spectra of the commercial Keggin POMs, and Keggin POM-1, 2, and 3 were shown in Fig. 5. It has been widely reported that the Keggin-type POMs show four characteristic bands, which are the fingerprint of the Keggin structure.[12;31] There are four kinds of oxygen atoms in Keggin POMs, e.g.; in $H_4SiMo_{12}O_{40}$.$6H_2O$

these characteristic bands were observed at ν_{as} (Mo-O_d) – 952 cm^{-1}, ν_{as} (Mo-O_b-Mo) – 794 cm^{-1}, ν_{as} (Mo-O_c-Mo) – 864 cm^{-1}, and ν_{as} (Si-O_a) – 902 cm^{-1}. $H_3PMo_{12}O_{40}$.$6H_2O$ exhibits these characteristic bands at ν_{as} (Mo-O_d) – 960 cm^{-1}, ν_{as} (Mo-O_b-Mo) – 870 cm^{-1}, ν_{as} (Mo-O_c-Mo) – 785 cm^{-1}, and ν_{as} (P-O_a) – 1065 cm^{-1} where as $H_3PW_{12}O_{40}$.$6H_2O$ exhibits these characteristic bands at ν_{as} (W-O_d) – 990 cm^{-1}, ν_{as} (W-O_b-W) – 890 cm^{-1}, ν_{as} (W-O_c-W) – 810 cm^{-1}, and ν_{as} (P-O_a) – 1080 cm^{-1}. The FTIR spectrum of the Keggin POM-1, 2, and 3 corresponds well to the superposition of the spectra of the commercial Keggin POMs and PB-P2VP polymer templates, which is an indication that the Keggin structure stayed intact when being grafted around the polymer templates. However, there is a shift observed in the frequencies for Mo-O-Mo, and W-O-W (both corner and edge shared) vibrations, the basal oxygens which are involved in de-protonation reactions of Keggin POMs. Both vibrations shift to higher wave numbers indicating that there is a change in the degree of protonation of the Keggin POMs dispersed in the polymer matrix in comparison to commercial Keggin POMs. The N_2 sorption measurements of Keggin POM-1, 2 and 3 show that the developed Keggin POM nanocomposites exhibit high surface areas. Keggin POM-1, 2, and 3 exhibit 39, 34, and 36 m^2g^{-1} surface areas, respectively where as the commercially available corresponding Keggin POMs only has 4, 3, and 4 m^2g^{-1} surface areas. Approximately 10 times increase in surface areas was observed.

Spherical polymer-Keggin POM nanocomposites. The crosslinking step offers easy control over the template structure. Therefore we are not limited to worm-like structures. To proof the general applicability we also synthesized composites applying spherical templates. The same procedure as for worm-like composites was followed for the synthesis of spherical polymer-Keggin POM nanocomposites. FESEM images of spherical polymer-Keggin POM nanocomposites, Keggin POM-4, 5, and 6, are shown in Fig. 3 (d, e, and f). The results are in accord with worm-like polymer-Keggin POM nanocomposites. TEM images of the spherical polymer-Keggin POM nanocomposites Keggin POM-4, and 5 were shown in Fig. 6. In comparison to the pure core-crosslinked polymer nanospheres (Fig. 1b), the roughness of the surfaces of Keggin POM-4 and 5 clearly indicats the composite

formation by grafting of Keggin POMs over the spherical polymer template (Fig. 6).

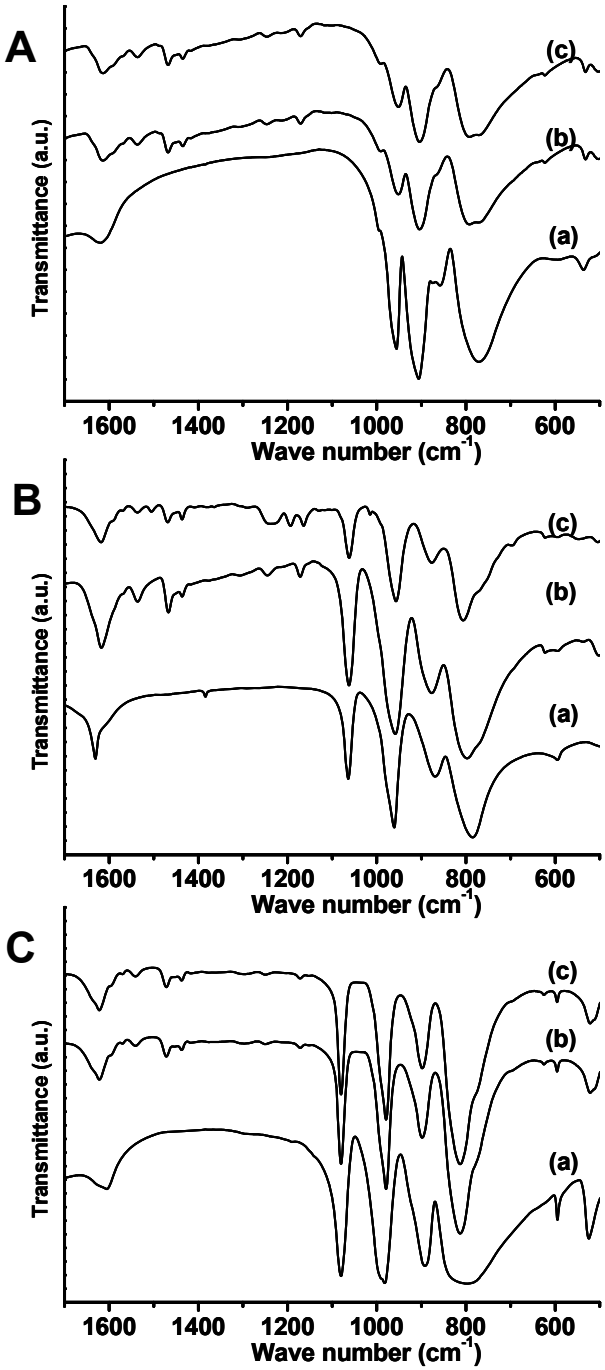

Figure 5. FTIR spectra of the pure Keggin POMs and corresponding polymer-Keggin POM nanocomposites; A: $H_4SiMo_{12}O_{40}$.$6H_2O$ (a), Keggin POM-1 (b), and Keggin POM-4 (c); B: $H_3PMo_{12}O_{40}$.$6H_2O$ (a), Keggin POM-2 (b), and Keggin POM-5 (c); C: $H_3PW_{12}O_{40}$.$6H_2O$ (a), Keggin POM-3 (b), and Keggin POM-6 (c).

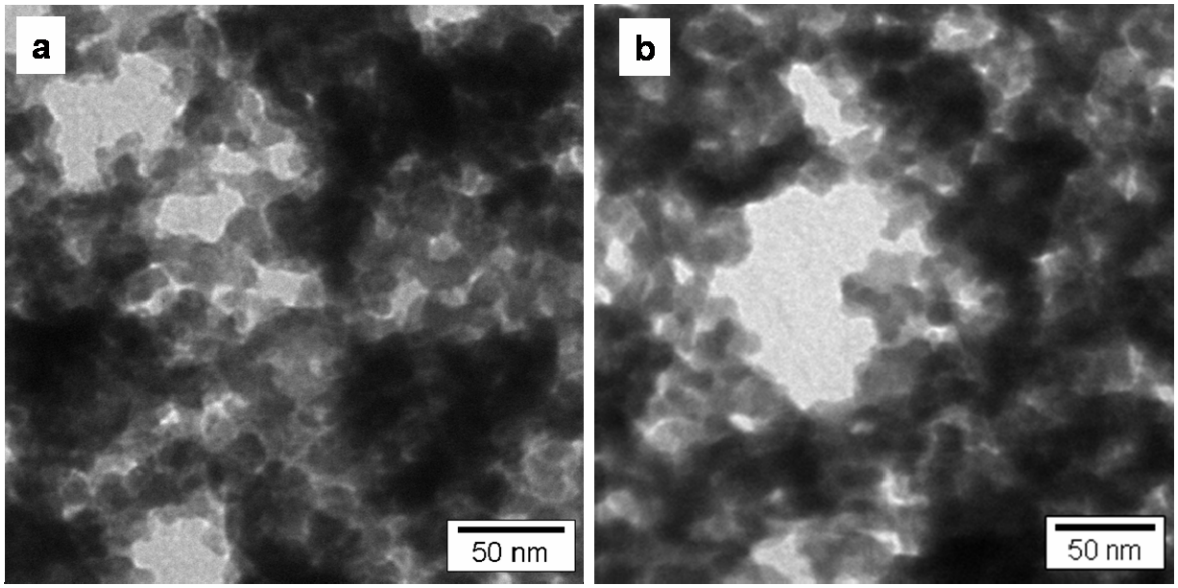

Figure 6. TEM images of the (a) Keggin POM-4 and (b) Keggin POM-5.

In the spherical polymer-Keggin POM nanocomposites the interaction of grafted Keggin POMs leads to a three-dimensional network of spherical composite particles forming mesopores and macropores. The N_2 sorption measurements of Keggin POM-Xs also show that the obtained Keggin POM nanocomposites exhibit high surface areas. Keggin POM-4, 5, and 6 exhibit 49, 58, and 54 m^2g^{-1} surface areas, respectively where as the commercially available corresponding Keggin POMs only have 4, 3, and 4 m^2g^{-1} surface areas. Approximately a 15 times increase in surface areas was observed. In comparison to the worm-like polymer-Keggin POM composites, spherical polymer-Keggin POM nanocomposites exhibit higher surface areas.

Calcination studies

Calcination studies. The acidic and oxidizing properties of Keggin POM have been used in the field of catalysis, in fundamental and applied research.[11;12] Many catalytic reactions are performed at temperatures above 300 °C, where the organic templates are no longer stable. Therefore it would be desirable to convert the composite materials into purely inorganic ones without loosing the morphology. Additionally one would expect an increase of surface area if the rods could be successfully turned into hollow tubes. Hence, the thermal behavior of Keggin POM-2 has been investigated in some detail using IR and PXRD. Above 450 ^oC, the Keggin structure is completely destroyed.[11;12] In general,

decomposition of $H_3PMo_{12}O_{40}$ $6H_2O$ occurs in a wide temperature range, leading to mixtures of α- and β-MoO_3. As mentioned earlier, core-crosslinked PB-P2VP was used for grafting Keggin POM which has hydrophilic P2VP block and sp^2 hybridized carbon containing hydrophobic PB blocks. When subsequently heat treated under an inert environment the sp^2 carbon containing PB block of the composites convert to amorphous carbon material. Such in-situ carbon has been shown to act as a rigid support for titania walls. Subsequently, the carbon support could be removed without collapse of the mesostructure. Following this strategy, Keggin POM-2 was calcined in two steps in a tube furnace in order to remove the template: Calcinations at 375 ^oC for 12 h in argon was followed by at calcinations at 300 ^oC for 5 h in air to remove the carbon formed in situ during the first step. It is worth noting that when first heat-treated under argon the characteristic 'fingerprint-like' band structure is lost, see Figure 7 c. During pyrolysis under argon some of the Mo(VI) centers apparently are reduced, resulting in the disappearances of the ν_{as} (Mo-O_b-Mo), and ν_{as} (Mo-O_c-Mo) vibrations. However, the final heat-treatment in air not only removes the carbon but it also re-oxidizes Mo to Mo(VI) centers and the characteristic 'fingerprint-like' band-structure of the Keggin POM is fully restored. (Fig. 7d).

PXRD patterns did not show any characteristic crystalline peaks indicating that the material is still amorphous (see ESI Fig. S3) after the heat treatment. FESEM images of argon calcined samples still show the rod-like morphology (Fig. 8a). Upon further calcinations in air FESEM images show that long rod-like structures were broken down into smaller but still rod-like morphologies. Unfortunately, the N_2 sorption measurements of calcined Keggin POM-2 show that the surface area is decreased to 27 m^2g^{-1}, and 22 m^2g^{-1} for argon and air calcined samples, respectively whereas the corresponding Keggin POM-2 has 34 m^2g^{-1} surface area. At the present stage, our attempts to increase the surface areas by removal of the polymer template were unsuccessful. But it might be possible by sonicating or grinding the argon calcined samples. An investigation of this aspect is ongoing. Additionally, the removal of the phosphorous from the herteropolyacids by gentle annealing in vacuum followed by a crystallization of the amorphous molybdenum oxide walls into stable and metastable phases MO_3 will be investigated.

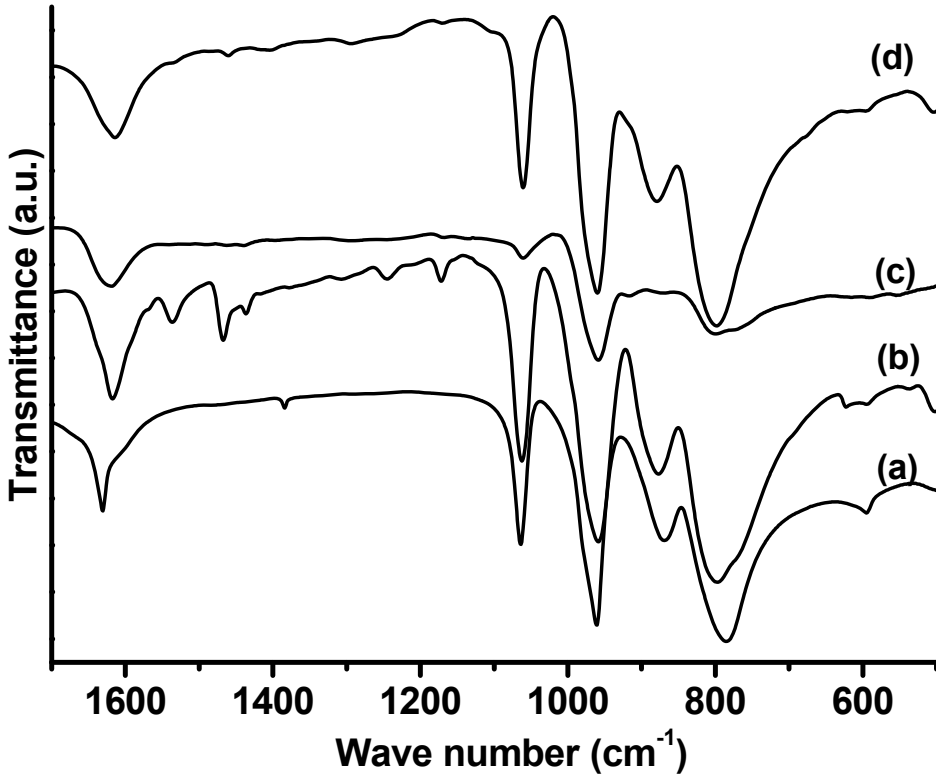

Figure 7. FTIR spectra of the (a) commercial $H_3PMo_{12}O_{40}$ $.6H_2O$, (b) Keggin POM-2, (c) corresponding argon calcined at 375 ^oC for 12 h, and (d) argon calcined and then air calcined at 300 ^oC for 5 h samples.

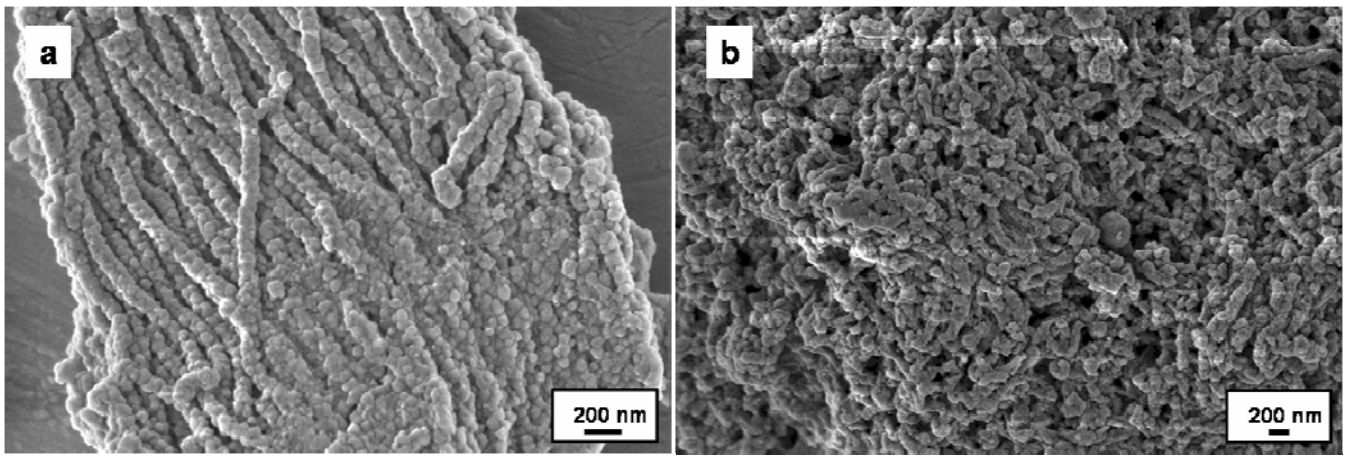

Figure 8. FESEM images of the (a) argon calcined POM-2 at 375 ^oC for 12 h, and (b) argon calcined and then air calcined POM-2 air calcined at 300 ^oC for 5 h.

Summary

In conclusion, we presented a new approach for the synthesis of high surface area Keggin-type polyoxometalates by grafting Keggin-type heteropolyoxometalates around the protonated, core-crosslinked PB-P2VP worm-like/spherical polymer templates. Composite formation is extremely robust because it is driven by Coulomb interactions between template and inorganic precursor. Our approach allows easy control over the synthesis and morphology of Keggin POM nanocomposites.

The produced polymer-Keggin POM nanocomposites exhibit high dispersion, greatly improved surface areas and are thus expected to be useful in catalytic and electrochemical related applications. To the best of our knowledge, we report the highest surface areas achieved for polymer-Keggin POM nanocomposites up to date.

Acknowledgement: This project is supported by Elite Network Bavaria (ENB). R. S. Y. and A. W. would like to acknowledge Elite Network Bavaria for a fellowship.

Reference List

(1) Hoffmann, F.; Cornelius, M.; Morell, J.; Fröba, M. *Angew.Chem.Int.Ed.* **2006**, *45*, 3216-3251.

(2) Ulrich, R.; Zwanziger, J. W.; De Paul, S. M.; Reiche, A.; Leuninger, H.; Spiess, H. W.; Wiesner, U. *Adv.Mater.* **2002**, *14*, 1134-1137.

(3) Huang, Z.; Bensch, W.; Sigle, W.; van Aken, P. A.; Kienle, L.; Vitoya, T.; Modrow, H.; Ressler, T. *J.Mater.Sci.* **2008**, *43*, 244-253.

(4) Forster, S. *Colloid Chemistry 1* **2003**, *226*, 1-28.

(5) Finnefrock, A. C.; Ulrich, R.; Du Chesne, A.; Honeker, C. C.; Schumacher, K.; Unger, K. K.; Gruner, S. M.; Wiesner, U. *Angew.Chem.Int.Ed.* **2001**, *40*, 1207.

(6) Schuth, F. *Angew.Chem.Int.Ed.* **2003**, *42*, 3604-3622.

(7) Davis, S. A.; Breulmann, M.; Rhodes, K. H.; Zhang, B.; Mann, S. *Chem.Mater.* **2001**, *13*, 3218-3226.

(8) Yelamanchili, R. S.; Walther, A.; Muller, A. H. E.; Breu, J. *Chem.Commun.* **2008**, 489-491.

(9) Walther, A.; Goldmann, A. S.; Yelamanchili, R. S.; Drechsler, M.; Schmalz, H.; Eisenberg, A.; Muller, A. H. E. *Macromolecules* **2008**, *41*, 3254-3260.

(10) M.T.Pope and A.Müller *Polyoxometalate Chemistry From Topology via Self-Assembly to Applications*; Kluwer Academic Publishers: Netherlands, 2001.

(11) J.B.Moffat *in Metal-Oxygen Clusters - The Surface and Catalytic Properties of Heteropoly Oxometalates*; Kluwer Academic / Plenum Publishers: New York, 2001.

(12) Rocchicciolideltcheff, C.; Aouissi, A.; Bettahar, M.; Launay, S.; Fournier, M. *Journal of Catalysis* **1996**, *164*, 16-27.

(13) Okamoto, K.; Uchida, S.; Ito, T.; Mizuno, N. *Journal of the American Chemical Society* **2007**, *129*, 7378-7384.

(14) Nomiya, K.; Murasaki, H.; Miwa, M. *Polyhedron* **1986**, *5*, 1031-1033.

(15) Katsoulis, D. E. *Chemical Reviews* **1998**, *98*, 359-387.

(16) Blasco, T.; Corma, A.; Martinez, A.; Martinez-Escolano, P. *Journal of Catalysis* **1998**, *177*, 306-313.

(17) Kresge, C. T.; Leonowicz, M. E.; Roth, W. J.; Vartuli, J. C.; Beck, J. S. *Nature* **1992**, *359*, 710-712.

(18) Shi, C. F.; Wang, R. W.; Zhu, G. S.; Qiu, S. L.; Long, J. *European Journal of Inorganic Chemistry* **2005**, 4801-4807.

(19) Yang, L.; Qi, Y. T.; Yuan, X. D.; Shen, H.; Kim, J. *Journal of Molecular Catalysis A-Chemical* **2005**, *229*, 199-205.

(20) Yu, S. Y.; Wang, L. P.; Chen, B.; Gu, Y. Y.; Li, J.; Ding, H. M.; Shan, Y. K. *Chemistry-A European Journal* **2005**, *11*, 3894-3898.

(21) Zhao, D. Y.; Feng, J. L.; Huo, Q. S.; Melosh, N.; Fredrickson, G. H.; Chmelka, B. F.; Stucky, G. D. *Science* **1998**, *279*, 548-552.

(22) Zhao, D. Y.; Huo, Q. S.; Feng, J. L.; Chmelka, B. F.; Stucky, G. D. *Journal of the American Chemical Society* **1998**, *120*, 6024-6036.

(23) Rao, P. M.; Wolfson, A.; Kababya, S.; Vega, S.; Landau, M. V. *Journal of Catalysis* **2005**, *232*, 210-225.

(24) Taguchi, A.; Abe, T.; Iwamoto, M. *Adv.Mater.* **1998**, *10*, 667-669.

(25) Stein, A.; Fendorf, M.; Jarvie, T. P.; Mueller, K. T.; Benesi, A. J.; Mallouk, T. E. *Chemistry of Materials* **1995**, *7*, 304-313.

(26) Janauer, G. G.; Dobley, A.; Guo, J. D.; Zavalij, P.; Whittingham, M. S. *Chemistry of Materials* **1996**, *8*, 2096-2101.

(27) Yun, H. S.; Kuwabara, M.; Zhou, H. S.; Honma, I. *Thin Solid Films* **2007**, *515*, 2842-2846.

(28) Zhang, R. F.; Yang, C. *Journal of Materials Chemistry* **2008**, *18*, 2691-2703.

(29) Maayan, G.; Popovitz-Biro, R.; Neumann, R. *Journal of the American Chemical Society* **2006**, *128*, 4968-4969.

(30) O'Reilly, R. K.; Hawker, C. J.; Wooley, K. L. *Chemical Society Reviews* **2006**, *35*, 1068-1083.

(31) Rocchiccioliideltcheff, C.; Fournier, M.; Franck, R.; Thouvenot, R. *Inorganic Chemistry* **1983**, *22*, 207-216.

Electronic Supplementary Information (ESI)

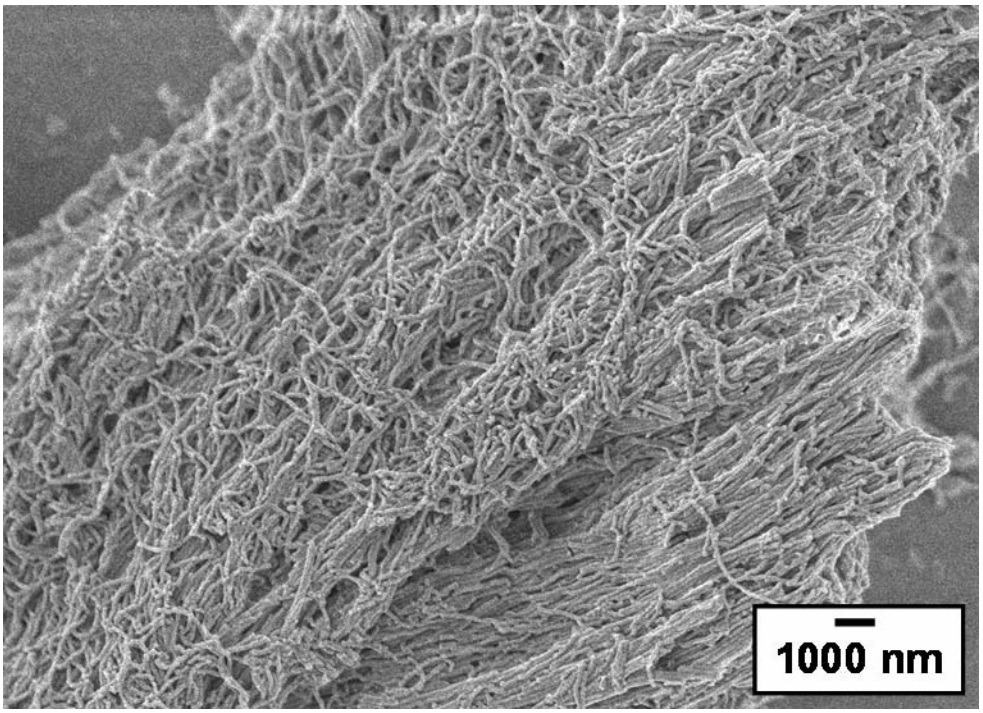

Figure S1. FESEM images of Keggin POM-2 using core-crosslinked long polymer templates.

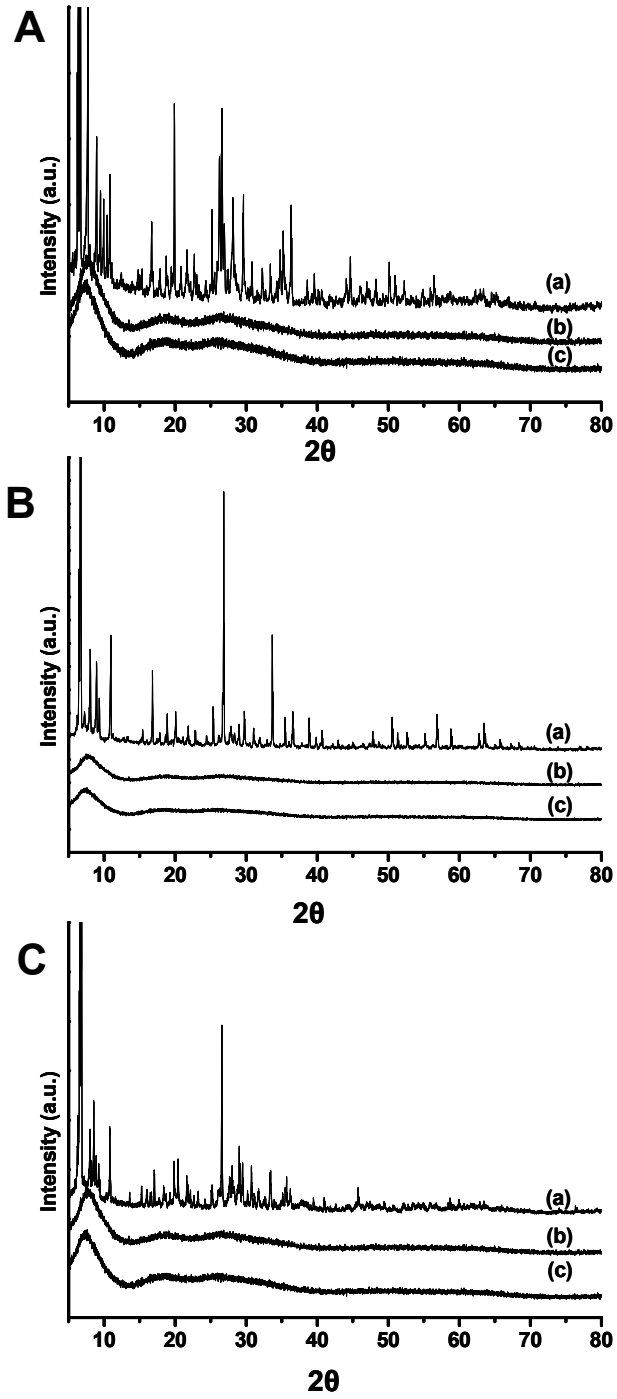

Figure S2. Powder X-ray diffraction patterns of (A): (a) $H_4SiMo_{12}O_{40}$.$6H_2O$, (b) Keggin POM-1, and (c) Keggin POM-4; (B): (a) $H_3PMo_{12}O_{40}$ $6H_2O$, (b) Keggin POM-2, and (c) Keggin POM-5; and (C): (a) $H_3PW_{12}O_{40}$.$6H_2O$, (b) Keggin POM-3, and (c) Keggin POM-6.

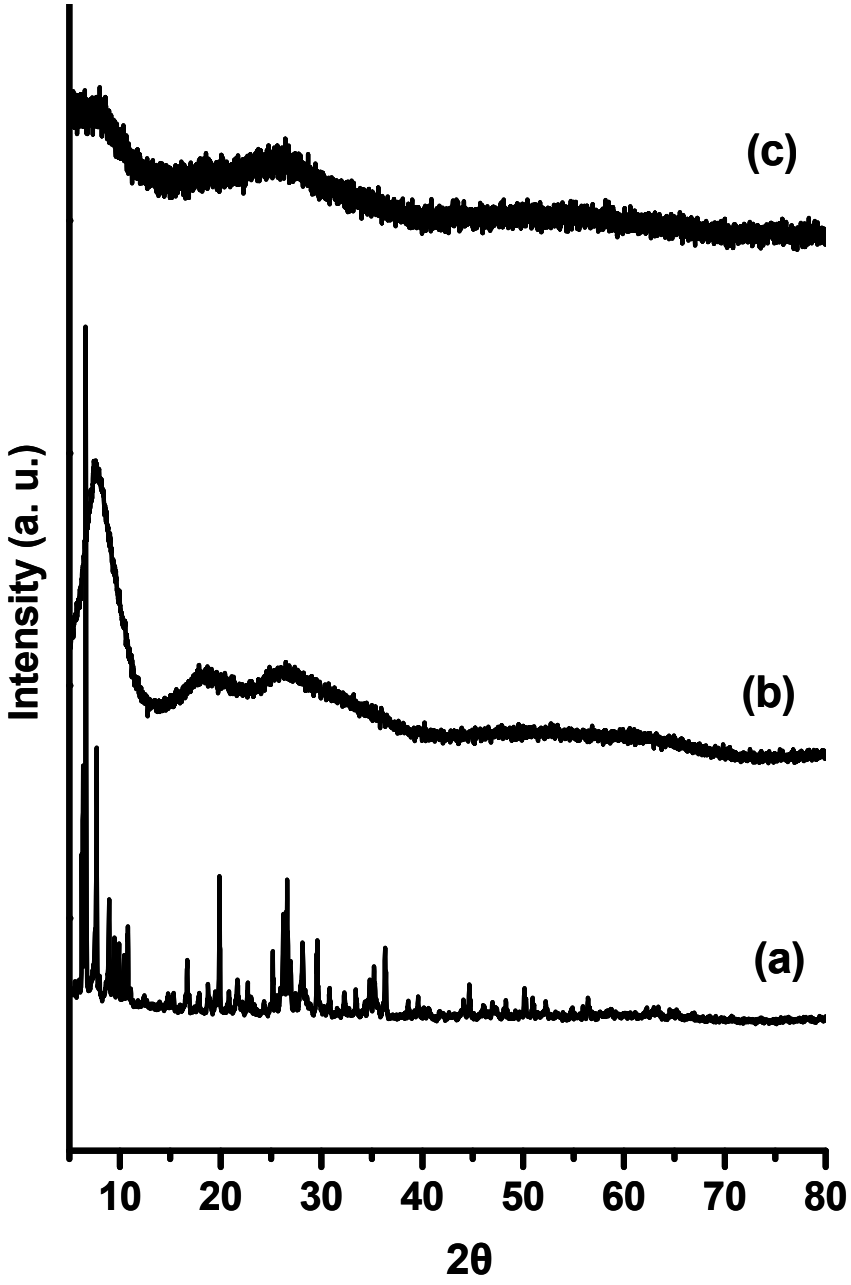

Figure S3. Powder X-ray diffraction patterns of (a) $H_3PMo_{12}O_{40}$ $6H_2O$, (b) Keggin POM-2, and (c) argon calcined Keggin POM-2.

A 3 Hexagonally ordered mesoporous Keggin-type polyoxometalates

This work with the title "**Hexagonally Ordered Mesoporous Keggin-type Polyoxometalates**" by Yelamanchili, R. S., Kamperman, M., Kiya, Y., Lee, Abruna, H. D., J., Breu, J., Wiesner, U., is to be submitted to *Nature Mater.*.

Hexagonally Ordered Mesoporous Keggin-type Polyoxometalates**

Ram Sai Yelamanchili,[a] Marleen Kamperman,[b] Yasuyuki Kiya,[c] Jinwoo Lee,[b]

Héctor D. Abruña,[c] Josef Breu[a] and Ulrich Wiesner*[b]*

[a]Department of Inorganic Chemistry I, University of Bayreuth, 95447 Bayreuth, Germany, [b]Department of Materials Science and Engineering and [c]Department of Chemistry and Chemical Biology, Cornell University, Ithaca, New York 14853

*To whom correspondence should be addressed (ubw1@cornell.edu and josef.breu@uni-bayreuth.de)

Keywords: block copolymers · mesoporous materials · organic-inorganic hybrid composites · polyoxometalates

[**] This project was supported by Elite Network Bavaria (ENB) and the NSF through a single investigator award (DMR-0605856). R. S. Y. would like to acknowledge Elite Network Bavaria for a fellowship.

Introduction

The ability of organic materials to self-assemble into a variety of nanostructures with well-defined shape and size has resulted in their role as structure directing agents (SDA) or templates in the discovery of fascinating organic-inorganic hybrid materials[1-3]. An important class of organic SDAs or templates used for the synthesis of hybrid and/or porous materials is the class of amphiphilic block copolymers[3-4]. Combined principles of self-assembly, polymer, colloidal, and inorganic chemistries were used to synthesize materials with unknown functionalities and properties[5-9]. On the other side, Keggin-type polyoxometalates (Keggin POM), discrete clusters with frameworks built mainly from transition metal oxo anions, exhibit unique properties leading to applications in fields such as catalysis, electrochemistry, and host-guest chemistry[10-14]. For instance, Keggin-type vanado-molybdo-phosphates have been extensively studied as active catalysts for the selective oxidation of several alkanes, aldehydes and acids[15-16].

Up until today, however, the relatively small surface areas of Keggin POMs (3 m^2g^{-1} for commercial $H_3PMo_{12}O_{40}$) hinders accessibility to the active sites and limits their applications[10]. High surface area mesoporous Keggin POMs are expected to be useful in a variety of applications such as high performance acid and redox catalysis, sensor devices and electrodes, due to their high ion conductivity, electron density, and rapid and reversible oxidative-reductive processes[12-14].

Since the discovery of mesoporous silica MCM-41[7], and SBA-15[8], these high surface area solids were used for the dispersion and/or encapsulation of Keggin POMs[17-19]. Even though the accessible surface area for Keggin POMs can be increased by these methods, limitations result from low Keggin POM loading, leaching of the active sites

into the reaction medium and pore blocking in porous supports[10]. Furthermore, attempts have been made to prepare mesostructured pure Keggin POM hybrid materials enroute to high surface area porous materials. Stein and co-workers have synthesized layered materials consisting of $H_2W_{12}O_{40}$[5]. Whittingham and co-workers have reported a similar material[6]. On the other hand, Ichinose and coworkers have described composite materials with a layered array of polyanions[20]. Iwamoto and co-workers prepared hexagonally mesostructured arrays of heteropolyanion composites[21]. Another approach involves the synthesis of POM nanocomposites using organic surfactants or polymers[22]. However, the accessible surface area for these composite materials is lower than that of the pure POM[5]. To allow free access to the Keggin POM active sites the organic templates need to be removed, but until now template removal resulted in collapse of the hybrid structures[21,5]. Neumann and co-workers used polymeric micelles to synthesize Keggin POM nanoparticles and observed improved catalytic activities[23]. Earlier, some of us have reported discrete polymer-Keggin POM worm-like nanostructures by grafting Keggin POMs on core-crosslinked block copolymers[24]. All together, these results show the general applicability of the use of organic materials (surfactants, and block copolymers) as SDAs and/or templates for the synthesis of mesostructured materials with polyanions such as Keggin ions. However, until now high surface area mesoporous materials with hexagonally ordered and uniform pores from Keggin ion frameworks have not been reported.

Here we describe the synthesis of hexagonally ordered mesoporous Keggin POM using amphiphilic diblock copolymers as structure directing agents. Scheme 1 summarizes the approach. Keggin POM itself is used as inorganic precursor. Because of

the small size of the Keggin cluster below 2 nm[5,10] it is not expected to perturb the polymer chain conformations much thus favouring molecular mixing with the hydrophilic block of the block copolymer[25]. Poly(isoprene-*block*-dimethylamino ethylmethacrylate) (PI-*b*-PDMAEMA) and poly(isoprene-*block*-ethylene oxide) (PI-*b*-PEO) were used as structure directing agents with hydrophilic PDMAEMA or PEO blocks and sp^2 hybridized carbon containing hydrophobic PI blocks[26] while the PEO block carries no ionizable groups, some of the amine units in the PDMAEMA block are protonated when solutions of this polymer are added to a Keggin POM (which is a heteropolyacid) solution. Thus, in the case of PDMAEMA the effect of Coulomb interactions with the Keggin POM anions can be studied as an additional driving force for organic-inorganic composite formation. When subsequently heat treated under an inert environment, the sp^2 hybridized carbon containing PI blocks of the composites convert to amorphous carbon material. This in-situ carbon acts as a rigid support to mesostructured Keggin POM walls and prevents structure collapse during heat treatment[27]. As we will show, at the same time some of the Mo(VI) centers of the Keggin POM are reduced. Final calcinations in air remove the in-situ formed carbon and re-oxidize the Mo(VI) centers of the Keggin POM, resulting in mesoporous materials with intact Keggin POM structures.

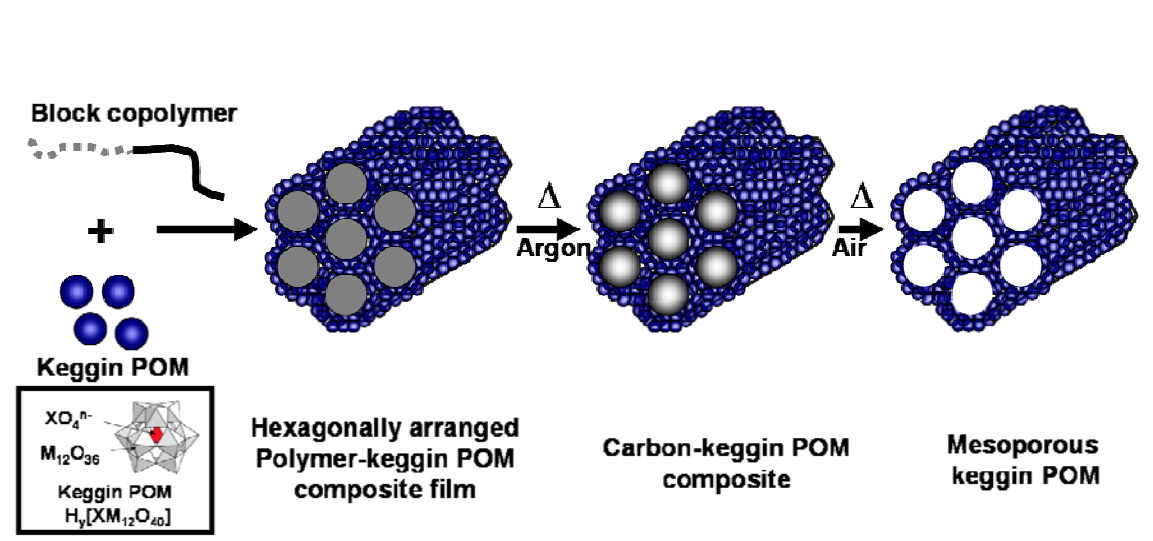

Scheme 1. Synthesis of mesoporous materials with Keggin POM framework using an amphiphilic diblock copolymer and $H_3[PMo_{12}O_{40}]$.

Well-defined PI-*b*-PDMAEMA and PI-*b*-PEO block copolymers with 33 wt% PDMAEMA and a molecular weight of 3.0×10^4 g mol^{-1} and 23 wt% PEO and a molecular weight of 1.6×10^4 g mol^{-1}, respectively, were synthesized by anionic polymerization (see experimental section). PI-*b*-PDMAEMA or PI-*b*-PEO and Keggin POM were separately dissolved in THF. The polymer solution was added slowly to the Keggin POM solution under stirring at room temperature. Volatiles were evaporated after casting the block copolymer/Keggin POM solutions into dishes in air at 50 °C resulting in amorphous hybrid films of 0.5-1 mm thickness. Films were prepared with seven different PI-*b*-PDMAEMA : Keggin POM and four different PI-b-PEO : Keggin POM weight ratios (1:0.5, 1:1, 1:1.5, 1:2, 1:3, 1:4, and 1:7 and 1:1, 1:1.5, 1:2 and 1:3, respectively).

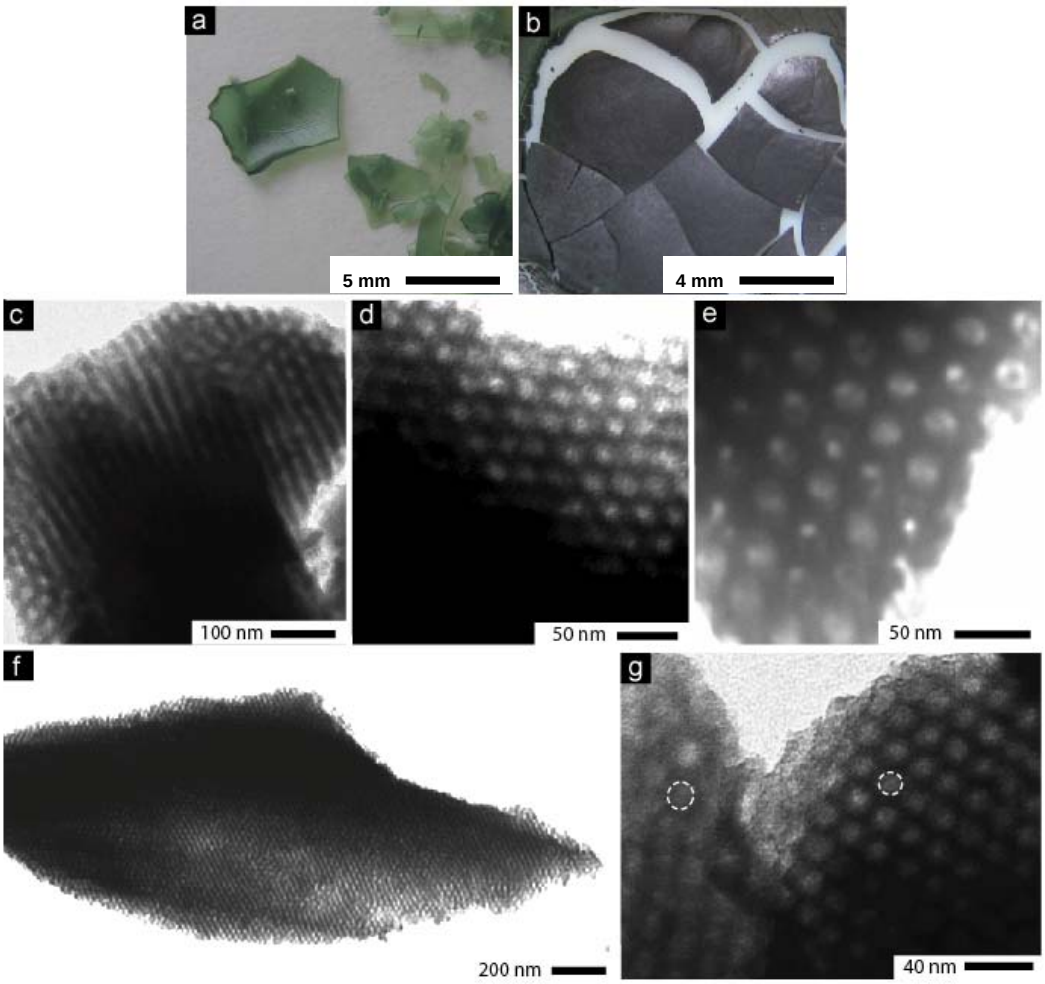

Figure 1. Materials characterization by photography and electron microscopy. Photographs of polymer-Keggin POM composite films prepared from PI-*b*-PDMAEMA and $H_3[PMo_{12}O_{40}]$ with different PI-*b*-PDMAEMA to Keggin POM loadings: **a,** 1: 0.5 and **b,** 1: 4. TEM images of as-made and heat-treated 1:4 PI-b-PDMAEMA/ Keggin POM composite materials: **c,** as-made material with PI appearing as bright cylinders in a PDMAEMA/ Keggin POM matrix (dark); **d,** argon calcined material; **e-g,** air calcined mesoporous Keggin POM materials at different magnifications. Dotted lines in **g** indicate mesopores of different sizes.

Figure 1a and b show representative images of films obtained from 1:0.5 and 1:4 weight ratios for the PI-*b*-PDMAEMA based composites (see ESI Figure S1 for images of the other compositions). At low Keggin POM content films were transparent with green colour. As the Keggin POM content increased films showed a dark blue colour. In general, the molybdenum compound turns blue in air because of both its partial reduction and hydrolysis to form the so-called molybdenum blues[10-11]. For all weight ratios films were homogeneous and did not show any signs of macrophase separation. The Keggin POM anions selectively swell the hydrophilic block of the block copolymers. The resulting polymer-Keggin POM composite films were calcined in two consecutive steps. Heating under argon atmosphere to 375 °C removed all organic components and converted the PI block into amorphous carbon. Additionally, some of the Mo(VI) centers become reduced. Subsequent heating in air to 300-350 °C oxidized this carbon away and re-oxidized all Mo to Mo(VI) again resulting in the final materials. Our preparation method could be referred to as a one-pot synthesis, as all the processing steps can be carried out in a single container from mixing the precursors, casting the films to the final calcined products.

As-made and calcined materials were characterized using combinations of small angle X-ray scattering (SAXS), powder X-ray diffraction (PXRD), transmission electron microscopy (TEM), Fourier transform infrared (FTIR) spectroscopy, Raman spectroscopy and N_2 sorption measurements. Here, we focus mostly on the discussion of materials with organic to inorganic reactant mass ratios of 1:3 – 1:4. Figure 2 shows small angle (a, b) and wide angle powder (c) X-ray scattering (SAXS and WAXS) traces of as-synthesized Keggin POM polymer hybrids and calcined materials.

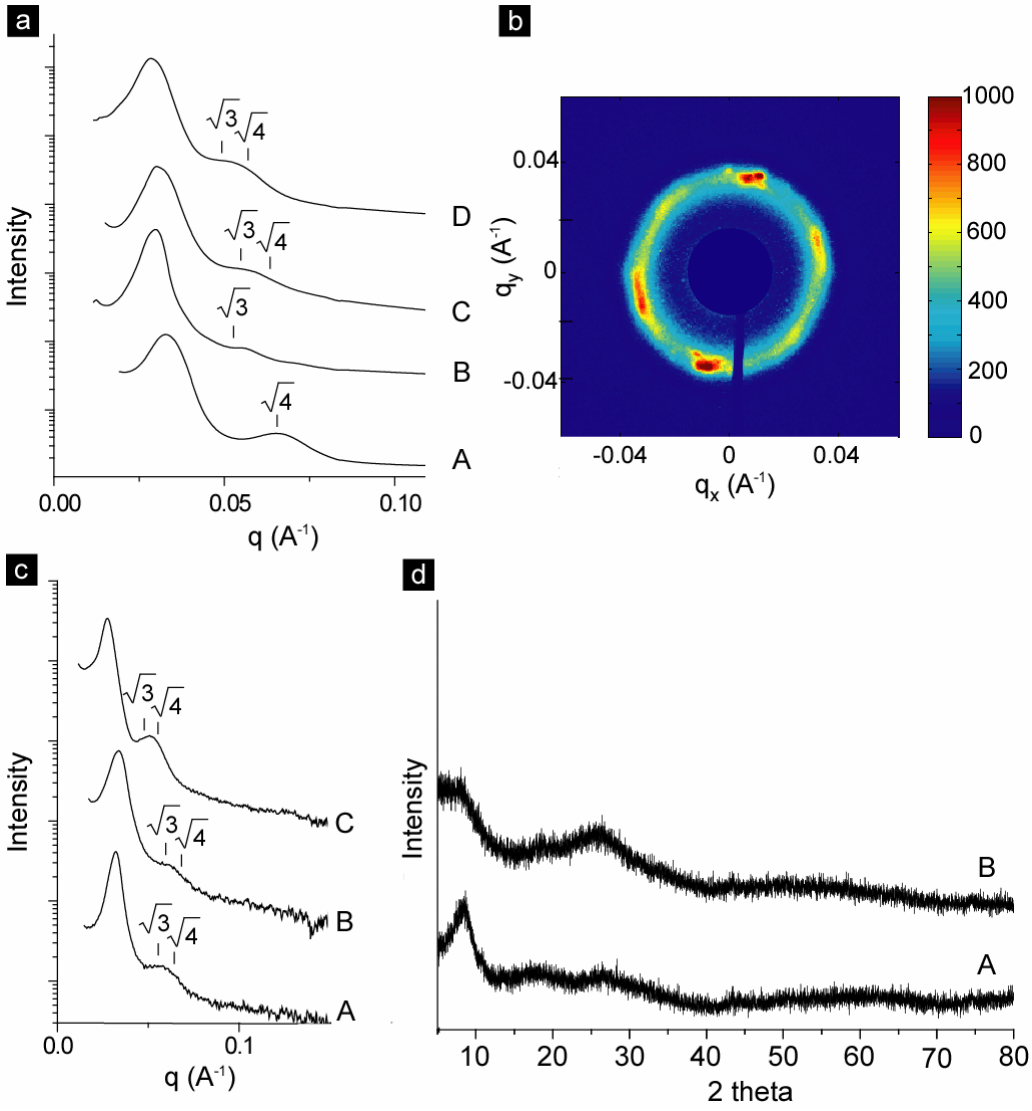

Figure 2. Materials characterization by X-ray scattering. a, SAXS patterns of as-made PI-*b*-PEO/ Keggin POM 1:3 composite (A) and as-made PI-*b*-PDMAEMA/ Keggin POM 1:4 composites (B-D). **b,** 2-D SAXS pattern of air-calcined mesoporous Keggin POM material obtained from PI-*b*-PDMAEMA/ Keggin POM 1:4 composite. **c,** SAXS patterns of argon calcined (A) and air calcined (B, C) mesoporous Keggin POM materials obtained from PI-*b*-PDMAEMA/ Keggin POM 1:4 composite. **d**, Wide angle PXRD patterns of as-made PI-*b*-PDMAEMA/ Keggin POM 1:4 composite (A) and air-calcined mesoporous Keggin POM material (B).

A representative SAXS trace of PI-*b*-PEO derived as-made organic-inorganic hybrids with 1:3 weight ratio is depicted in Figure 2a(A). It exhibits a first order maximum with corresponding *d*-spacing of 19.2 nm and at least one higher order reflection at angular position of $\sqrt{4}$ of the first-order maximum, consistent with a lamellar structure. SAXS traces of three PI-*b*-PDMAEMA derived as-made hybrids with 1:4 weight ratio, Figure 2aB, C and D, show first-order peaks with corresponding *d*-spacing of 20.7, 19.9 and 22.1 nm, respectively, and at least two higher order reflections at angular position of $\sqrt{3}$ and $\sqrt{4}$ of the first-order maximum, consistent with PI cylinders packed in a hexagonal lattice. As is evident from these traces there is a noticeable variation in *d*-spacing between samples prepared with essentially identical Keggin POM/ PI-b-PDMAEMA block copolymer weight ratios under the same experimental conditions as well as between different measurements on the same sample (see below). These variations may be due to strong cluster formation between oppositely charged block copolymer chains and the Keggin POM structures in solution. Upon film casting the mobility of the clusters is obviously high enough to form structures with long-range order. But due to the relatively strong Coulomb interactions the distribution of cluster sizes may lead to variations in domain thickness in the bulk.

TEM studies corroborated structure assignments from SAXS experiments. Figure 1C shows a representative image of a 1:4 PDMAEMA/ Keggin POM composite with hexagonal mesostructure. As-made Keggin POM polymer hybrids did not show any peaks in PXRD patterns characteristic for the parent crystalline Keggin POM suggesting that the Keggin POM is well dispersed in the polymer matrix (see Figure 2dA).

Table 1. Wave number values (cm^{-1}) and assignment of FTIR bands of the Keggin POM composites and mesoporous materials

sample	ν_{as} (P-O_a)	ν_{as} (Mo-O_b-Mo)	ν_{as} (Mo-O_c-Mo)	ν_{as} (Mo-O_d)
commercial Keggin POM ($H_3PMo_{12}O_{40}$)	1064	869	785	961
polymer-Keggin POM composite	1060	878	794	956
air calcined mesoporous Keggin POM	1061	874	799	960

Figure 3a shows representative FTIR spectra of (A) the parent Keggin POM ($H_3PMo_{12}O_{40}$) and (B) 1:4 PI-*b*-PDMAEMA-Keggin POM hybrid material. Keggin POMs generally show four characteristic bands, which is a fingerprint of the Keggin structure[10,28]. There are four kinds of oxygen atoms in $H_3PMo_{12}O_{40}$ (O_a – oxygen in PO_4 tetrahedra, O_d – terminal oxygen atom to Mo, O_b – corner sharing oxygen and O_c – edge sharing oxygen) giving rise to characteristic bands at ν_{as} (Mo-O_d) – 963 cm^{-1}, ν_{as} (Mo-O_b-Mo) – 870 cm^{-1}, ν_{as} (Mo-O_c-Mo) – 785 cm^{-1}, and ν_{as} (P-O_a) – 1067 cm^{-1}, in agreement with what was observed for the commercial Keggin POM (Figure 3a(A)). The FTIR spectrum of the as-made PI-*b*-PDMAEMA-Keggin POM hybrid (Figure 3a(B)) corresponds well with an overlay of the spectra of PI-*b*-PDMAEMA and commercial Keggin POM, suggesting that the Keggin structure stayed intact upon composite formation. A summary of the peak positions of the various materials is given in Table 1. The observed shift in wavenumber for both of the Mo-O-Mo vibrations is likely due to a change in the environment of the Keggin POM anions dispersed in the polymer matrix in comparison to the commercial Keggin POM.

Table 2. Properties of mesoporous Keggin POM materials

sample	surface area[a] (m^2g^{-1})	pore size[b] (nm)
commercial non-porous Keggin POM	3.0	3.7
argon calcined mesoporous Keggin POM	27.0	9.5
air calcined mesoporous Keggin POM	30.0	12.2

[a] 5 point BET [b] BJH desorption branch

The as-made films were subsequently heat treated under argon in a tube furnace to 375 °C in several stages. During this process, the hydrophilic block is burnt off and the Keggin POM is thought to sinter into wall material. At the same time, part of the PI is converted to an amorphous carbon that lines the Keggin POM walls of the resulting cylindrical pores in analogy to what has recently been observed for transition metal oxides based composites[27]. Structural characterization of samples heat-treated under argon suggested that the nanostructure was preserved. Diffractograms of heat-treated 1:4 PI-*b*-PDMAEMA/ Keggin POM composites (Figure 2cA) show a first-order peak with corresponding *d*-spacing of 19.5 nm and at least two higher order reflections at angular position of $\sqrt{3}$ and $\sqrt{4}$ of the first-order maximum consistent with a hexagonal lattice. This structural assignment was corroborated by TEM studies (Figure 1d). Nitrogen physisorption measurements (Figure 3bA) of porous Keggin POMs calcined under argon exhibit a type IV nitrogen sorption isotherm with specific surface area of 27 m^2g^{-1}. In contrast, the commercial Keggin POM ($H_3PMo_{12}O_{40}$) only has a surface area of 3 m^2g^{-1}, see Table 2. The pore size estimate of the mesoporous material based on the Barrett-Joyner-Halenda (BJH) method[29] is 9.5 nm, see insert (A) in Figure 3b.

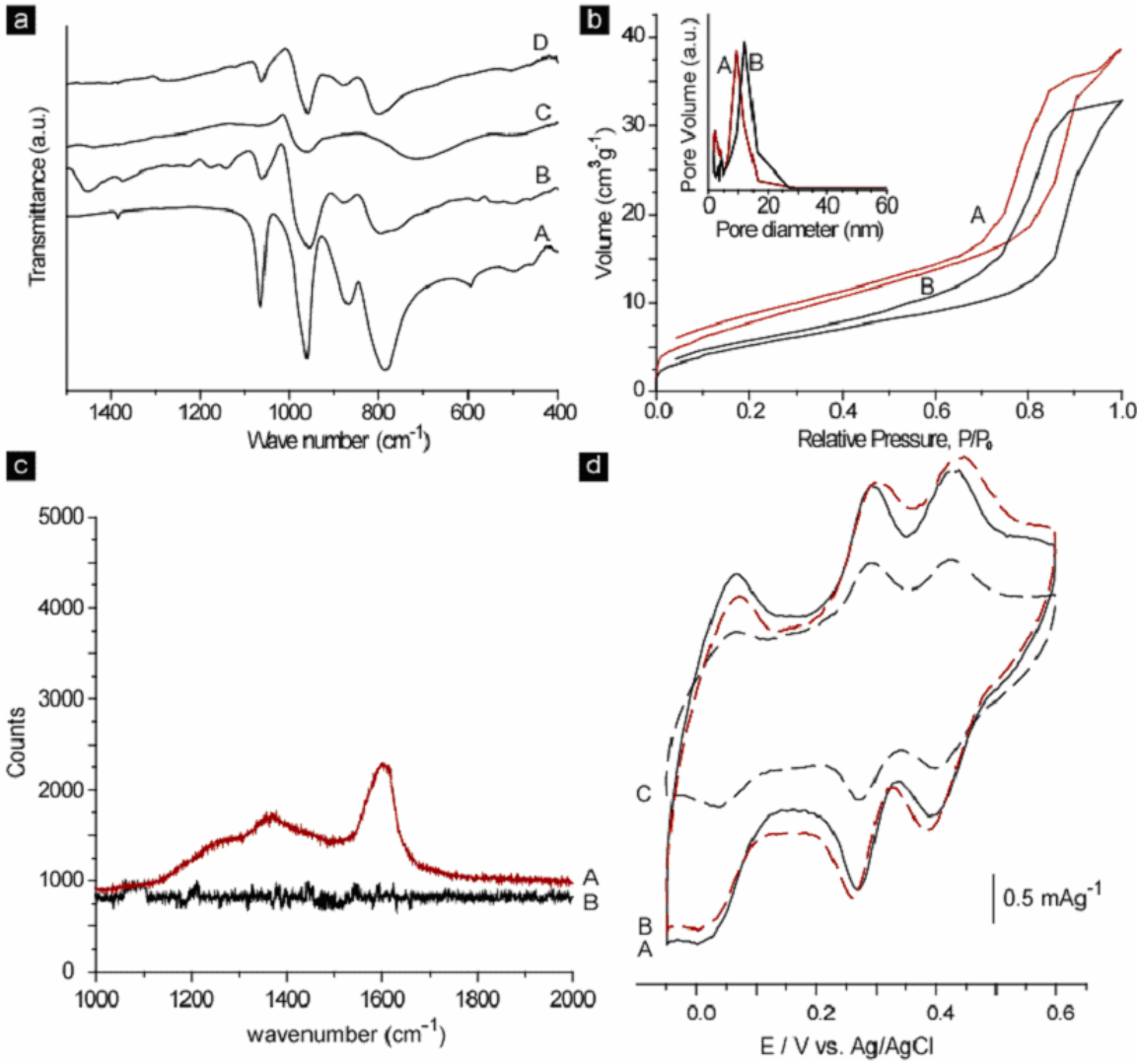

Figure 3. Materials characterization. a, FTIR spectra of the commercial Keggin POM $H_3[PMo_{12}O_{40}]$ (A), as-made 1:4 PI-*b*-PDMAEMA/ Keggin POM composite (B), corresponding argon calcined (C), and air calcined (D) mesoporous Keggin POM materials. **b,** Nitrogen physisorption isotherms of argon calcined (A) and air calcined (B) mesoporous Keggin POM materials obtained from PI-*b*-PDMAEMA/ Keggin POM 1:4 composite (inset: corresponding pore size distributions). **c,** Raman spectra of argon calcined (A) and air calcined (B) mesoporous Keggin POM materials obtained from PI-*b*-PDMAEMA/ Keggin POM 1:4 composite. **d,** CVs for (A) commercial Keggin POM, (B) as-made 1:4 PI-*b*-PDMAEMA/ Keggin POM composite , and (C) mesoporous Keggin-

type $H_3PMo_{12}O_{40}$ modified GCEs in 2 M H_2SO_4. The scan rate in all cases was 50 mV/s. Note that the current values are normalized to the amount of $H_3PMo_{12}O_{40}$ modified on GCEs.

Subsequent calcinations of the argon-heated material in air to 300-350 °C preserved the inverse hexagonal structure. SAXS diffractograms of two different pieces of the same air calcined material (Figure 2c,B and C) show first-order peaks with corresponding d-spacings of 18.4 and 22.7 nm, respectively, and at least two higher order reflections at angular positions of $\sqrt{3}$ and $\sqrt{4}$ of the first-order maxima, consistent with a hexagonal lattice. Variations in *d*-spacing within one sample are also evident from the 2-D SAXS pattern in Figure 2b showing first-order Bragg spots at slightly different radial positions. The structural assignment was corroborated and *d*-spacing variations within one sample were confirmed by TEM studies. The TEM image in Figure 1g shows variations in lattice spacings and pore sizes between different grains of the same hexagonally ordered sample. From SAXS (Figure 2cB and C) and TEM results (Figure 1E and F) it is evident, however, that this does not result in loss of long range order in the final materials.

Retention of the structure upon heating in air was also corroborated by N_2 physisorption (Figure 3bB). The oxidized material shows again a type IV nitrogen sorption isotherm with specific surface area of 30 m^2g^{-1}. The pore size according to the BJH method is 12.2 nm. This is slightly larger than the pore size of the material heat-treated under argon and is expected from the loss of in-situ formed carbon. WAXS patterns of the calcined (under argon or under air) material did not show any of the characteristic reflections expected from crystalline Keggin POM (see Figure 2d,B). When

studied by FTIR, however, the material calcined under argon and subsequently under air clearly showed the four 'fingerprint-like' bands characteristic of the Keggin structure (Figure 3aD). This is consistent with the results of electrochemical studies, see below. It is worth noting that when first heat-treated under argon the characteristic 'fingerprint-like' band structure is lost, see Figure 3a,C. During pyrolysis under argon some of the Mo(VI) centers apparently are reduced, resulting in the disappearances of the ν_{as} (Mo-O_b-Mo), and ν_{as} (Mo-O_c-Mo) vibrations. Our results suggest that final heat-treatment in air removes the carbon and re-oxidizes Mo to Mo(VI) centers of the Keggin POM.

Separate Raman spectroscopy studies were performed to establish the presence of the *in-situ*-formed carbon and its removal in the final material. A spectrum for a Keggin POM material heat-treated under argon to 375 °C is shown in Figure 3c,A. Two bands appear around 1600 cm^{-1} and 1350 cm^{-1} from graphitic carbon (G-band) and disordered carbon (D-band), respectively, typical for amorphous carbon materials[27]. On subsequent calcination in air at 350 °C, the bands disappeared (Fig. 3c,B), suggesting removal of the carbon.

Figure 3d compares representative cyclic voltammograms (CVs) for PI-*b*-PDMAEMA derived nanocomposite (as-made) and mesoporous (heated first under argon and then under air) $H_3PMo_{12}O_{40}$ modified glassy carbon electrodes (GCEs) in 2 M H_2SO_4, with that of commercial $H_3PMo_{12}O_{40}$ Keggin POM. It should be noted that these experiments were primarily performed to establish the preservation of the Keggin POM structure and catalytic activity after mesoporous materials formation. Indeed, all samples exhibited three two-electron redox processes, characteristic of a Keggin structure[30], over the potential range from -0.05 V to +0.60 V vs. Ag/AgCl. This is clear proof that the

Keggin structure is intact even after conversions to nanocomposite and mesoporous materials.

In summary, we have demonstrated that the block copolymers PI-*b*-PDMAEMA and PI-*b*-PEO can be used as structure directing agents for Keggin POM. We have reported on nanocomposites with lamellar and hexagonal morphologies. High temperature treatment of hexagonally ordered nanocomposites resulted in mesoporous Keggin POM with open and accessible pores. To the best of our knowledge, this is the first time that an ordered mesoporous Keggin POM material has been obtained through a block copolymer-type bottom-up approach. This approach has the potential to open a new field for the development of nanostructured Keggin POM materials with novel property profiles.

Experimental Section

Block copolymer synthesis: The block copolymers PI–*b*–PDMAEMA and PI-b-PEO were polymerized by anionic polymerization as described elsewhere[31-33]. Gel permeation chromatography (GPC) was used to determine the molecular weight of the first blocks (polyisoprene, PI) and the polydispersity of the block copolymers. ^{1}H NMR was used to determine the overall molecular weights of the block copolymers. The resulting PI-*b*-PDMAEMA polymer had a molecular weight of 31 kg/mol and 33 wt.-% PDMAEMA with a polydispersity of 1.04 and the PI-b-PEO polymer had a molecular weight of 16 kg/mol and 23 wt.-% PEO with a polydispersity of 1.05.

Synthesis of composites: The polymer-Keggin POM composite films were prepared by adding the PI-*b*-PDMAEMA or PI-*b*-PEO polymer solution in THF (J. T.

Baker, 99%, used as received) to a separate solution of $H_3PMo_{12}O_{40}$ xH_2O (Aldrich, used as received) in THF under continuous stirring. In a typical synthesis of a 1: 4 polymer:Keggin POM composite film, 0.1 g of block copolymer was dissolved in 2 mL of THF. This solution was added to the $H_3PMo_{12}O_{40}$ in THF solution (0.4 g Keggin POM in 3 mL of THF) at room temperature under continuous stirring. After 30 min, films were cast by evaporation of the solvent in air on a hot plate at 50 °C. Following the same procedure films with different polymer:Keggin POM weight ratios were obtained.

Calcination of the samples: Calcinations were always performed in 2 steps. First, under argon atmosphere with step-wise heating (150 °C – 5 h, 250 °C - 3 h, and 375 °C – 10 h), followed with a second calcination in air with step-wise heating (100 °C – 2 h, 200 °C – 3 h, 300 °C – 5 h (and 350 °C – 5 h)).

Characterization:

FTIR: data was collected on a Brucker IFS66V using KBr pellets. Before the measurements, samples were heated to 100 ^{o}C for 12 hours and KBr pellets were pressed.

Raman: Ambient-temperature Raman spectroscopy experiments were performed using a Jobin Yvon Labram spectrometer with a 632.8 nm He-Ne excitation line and laser output power of 8 mW. The laser beam was focused using a 50× objective, resulting in a spot having a diameter of ~5 μm.

SAXS: data was obtained at the Cornell High Energy Synchrotron Source (CHESS) and on a Rigaku RU300 copper rotating anode X-ray spectrometer (λ = 1.54 Å) operated at 40 kV and 50 mA. Data were collected with a CCD 2-D detector operating at X-ray energy of 1.223 Å and with a homebuilt 1 K × 1 K pixel CCD detector, respectively.

PXRD: patterns were collected using a PANalytical X-ray diffractometer with Ni-filtered Cu Kα radiation (40 kv, 40 mA) at 0.008° step size and 1.2 s step time over $5 < 2\theta < 80°$ range.

TEM: was performed on a Zeiss CEM 902 microscope at an accelerating voltage of 80 kV. Samples for TEM analysis were prepared by sonicating the samples in ethanol for 2 min followed by depositing one drop on a holey carbon film supported by a copper grid using a Pasteur pipette.

BET: Nitrogen physisorption was conducted at 77 K on a Quantachrome Autosorb 1 instrument. Prior to the measurements, the samples were degassed at 373 K for 24 h.

Preparation and Characterization of Polyoxometalate, $H_3PMo_{12}O_{40}$, Modified Electrodes: $H_3PMo_{12}O_{40}$ modified electrodes were prepared by casting dispersions containing $H_3PMo_{12}O_{40}$, Nafion® (5 wt% solution in lower aliphatic alcohols/H_2O mix, Aldrich, used as received), isopropanol (IPA, Mallinckrodt Chemicals, used as received), and H_2O on glassy carbon electrodes (GCEs) (Pine Instrument Co., 5.0 mm diameter). The dispersions were prepared by mixing $H_3PMo_{12}O_{40}$, 20 µl of a Nafion solution, 1000 µl of IPA, and 3980 µl of H_2O. The mixtures were sonicated for 10 minutes to homogenize. 8 µl of the dispersion was cast on a GCE with a micro-pipet (10 µl, Gilson, Inc.) and subsequently dried under vacuum at room temperature for an hour to obtain the $H_3PMo_{12}O_{40}$ modified GCEs.

Electrochemical characterization of $H_3PMo_{12}O_{40}$ modified electrodes was carried out at room temperature via cyclic voltammetry (CV) (Hokuto Denko Co. (Japan), model HSV-100). Measurements were taken in a three-electrode cell configuration using a

GCE, a large area Pt coil counter electrode, and a potassium chloride-saturated Ag/AgCl (Bioanalytical Systems, Inc., BAS) reference electrode without regard to the liquid junction potential, and against which all potentials are reported. The working electrode was polished with 0.3 μm and 0.05 μm alumina slurries (REFINETEC Ltd.), rinsed with Millipore water and acetone, and dried prior to use. Unless otherwise noted, all experiments were carried out in a 2 M sulfuric acid (H_2SO_4, 99.999%, Aldrich, used as received) solution, which was thoroughly purged using pre-purified nitrogen gas. The 2 M H_2SO_4 electrolyte solutions employed were prepared with Millipore water (18 MΩcm, Millipore Milli-Q).

The specific electrochemical activity of the three samples, a total faradaic charge due to redox reactions of $H_3PMo_{12}O_{40}$ normalized to the amount of $H_3PMo_{12}O_{40}$ on GCEs, was 2.3, 4.4 and 4.1 Cg^{-1} for the parent Keggin POM, nanocomposite and mesoporous material, respectively. However, the $H_3PMo_{12}O_{40}$ materials studied (i.e., parent, nanocomposite, and mesoporous materials) were found to partially dissolve in the IPA/H_2O solution during the modification of $H_3PMo_{12}O_{40}$ on GCEs. Therefore, comparison of the specific electrochemical activity of the different samples is only qualitative. In particular, under the experimental conditions employed in this study, the full potential of the high-surface-area property of the mesoporous $H_3PMo_{12}O_{40}$ is not taken advantage of.

Reference List

1. Hoffmann,F., Cornelius,M., Morell,J. & Fröba,M. Silica-based mesoporous organic-inorganic hybrid materials. *Angew. Chem. Int. Ed.* **45**, 3216-3251 (2006).
2. Schüth,F. Endo- and exotemplating to create high-surface-area inorganic materials. *Angew. Chem. Int. Ed.* **42**, 3604-3622 (2003).

3. Templin,M. *et al.* Organically modified aluminosilicate mesostructures from block copolymer phases. *Science* **278**, 1795-1798 (1997).

4. Förster,S. Amphiphilic block copolymers for templating applications. *Colloid Chemistry 1* **226**, 1-28 (2003).

5. Stein,A. *et al.* Salt Gel Synthesis of Porous Transition-Metal Oxides. *Chem. Mater.* **7**, 304-313 (1995).

6. Janauer,G.G., Dobley,A., Guo,J.D., Zavalij,P. & Whittingham,M.S. Novel tungsten, molybdenum, and vanadium oxides containing surfactant ions. *Chem. Mater.* **8**, 2096-2101 (1996).

7. Kresge,C.T., Leonowicz,M.E., Roth,W.J., Vartuli,J.C. & Beck,J.S. Ordered Mesoporous Molecular-Sieves Synthesized by A Liquid-Crystal Template Mechanism. *Nature* **359**, 710-712 (1992).

8. Zhao,D.Y. *et al.* Triblock copolymer syntheses of mesoporous silica with periodic 50 to 300 angstrom pores. *Science* **279**, 548-552 (1998).

9. Yang,P.D., Zhao,D.Y., Margolese,D.I., Chmelka,B.F. & Stucky,G.D. Block copolymer templating syntheses of mesoporous metal oxides with large ordering lengths and semicrystalline framework. *Chem. Mater.* **11**, 2813-2826 (1999).

10. J.B.Moffat. in Metal-Oxygen Clusters - The Surface and Catalytic Properties of Heteropoly Oxometalates. Kluwer Academic / Plenum Publishers, New York (2001).

11. M.T.Pope and A.Müller. Polyoxometalate Chemistry From Topology via Self-Assembly to Applications. Kluwer Academic Publishers, Netherlands (2001).

12. Nomiya,K., Murasaki,H. & Miwa,M. Catalysis by Heteropolyacids .8. Immobilization of Keggin-Type Heteropolyacids on Poly(4-Vinylpyridine). *Polyhedron* **5**, 1031-1033 (1986).

13. Katsoulis,D.E. A survey of applications of polyoxometalates. *Chem. Rev.* **98**, 359-387 (1998).

14. Rhule,J.T., Hill,C.L. & Judd,D.A. Polyoxometalates in medicine. *Chem. Rev.* **98**, 327-357 (1998).

15. Jentoft,F.C. *et al.* The structure of molybdenum-heteropoly acids under conditions of gas-phase selective oxidation catalysis: a multi-method in situ study. *Appl. Catal. A* **256**, 291-317 (2003).

16. Herzog,B., Bensch,W., Ilkenhans,T., Schlogl,R. & Deutsch,N. Single-Crystal and Powder Diffraction Studies of the Structure of Heteropolymolybdophosphoric Acid Catalysts. *Catal. Lett.* 20, 203-219 (1993).

17. Inumaru,K., Ishihara,T., Kamiya,Y., Okuhara,T. & Yamanaka,S. Water-tolerant, highly active solid acid catalysts composed of the Keggin-type polyoxometalate H3PW12O40 immobilized in hydrophobic nanospaces of organomodified mesoporous silica. *Angew. Chem. Int. Ed.* **46**, 7625-7628 (2007).

18. Shi,C.F., Wang,R.W., Zhu,G.S., Qiu,S.L. & Long,J. Synthesis, characterization, and catalytic properties of SiPW-X mesoporous silica with heteropolyacid encapsulated into their framework. *Eur. J. Inorg. Chem.* 4801-4807 (2005).

19. Blasco,T., Corma,A., Martinez,A. & Martinez-Escolano,P. Supported heteropolyacid (HPW) catalysts for the continuous alkylation of isobutane with 2-butene: The benefit of using MCM-41 with larger pore diameters. *J. Catal.* **177**, 306-313 (1998).

20. Ichinose,I., Asai,T., Yoshimura,S., Kimizuka,N. & Kunitake,T. 2-Dimensional Arrangement of Polynuclear Metal-Complexes in the Interlayer of Multibilayer Cast Films. *Chem. Lett.* 1837-1840 (1994).

21. Taguchi,A., Abe,T. & Iwamoto,M. Non-silica-based mesostructured materials: Hexagonally mesostructured array of surfactant micelles and 11-tungstophosphoric heteropoly anions. *Adv. Mater.* **10**, 667-669 (1998).

22. Yun,H.S., Kuwabara,M., Zhou,H.S. & Honma,I. Synthesis of heteropoly oxometalate/amphiphilic block copolymer composite thin films with self-ordered mesostructures. *Thin Solid Films* **515**, 2842-2846 (2007).

23. Maayan,G., Popovitz-Biro,R. & Neumann,R. Micelle directed synthesis of polyoxometalate nanoparticles and their improved catalytic activity for the aerobic oxidation of sulfides. *J. Am. Chem. Soc.* **128**, 4968-4969 (2006).

24. Yelamanchili,R.S., Walther,A., Muller,A.H.E. & Breu,J. Core-crosslinked block copolymer nanorods as templates for grafting [SiMo12O40](4-) Keggin ions. *Chem. Commun.* 489-491 (2008).

25. Warren,S.C., Disalvo,F.J. & Wiesner,U. Nanoparticle-tuned assembly and disassembly of mesostructured silica hybrids. *Nature Mater.* **6**, 156-U23 (2007).

26. Kamperman,M., Garcia,C.B.W., Du,P., Ow,H.S. & Wiesner,U. Ordered mesoporous ceramics stable up to 1500 degrees C from diblock copolymer mesophases. *J. Am. Chem. Soc.* **126**, 14708-14709 (2004).

27. Lee,J. *et al.* Direct access to thermally stable and highly crystalline mesoporous transition-metal oxides with uniform pores. *Nature Mater.* **7**, 222-228 (2008).

28. Rocchicciolideltcheff,C., Fournier,M., Franck,R. & Thouvenot,R. Vibrational Investigations of Polyoxometalates .2. Evidence for Anion Anion Interactions in Molybdenum(Vi) and Tungsten(Vi) Compounds Related to the Keggin Structure. *Inorg. Chem.* **22**, 207-216 (1983).

29. Barrett,E.P., Joyner,L.G. & Halenda,P.P. The Determination of Pore Volume and Area Distributions in Porous Substances .1. Computations from Nitrogen Isotherms. *J. Am. Chem. Soc.* **73**, 373-380 (1951).

30. Sadakane,M. & Steckhan,E. Electrochemical properties of polyoxometalates as electrocatalysts. *Chem. Rev.* **98**, 219-237 (1998).

31. Renker,S. *et al.* Nanostructure and shape control in polymer-ceramic hybrids from poly(ethylene oxide)-block-poly(hexyl methacrylate) and aluminosilicates derived from them. *Macromolecular Chem. and Phy.* **205**, 1021-1030 (2004).

32. Creutz,S., Teyssie,P. & Jerome,R. Anionic block copolymerization of 4-vinylpyridine and tert-butyl methacrylate at "elevated" temperatures: Influence of various additives on the molecular parameters. *Macromolecules* **30**, 5596-5601 (1997).

33. Allgaier,J., Poppe,A., Willner,L. & Richter,D. Synthesis and characterization of poly[1,4-isoprene-b-(ethylene oxide)] and poly[ethylene-co-propylene-b-(ethylene oxide)] block copolymers. *Macromolecules* **30**, 1582-1586 (1997).

Electronic Supporting Information (ESI)

Hexagonally Ordered Mesoporous Keggin-type Polyoxometalates**

Ram Sai Yelamanchili,[a] *Marleen Kamperman,*[b] *Yasuyuki Kiya,*[c] *Jinwoo Lee,*[b]

Héctor D. Abruña,[c] *Josef Breu**[a] *and Ulrich Wiesner**[b]

[a] Prof. Dr. Josef Breu and Mr. Ram Sai Yelamanchili
Department of Inorganic Chemistry I
University of Bayreuth
95447 Bayreuth, Germany
Fax: (+49921552788)
E-mail: josef.breu@uni-bayreuth.de

[b] Prof. Dr. Ulrich Wiesner, Marleen Kampermann and Dr. Jinwoo Lee
Department of Materials Science and Engineering
Cornell University
Ithaca, New York 14853, USA
Fax: (+49921553393)
E-mail: ubw1@cornell.edu

[c] Prof. Dr. Héctor D. Abruña and Dr. Yasuyuki Kiya
Department of Chemistry and Chemical Biology
Cornell University, Ithaca, New York 14853

[**] This project was supported by Elite Network Bavaria (ENB) and the NSF through a single investigator award (DMR-0605856). R. S. Y. would like to acknowledge Elite Network Bavaria for a fellowship.

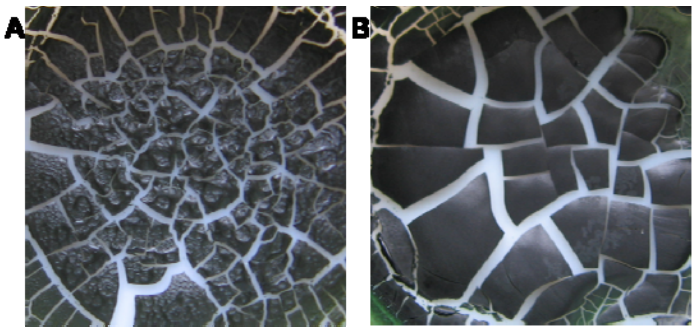

Figure S1 Digital images of the polymer composite films prepared with PI–PDMAEMA and $H_3[PMo_{12}O_{40}]$ with different polymer : keggin-POM loadings; 1: 2 (A), and 1: 3 (B).

A 4 Shaping colloidal rutile into thermally stable and porous mesoscopic titania-balls

This work with the title “Shaping colloidal rutile into thermally stable and porous mesoscopic titania-balls” by Yelamanchili, R. S., Lu, Y., Lunkenbein, T., Miyajima, N., Yan, L., Ballauff, M., Breu, J., has been submitted to *Small.*

Submitted to NANO MICRO small

The table of contents

We present a new approach to the direct synthesis of crystalline polymer-metal oxide composites by structure directing electrostatically stabilized rutile nanocrystals over spherical polyelectrolyte brush (SPB) particles. The as-synthesized crystalline composites exhibit high surface areas and porosity can be achieved through controlled step-wise calcinations under inert argon atmosphere followed by a second calcination under air. Original morphology and phase were retained after calcinations and the surface areas increased dramatically. In this report we proved that this alternative route is not just limited to zeolitie materials and it is expected that this hierarchical route to structure oxides at the mesoscale is generally applicable.

TOC Keyword

Nanocomposite, Polyelectrolyte brush particles, Mesoporous materials, Nanocrystalline materials, Photo-catalyst

Ram Sai Yelamanchili, Yan Lu*, Thomas Lunkenbein, Nobuyoshi Miyajima, Li-Tang Yan, Matthias Ballauff* and Josef Breu* ■<B>…<B>■

Title: Shaping colloidal rutile into thermally stable and porous mesoscopic titania-balls

ToC figure

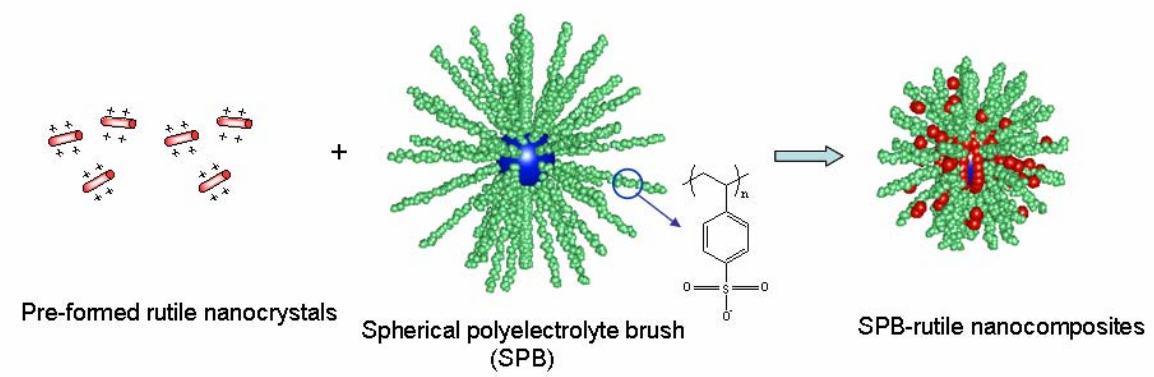

Submitted to small

DOI: 10.1002/smll.((please add manuscript number))

Shaping colloidal rutile into thermally stable and porous mesoscopic titania-balls**

Ram Sai Yelamanchili, Yan Lu[*], Thomas Lunkenbein, Nobuyoshi Miyajima, Li-Tang Yan, Matthias Ballauff[*] and Josef Breu[*]

((Optional Dedication))

[*] Prof. Dr. Josef Breu, Mr. Ram Sai Yelamanchili, Mr. Thomas Lunkenbein
Department of Inorganic Chemistry I
University of Bayreuth, 95447 Bayreuth (Germany)
E-mail: josef.breu@uni-bayreuth.de
Prof. Dr. Matthias Ballauff, Dr. Yan Lu
Department of Physical Chemistry I
University of Bayreuth, 95447 Bayreuth (Germany)
E-mail: matthias.ballauff@uni-bayreuth.de; yan.lu@uni-bayreuth.de
Dr. Nobuyoshi Miyajima
Bayerisches Geoinstitut,
University of Bayreuth, 95440 Bayreuth (Germany)
Dr. Li-Tang Yan
Department of Physical Chemistry II
University of Bayreuth, 95440 Bayreuth (Germany)

Supporting Information is available on the WWW under http://www.small-journal.com or from the author.

Keywords: Nanocomposite, Polyelectrolyte brush particles, Mesoporous materials, Nanocrystalline materials, Photo-catalyst

Abstract

High crystallinity and controlled porosity are advantageous for many applications such as energy conversion and power generation. Despite many efforts in the last decades, the direct synthesis of organic-inorganic composite materials with well crystalline transition metal oxides is still a major challenge. In general molecular precursors serve as inorganic precursors and heat treatment is required to convert as-synthesized amorphous composites to stable crystalline materials. Herein, we present an alternative approach to the direct synthesis of crystalline polymer-metal oxide composites by using spherical polyelectrolyte brush (SPB) as

the template system. Pre-synthesized electrostatically stabilized rutile nanocrystals which carry a positive surface charge were used as inorganic precursors. In this approach, the strong Coulomb interactions between anionic polyelectrolyte brush chains and cationic crystalline rutile colloids, which surfaces are naked and therefore reactive, are the key factors for the organic-inorganic crystalline composite formation. Stepwise calcinations first under argon followed with a second calcination in air lead to the complete removal of polymer template without collapse and porous rutile balls are obtained. The results suggest that any colloids that carry a surface charge might serve as inorganic precursors when charged templates are used. It is expected that this hierarchical route to structure oxides at the mesoscale is generally applicable.

1. Introduction

Extensive research efforts have been devoted to the development of rational synthesis pathways for porous inorganic materials. Potential applications in catalysis, photocatalysis, adsorbents, sensors, and electrode materials have been driving this research. [1-3] However, for distinct applications the potential can only be optimized for well crystalline materials. It is well known, for instance, that amorphous volumes in mesoporous titania promote the recombination of photo-excited electrons and holes and by this way limit the photocatalytic efficiency.[4,5] In addition the crystalline state will increase thermal and mechanical stability. When using soft organic materials such as block copolymers as structure directing templates, only very few examples are known where the inorganic material in the organic-inorganic hybrids obtained spontaneously, is indeed well crystalline.[4,6] Even if colloidal crystals are used as templates,[7] usually, the precipitated walls of the as-made hybrid materials turn out to be amorphous and have to be converted to completely crystalline walls in a subsequent tedious crystallization treatment. Often this post-synthesis treatment is some kind of annealing at elevated temperatures which bears the risk of loosing the hierarchical structure. Moreover,

when the inorganic materials show polymorphism, controlling the crystal structure and thus the materials properties is an additional challenge that needs to match with the heat treatment. Often, the original phase, structures or morphologies change/collapse during the crystallization process.[4,8,9]

While in the vast majority of synthesis pathways molecular[4,6] or oligomeric[10] building blocks serve as inorganic precursors, a rather obvious strategy has been neglected in the past: When using polyelectrolytes as organic templates, the surface potential of pre-synthesized nanocrystals might be utilized to overcome phase segregation and arrange the inorganic material around the template. If the nanocrystals are only electrostatically stabilized, the surfaces might still be reactive enough to render covalent bonding between the nanocrystals in the walls of the hybrid material possible, leading to thermally and mechanically stable materials. A proof of this synthesis concept has been delivered already some years ago when synthesis methods were developed that produce zeolites which show hierarchical bimodal pore size distributions.[11-17] Nanosized zeolite “seeds” (protozeolitic nanoclusters) were used as building blocks, which were directly assembled into hexagonal, cubic, wormhole, and foamlike framework structures applying supramolecular structure-directing templates. Unfortunately, to our knowledge the general applicability of this very appealing synthesis concept for other oxide materials has not been explored.

Here we report the assembly of electrostatically stabilized nanoscopic rutile around spherical polyelectrolyte brushes (SPB).[18-20] SPB are colloidal particles consisting of a solid polystyrene core and a dense surface layer of polyelectrolytes. During the calcination of the rutile-SPB-hybrid, the “naked” nanocrystals are crosslinked and thermally and mechanically stable mesoscopic rutile balls with interparticle mesoporosity are obtained. Colloidal rutile has been chosen as inorganic precursor because crystalline titania-based materials are of

considerable interest due to their technological applications as photoconductors, sensors, photocatalysts, and dye sensitized solar cells, optoelectronic devices.[16,21-33]

2. Results and Discussion

Outline of the synthesis concept:

Titania comes in three crystalline polymorphs: anatase, rutile, and brookite. Each crystalline phase has different physical properties, such as refractive index, chemical reactivity, and photochemical reactivity.[25,27,34-36] Consequently, different applications ask for distinct polymorphs and control of crystal structure might be a prerequisite. Versatile synthesis methods such as chemical vapour deposition,[37] liquid phase deposition,[38] sol-gel,[39] non-hydrolytic sol-gel, hydrothermal/solvothermal,[40] and template methods[41,42] were developed for the synthesis of titania composites. Generally, as-made composites are amorphous materials and additional efforts are needed for the crystallization of these amorphous materials, which is a quite tricky process as mostly, the original structures or morphologies used to change/collapse during this crystallization process.[4,8,9]

There are only two reports in the literature where highly crystalline composite materials have been obtained spontaneously, i.e., in a simple “one-pot”-type procedure. Firstly, Lee et al. [4] have used a block copolymer which converts to a sturdy, amorphous carbon material under appropriate heating conditions that is sufficiently rigid to allow crystallization at high temperatures. This approach resulted in mesoporous anatase.

Secondly, in an earlier paper we have demonstrated that SPB particles can be used as well-defined nanoreactors for the spontaneous “one-pot” generation of well crystalline, photocatalytically active anatase nanoparticles at room temperature.[6] The sulfonate groups (SO_3^-) on the polyelectrolyte brush chains preferentially associate with titanium metallorganic compounds.[43,44] Consequently, the **molecular** titanium precursor is hydrolysed and titania condenses around the brush particles.[6] However, when using molecular precursors the crystal

structure of the precipitated walls is controlled by the polyelectrolyte template and the synthesis of other titania polymorphs like rutile is impossible. This is because strong ligands like sulphate, sulfonate, and phosphate show strong affinity to titania surfaces which strictly paves the way to the nucleation of anatase.[45-47]

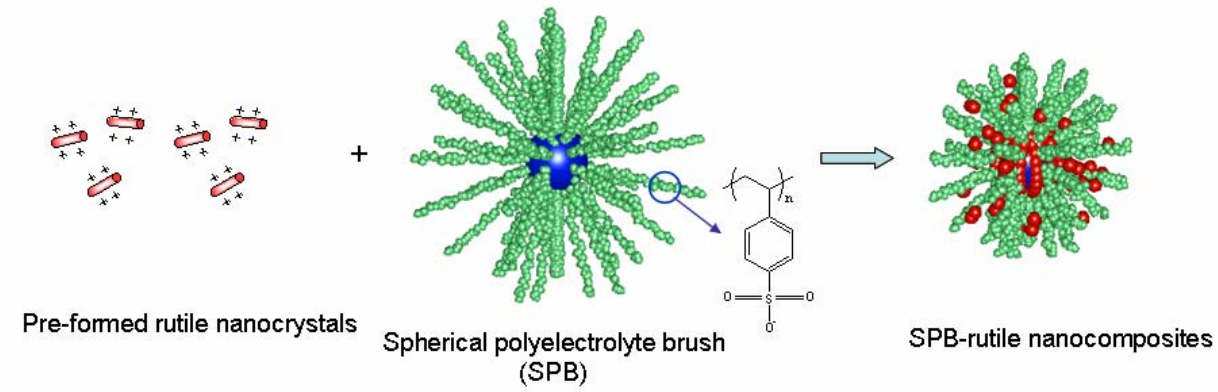

Scheme 1. Synthesis of rutile composites using cationic rutile colloids and anionic SPB.

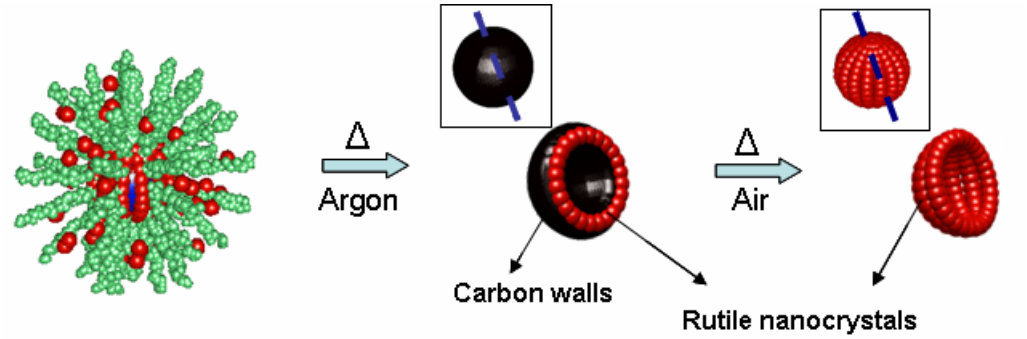

Scheme 2. Formation of porous rutile balls by two-step calcination. Firstly, by heat treatment of rutile composite under argon, the sp^2 carbon containing SPB is converted to a amorphous carbon material, which acts as a rigid support to rutile nanocrystals and prevents the mesostructure from collapse. Secondly, further calcination in air will remove carbon and porous rutile balls with mesoporous crystalline walls are obtained.

Since the crystal structure can not be controlled in the presence of the soft template, it is essential to follow the alternative route for mesostructuring as outlined in the introduction. Firstly, nanoscopic rutile is synthesized under acidic aqueous conditions. Because of the low pH (1.0), which is far below the isoelectric point of rutile, these nanocrystals exhibit high

positive surface charge. Secondly, these crystalline and surface charged rutile colloids can be structure directed onto the anionic SPB particles to form crystalline rutile nanocomposites with well-defined structure, shape, and size (**Scheme 1-2**). The strong Coulomb interactions between anionic polymer chains and the cationic crystalline rutile colloids, whose surfaces are naked and therefore reactive, are the key factors in this approach for the organic-inorganic crystalline composite formation. It is the surface reactivity of the naked rutile colloids that, thirdly, paves the way to thermally and mechanically stable mesostructured porous rutile balls obtained by the subsequent calcination. Please note that in contrast to the earlier report,[6] synthesis in this approach was done using colloidal rutile crystals as titania source instead of starting from titanium molecular precursors.

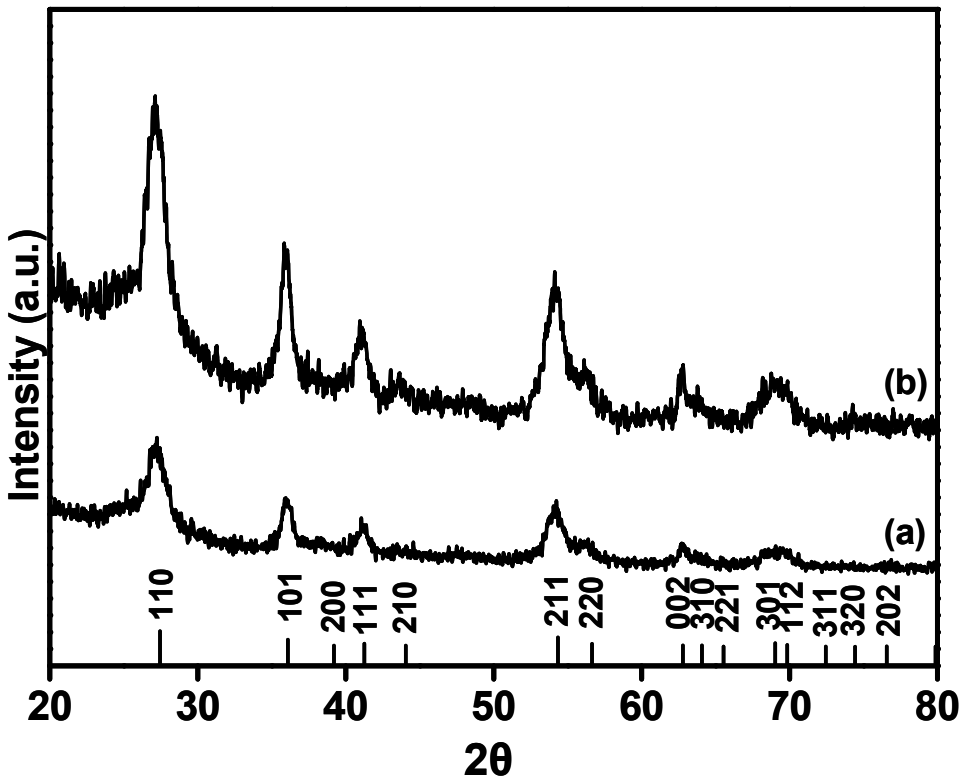

Figure 1. PXRD patterns of as-synthesized rutile composite (a), and porous rutile balls after calcinations (b). For comparison standard rutile (bottom) peaks are included.

Synthesis of nanoscopic rutile precursors:

As stressed above for this synthesis strategy control of both, size and the chemical nature of the surface of the colloid is essential. Therefore, we have developed a modified low-temperature, non-hydrothermal synthesis route for colloidal rutile which is only electrostatically stabilized. Any kind of steric stabilization would be detrimental by reducing the surface reactivity. To emphasize and clarify the subtle peculiarities of our nanorutile synthesis, published procedures shall be reviewed briefly first. Obviously, this review cannot claim to be exhaustive.

Generally, anatase is easier to be made nanocrystalline and various particle shapes and sizes have been synthesized by several synthesis routes.[48-50] Direct synthesis of nanoscopic rutile under mild conditions is difficult and often needs very stringent hydrothermal/solvothermal treatments because low-temperature routes generally tend to produce the kinetically favoured anatase polymorph.[45-47,51,52] Several synthesis routes were proposed for the synthesis of rutile using non-aqueous solvents, organic surfactants and ionic liquids. [45-47,52] However, as outlined above for our synthesis approach, TiO_2 nanocrystals capped/stabilized with organic surfactants can not be readily used because their surface is coated or stabilized with organic material. In the present study, rutile nanoparticles were synthesized under aqueous conditions by using 2M HCl as the reaction medium and titanium n-butoxide as the precursor. Please note that under these “simple” conditions, rutile colloids could be obtained under very mild conditions at 40 ^{o}C in 2 hours. Phase purity was confirmed by powder X-ray diffraction (PXRD), and high resolution transmission electron microscopy (HRTEM) (see ESI Figure S1-2). HRTEM images show a rather rough and therefore reactive surface. Surface roughness might be crucial for the subsequent connection between nanocrystals.

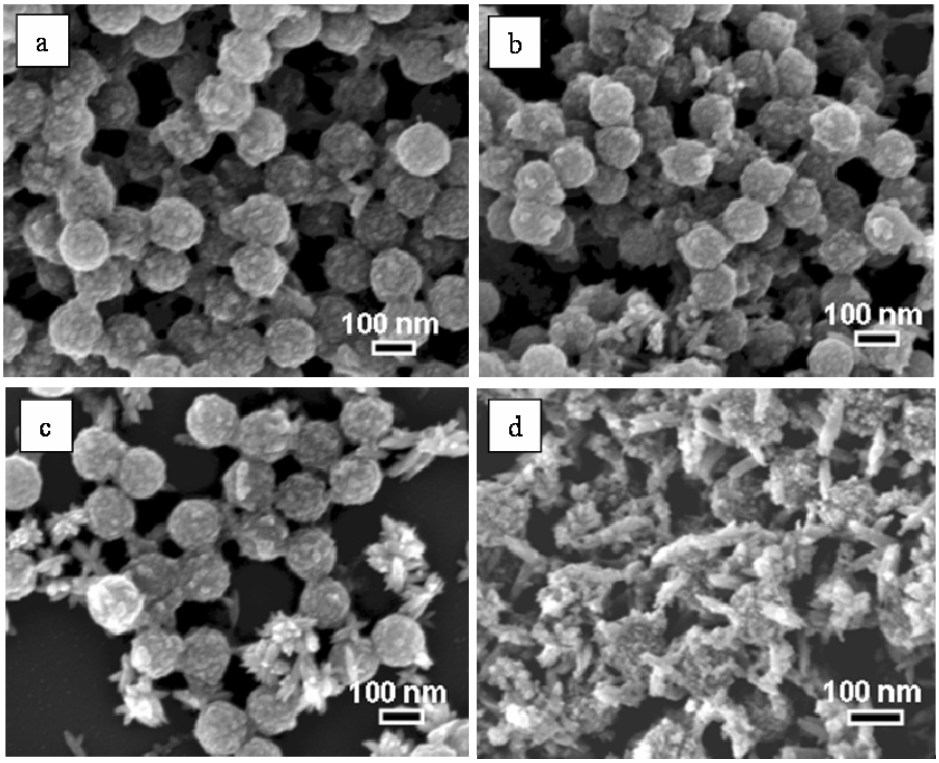

Figure 2. FESEM images of rutile composites with different polymer:rutile ratio (weight), 1:0.2 (a), 1:0.4 (b), 1:0.6 (c), and 1:1 (d).

Mesostructuring of nanoscopic rutile precursors:

In all cases freshly prepared colloidal rutile solutions were used for the crystalline titania-composite synthesis. As-synthesized rutile colloids are positively charged with zeta potentials of 51 mV and SPB particles are negatively charged with zetapotentials of -51 mV, both at pH 1. The strong Coulombic interactions reliably control the supramolecular assembly of charged colloids over the oppositely charged soft templates. After mixing the anionic SPB solution with the as-synthesized rutile colloids, the Coulomb interactions of rutile colloids and brush chains lead to the formation of organic-inorganic rutile composite. Figure 1a shows the PXRD patterns of the as-synthesized rutile composites. Please note that PXRD patterns of polymer brush particles do not show any reflections (see ESI Figure S3). From Figure 1a, it can be seen that when pre-formed rutile nanocrystals were used to prepare the composite, only rutile peaks are observed. Addition of SPB to colloidal rutile solutions did not change the

crystalline form of the pre-formed rutile nanocrystals. Thus, crystalline titania-composites with designed shape, size and crystalline forms can be obtained by this approach.

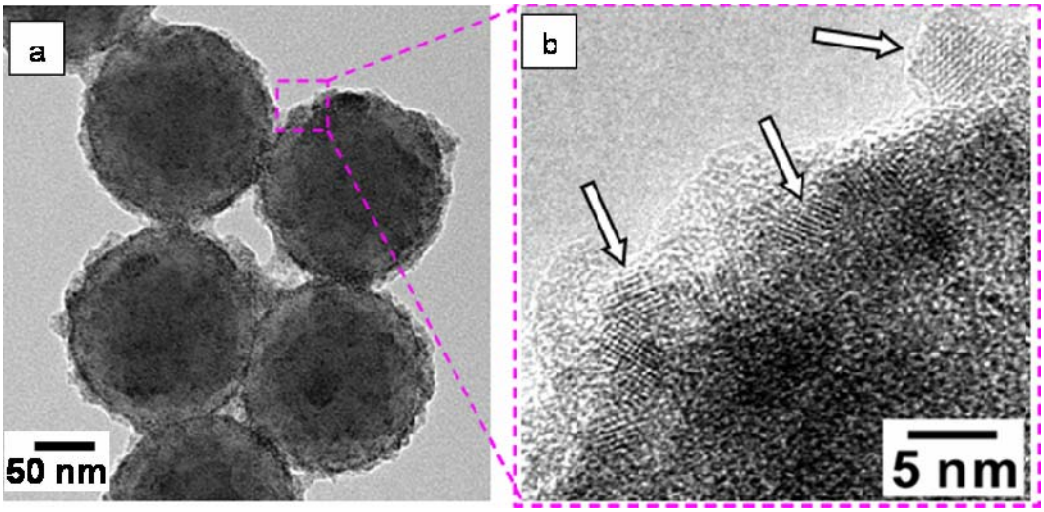

Figure 3. TEM (a) and HRTEM (b) images of rutile composites prepared from rutile nanocrystals.

The influence of different amounts of rutile colloids on the morphology of rutile composites has been studied (Figure 2). Comparison to the as-synthesized rutile composites, pure SPB particles show smooth surfaces (see ESI Figure S4). Rutile composite formation due to incorporation of rutile colloids into the polyelectrolyte brush layer of the SPB templates generates rough surfaces. At low rutile to SPB weight ratio, the SPB particle surfaces are homogeneously covered with a thin layer of rutile nanocrystals (Figure 2a and b). When further increasing the relative amount of rutile colloids, eventually leads to the generation of phase segregated secondary rutile besides the rutile composites (Figure 2c). More of these secondary rutile aggregates were observed with even higher relative concentration of rutile (Figure 2d). For further investigations, rutile composites prepared with the polymer to rutile weight ratio at 1:0.4 were used in order to avoid the influence from the secondary rutile aggregates.

Table 1. Properties of synthesized rutile composites and porous rutile balls.

sample	surface area[a] (m^2g^{-1})	pore size[b] (nm)
Rutile composite		
As-synthesized	76.9	non-porous
Argon calcined	122.9	17-32
Air calcined	134.5	17-33

[a] 5 point BET [b] BJH desorption branch

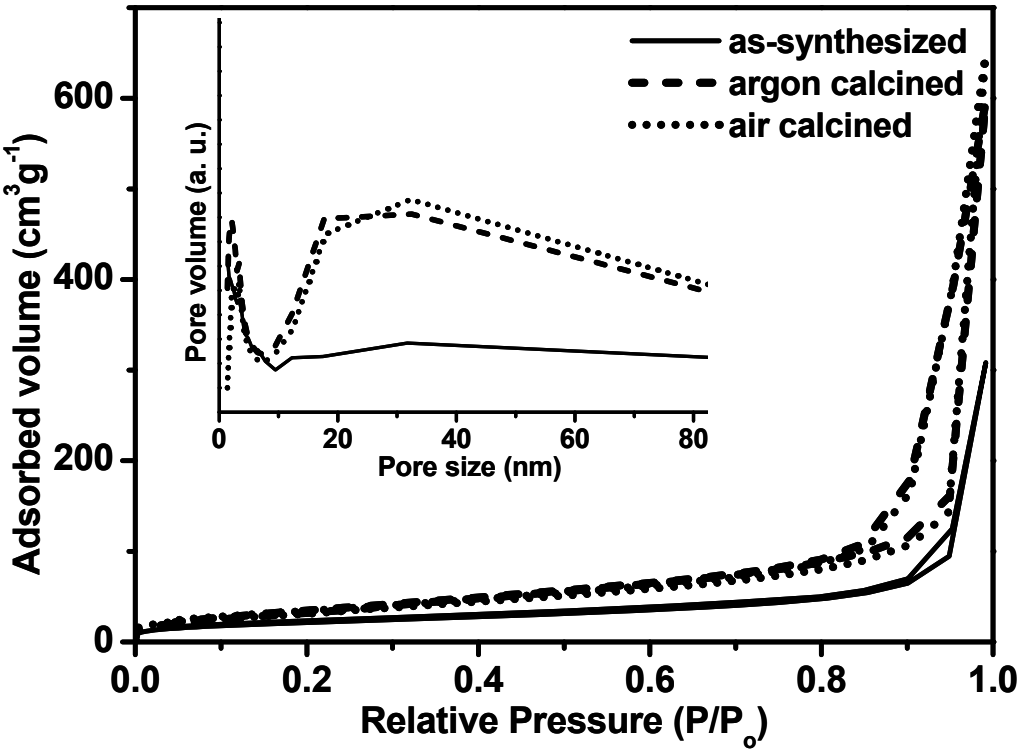

Figure 4. N_2 sorption isotherms of rutile composites and porous rutile balls obtained after argon and air calcinations (inset: corresponding pore size distribution).

Figure 3 show TEM and HRTEM images of the rutile composite with 1:0.4 (polymer:rutile/wt:wt) composition. It is evident from the TEM image that the rutile colloids were immobilized homogeneously into the brushes. Fig. 3b shows a HRTEM image of the

rutile composite, in which the crystal lattice planes can be clearly seen on the surface of the PS core. Zeta potential measurement at pH 1 indicates that rutile composite exhibits negative zeta potential of -35 mV where as as-synthesized rutile colloids are positively charged with zeta potentials of 51 mV and SPB particles are negatively charged with zeta potentials of -51 mV. The zeta potential measurements show that even after composite formation rutile composites are electrostatically stabilized. N_2 sorption analysis of the as-synthesized rutile composites revealed a high surface area of 76.9 m^2g^{-1} and the rutile composites are non-porous (Table 1 and Figure 4).

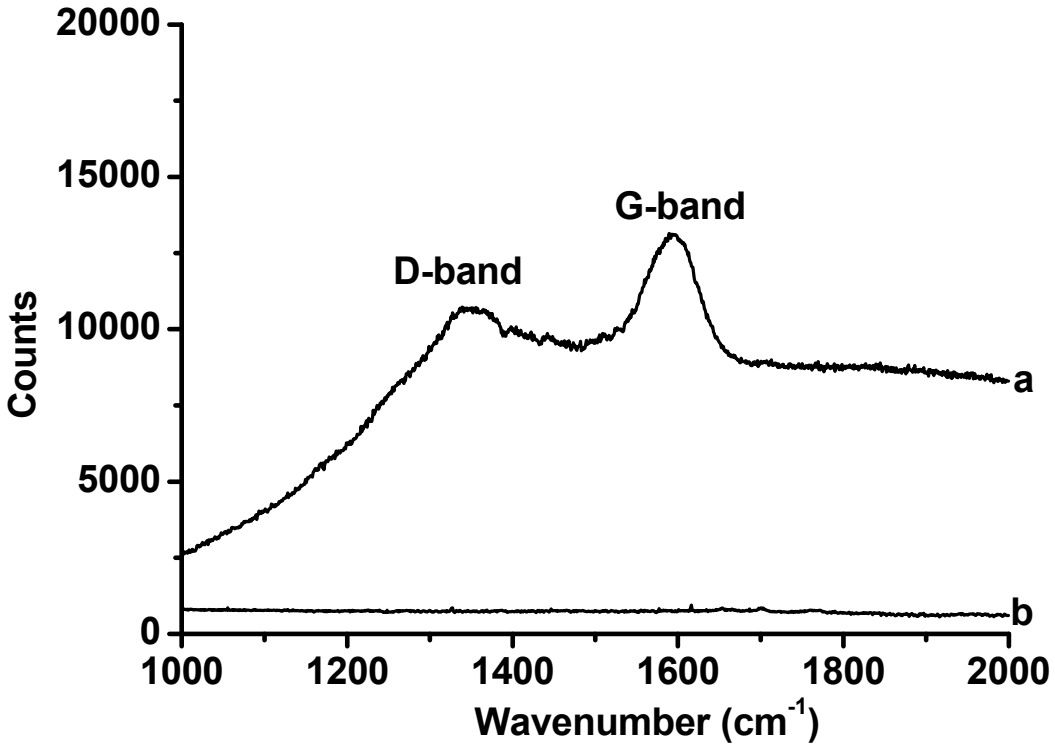

Figure 5. Raman spectra of rutile composites after (a) argon and (b) air calcinations showing the characteristic carbon D- and G-bands.

The subsequent heat treatment of the as-synthesized rutile composite under an inert environment leads to the conversion of the sp^2 carbon containing SPB particles to amorphous carbon material. This in-situ carbon acts as a rigid support to rutile nanocrystals and prevents structure collapse during heat treatment. Further calcinations in air will remove carbon walls

and porous structures with rutile framework are obtained by this approach.[4] Following these principles, the as-synthesized rutile composites are heated in a tube furnace under argon, followed by further heating in air, both at 500°C. During this process, SPB particles are first converted to an amorphous carbon that lines the rutile nanocrystals resulting macropores. Raman spectra establish the presence of the *in-situ* formed carbon during argon calcinations and its consequent removal in the final air calcined materials (Figure 5a and 5b). After argon calcinations, two bands appear around 1600 cm^{-1} and 1350 cm^{-1} from graphitic carbon (G-band) and disordered carbon (D-band), respectively, typical for amorphous carbon materials.[4] The carbon walls can be completely removed by subsequent air calcinations, which lead to the formation of hollow spheres built from interconnected rutile nanocrystals. The original spherical morphology is preserved during both calcinations steps as evidenced from the FESEM and TEM images (Figure 6a and 6b). Calcination of the rutile composite leads to a macroporous scaffold of interconnected rutile nanocrystals. Macropores (diameter ~100 nm) are formed by removing the PS core of the template while mesopores are formed between the rutile crystals by removal of the polyelectrolyte brush. PXRD measurements were done to check if any TiC was formed and reflections corresponding to TiC were not observed.

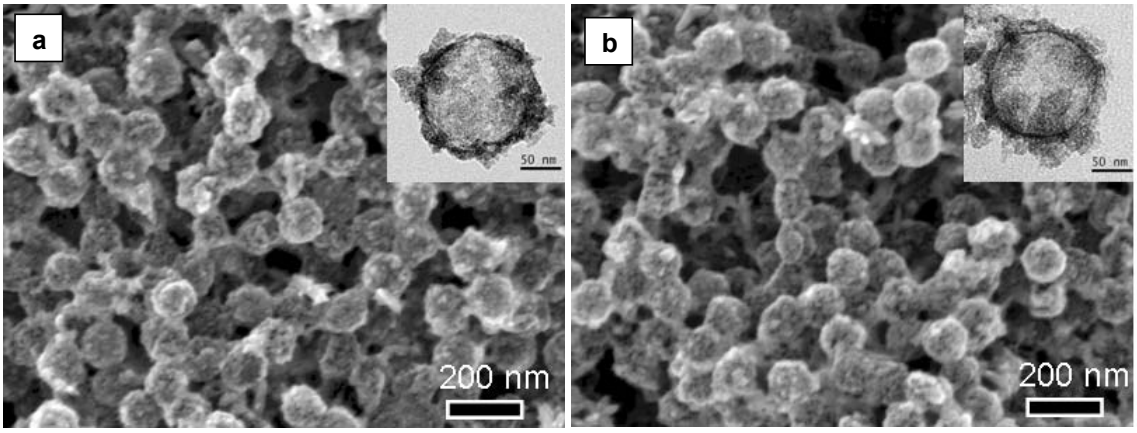

Figure 6. FESEM images of porous rutile balls obtained after calcinations (a: argon calcined, b: air calcined), inserts are the TEM images of the samples.

The N_2 sorption isotherm of the argon calcined porous rutile balls shows the formation of mesopores (Table 1 and Figure 4). The BET surface area increased to 122.9 m^2g^{-1}, with pore sizes ranging from 17 to 32 nm. Subsequent calcinations in air to remove the carbon lead to a further increase of surface area, 134.5 m^2g^{-1}, with pores ranging from 17 to 33 nm (Table 1 and Figure 4). This indicates that rutile balls with porous walls are formed after two-step heat treatment of the rutile composites. As evidenced by PXRD (Figure 1b), the walls of the porous balls are built by rutile nanocrystals that are interconnected to construct thermally and mechanically stable porous rutile balls. It is worth to note that calcinations of pure rutile nanocrystals under similar conditions causes strong densification of the material and no porosity can be observed, which demonstrates that SPB particles play an important role in the formation of structure-stable porous rutile balls.

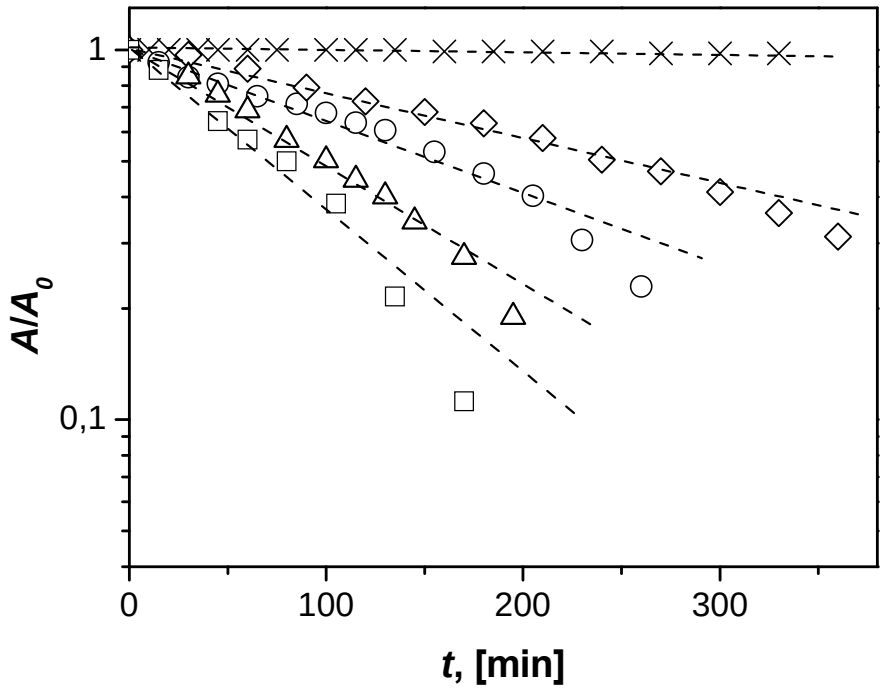

Figure 7. A/A_0 versus time of porous rutile balls on the photodegradation of RhB. Parameter of the different curves is the concentration of porous rutile balls in the solution. Quadrangles: 1g/l; triangles: 0.75g/l; circles: 0.5g/l; diamonds: 0.25g/l; crosses: without porous rutile balls. The concentration of the reactants was as follows: [RhB] = 0.02mmol/l, T = 20°C.

Photocatalysis measurements:

The photocatalytic activity of the porous rutile balls was evaluated by measuring the degradation of the organic dye, Rhodamine B (RhB). When UV light irradiated the dispersion containing porous rutile balls and RhB, a decoloration phenomenon occurred, which indicates that the RhB dye decomposed in the presence of porous rutile balls under UV irradiation.[53] The kinetics of this reaction can be monitored by UV/VIS spectroscopy as shown in Figure S5. After addition of porous rutile balls the absorption band of RhB at 552 nm decreased rapidly under UV irradiation and had a slight blue shift, which indicates the formation of some N-di-ethylated intermediates during the photocatalytic degradation of RhB.[53] Additional experiment demonstrates that when RhB solution was irradiated by UV in the absence of porous rutile balls the degradation of RhB is negligible.

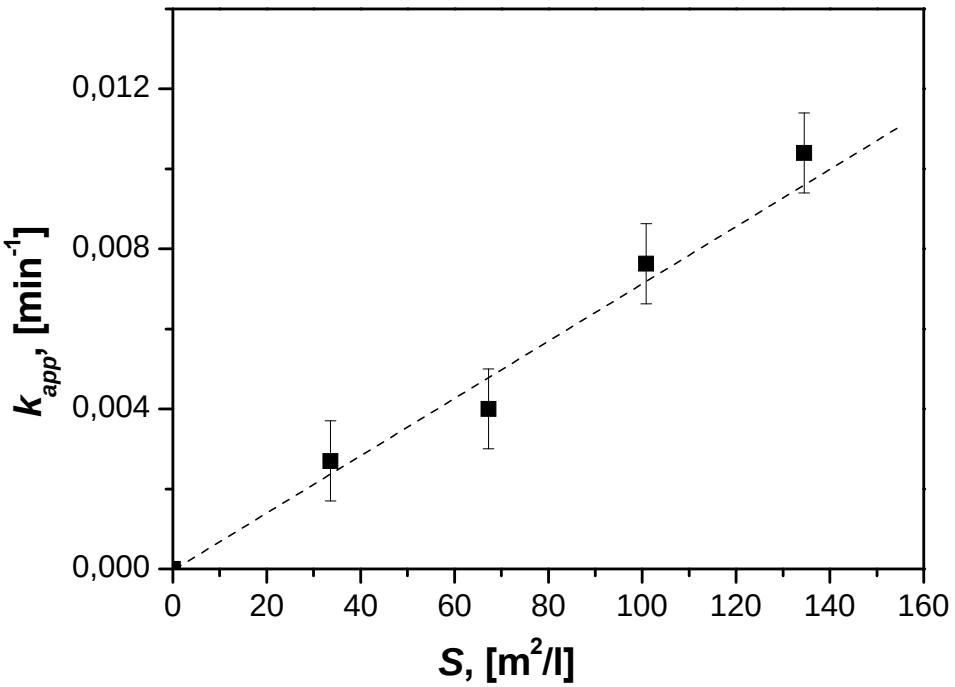

Figure 8. Analysis of the rate constant k_{app} obtained from Figure 7 as a function of the surface area of porous rutile balls normalized to the unit volume of the system.

Moreover, as shown in Figure 7 a linear relation between $\ln(c_t/c_0)$ versus time t has been obtained at the initial stage when porous rutile balls were used as catalyst, which could

be directly used to evaluate the apparent photocatalytic rate. From Figure 7, it can be seen that porous rutile balls can work effectively as the photo-catalyst for the degradation of RhB. Also, the rate constants are found to increase with the concentration of porous rutile balls. Furthermore, we assume the catalysis takes place on the surface of the rutile balls, and the apparent rate constant k_{app} will be proportional to the total surface S of the porous rutile balls present in the system:[19,20]

$$-\frac{dc_t}{dt} = k_{app}c_t = k_1 S c_t \qquad (1)$$

where c_t is the concentration of RhB at time t, k_1 is the rate constant normalized to S, the surface area of porous rutile balls normalized to the unit volume of the system. Here, surface area obtained from N_2 sorption measurements has been used to calculate S (Table 1). Figure 8 shows apparent rate constant as a function of the total surface area of porous rutile balls in the system. Evidently, k_{app} is found to vary linearly with the total surface S of the porous rutile balls, which demonstrates that the catalysis takes place on the surface of rutile balls as expected. From Figure 8, a photo-catalytic activity $k_1 = 7.77*10^{-5}$ $min^{-1}m^{-2}L$ can be obtained. Since anatase is the better photocatalyst, this value is of course lower than that of the as-prepared anatase composites ($k_1 = 8.41*10^{-3}$ $min^{-1}m^{-2}L$) we reported recently.[6]

3. Conclusions

In conclusion, we demonstrated that crystalline nanoscopic rutile can be obtained at temperatures as low as 40 ^{o}C under aqueous conditions. This nanoscopic, electrostatically stabilized rutile can be used as inorganic precursor and crystalline nanocomposites can be directly synthesized using spherical polyelectrolyte brush particles as the template. Stepwise calcinations first under argon followed with a second calcination in air lead to the complete removal of polymer template without collapse of the mesostructure. The rutile nanocrystals are connected upon heat treatment and porous titania balls with a crystalline framework are

obtained. Pore volumes and surface areas increased dramatically after stepwise calcinations. Moreover, the porous rutile balls are photocatalytic active. Most importantly, the results proof that the alternative route to mesostructured hybrid materials using preformed colloids as inorganic precursors is not limited to zeolite materials. This alternative approach was tested also using electrostatically stabilized anatase nanocrystals which carry a positive surface charge and, as expected, lead to the thermally stable and mesoscopic porous anatase balls. Hence, it is expected that this hierarchical route to structure oxides at the mesoscale is generally applicable.

4. Experimental Section

Synthesis of polyelectrolyte brush: PS core covered with a thin layer of photo initiator, 2-[*p*-(2-Hydroxy-2-methylpropiophenone)]-ethyleneglycol methacrylate (HMEM), was prepared by conventional emulsion polymerization, which has been described in detail previously.[18] The polyelectrolyte brushes were prepared by photo-emulsion polymerization. Diluted PS core solution (2.5 wt.-%) was mixed with defined amount of functional monomer styrene sulfonic acid sodium salt (NaSS; Aldrich, 30 mol-% with regard to the amount of styrene) under stirring. Photo-emulsion polymerization was done by use of UV irradiation at room temperature for 60 minutes. Thereafter the brush particles were cleaned 10 times by dialysis against purified water (membrane: cellulose nitrate with 100 nm pore size supplied by Schleicher & Schuell).

Synthesis of rutile nanocomposites from crystalline colloids: For the synthesis of crystalline rutile nanocomposite starting from crystalline rutile colloids, titanium (IV) n-butoxide (0.4 mL) was added dropwise at a rate of 1 mL/min to 1.0 mL of a 2M HCl solution at 40 ^{o}C, while continuously stirring. Initially precipitate appears with the addition of titanium n-butoxide and disappears with stirring. Precipitation starts again in 30 mins. After 2 h, pH was adjusted to 1 using 1M NaOH. PS-NaSS brush solution (1.0 g PS-NaSS in 5 mL of 2M

HCl) was adjusted to pH 1 using 1M NaOH and then added to crystalline rutile reaction mixture while continuously stirring at 40 ^{o}C. After 4 h, stirring was stopped and let it settle down over night. Settled rutile composite was washed three times with water and then freeze dried.

Photocatalytic activity measurements: The photocatalytic activity of porous rutile balls were measured in terms of the decolourisation of Rhodamine B (RhB). The UV source was a 150 W Hg lamp (44 mm long) with higher radiation intensity level in wavelength ranges 280-360 and 460-510 nm, which was surrounded by a circulating water jacket (Heraeus) to cool the lamp. All runs were conducted at ambient pressure and temperature. The distance between the Hg lamp and the reactor was 10 cm for each experiment. For a typical run, 0.02 g porous rutile balls and 20 ml RhB (2×10^{-5} M) aqueous solution were mixed together in a quartz glass reactor under stirring. This reaction dispersion was magnetically stirred in the dark for ca. 30 min prior to irradiation to establish the adsorption/desorption equilibrium of the dye on the catalyst surface. At given irradiation time intervals, 1.5 ml of sample was taken out and separated by centrifugation at 5000 rpm for 10 minutes. UV-Vis spectra were taken for the supernatant in the range of 400-650 nm. The rate constant of the reaction was determined by measuring the change in intensity of the peak at 552 nm with time.

Instruments and measurements: Photo-emulsion polymerization was done in a UV-reactor (Heraeus TQ 150 Z3, range of wavelengths 200-600 nm). Cryogenic transmission electron microscopy was done as reported.[54] Field-emission scanning electron microscopy (FESEM) was performed using a LEO Gemini microscope equipped with a field emission cathode. The UV-spectra were measured by Lambda 25 spectrometer supplied by Perkin Elmer. Powder X-ray diffraction (PXRD) measurement was performed at 25 °C on a Panalytical XPERT-PRO diffractometer in reflection mode using Cu K_{α} radiation. Zeta potential measurements were done using Malvern Zetasizer ZS instrument. All the solutions

were prepared using 0.001M KCl and 1gl^{-1} sample concentration. Nitrogen physisorption was conducted at 77 K on a Quantachrome Autosorb 1 instrument. Prior to the measurements, the samples were degassed at 373 K for 24 h. Ambient-temperature Raman spectroscopy experiments were performed using a Jobin Yvon Labram spectrometer with a 632.8 nm He-Ne excitation line and laser output power of 8 mW. The laser beam was focused using a 50× objective, resulting in a spot having a diameter of ~5 μm. All calcinations were done step-wise in a tube furnace, first under argon atmosphere with step-wise heating (200 ^{o}C – 5 h, and 500 ^{o}C – 2 h), followed with a second calcination in air with step-wise heating (200 ^{o}C – 2 h, and 500 ^{o}C – 2 h) at 3 ^{o}C min^{-1} heating and cooling rate.

Acknowledgements

The authors thank the Deutsche Forschungsgemeinschaft, SFB 481, Bayreuth, Elite Network Bavaria (ENB), Schwerpunktprogramm "Hydrogele" (SPP1259/1), the BASF-AG and Fonds der Chemischen Industrie for financial support. R. S. Y. would like to acknowledge Elite Network Bavaria for the fellowship.

[1] T. Ressler, A. Walter, Z. D. Huang, W. Bensch, *J. Catal.* **2008,** *254,* 170-179.

[2] F. Hoffmann, M. Cornelius, J. Morell, M. Fröba, *Angew. Chem. Int. Ed.* **2006,** *45,* 3216-3251; *Angew. Chem.* **2006,** *118,* 3290-3328.

[3] M. Tiemann, *Chem. Mater.* **2008,** *20,* 961-971.

[4] J. Lee, M. C. Orilall, S. C. Warren, M. Kamperman, F. J. Disalvo, U. Wiesner, *Nature Mater.* **2008,** *7,* 222-228.

[5] B. Ohtani, Y. Ogawa, S. Nishimoto, *J. Phys. Chem. B* **1997,** *101,* 3746-3752.

[6] Y.Lu, M. Hoffmann, R. S. Yelamanchili, A. Terrenoire, M. Schrinner, M. Drechsler, M. Möller, J. Breu, M. Ballauff, *J. Mater. Chem.* **2008,** *Submitted*.

[7] Z. Y. Yuan, B. L. Su, *J. Mater. Chem.* **2006,** *16,* 663-677.

[8] Y. B. Mao, S. S. Wong, *J. Am. Chem. Soc.* **2006,** *128,* 8217-8226.

[9] H. Z. Zhang, M. Finnegan, J. F. Banfield, *Nano Lett.* **2001,** *1,* 81-85.

[10] R. S. Yelamanchili, A. Walther, A. H. E. Müller, J. Breu, *Chem. Commun.* **2008,** 489-491.

[11] K. S. Triantafyllidis, E. F. Iliopoulou, E. V. Antonakou, A. A. Lappas, H. Wang, T. J. Pinnavaia, *Microporous and Mesoporous Mater.* **2007,** *99,* 132-139.

[12] Y. Liu, W. Z. Zhang, T. J. Pinnavaia, *J. Am. Chem. Soc.* **2000,** *122,* 8791-8792.

[13] Y. Liu, W. Z. Zhang, T. J. Pinnavaia, *Angew. Chem. Int. Ed.* **2001,** *40,* 1255-1258; *Angew. Chem.* **2001,** *113,* 1295-1298.

[14] Y. Liu, T. J. Pinnavaia, *J. Mater. Chem.* **2002,** *12,* 3179-3190.

[15] Z. T. Zhang, Y. Han, F. S. Xiao, S. L. Qiu, L. Zhu, R. W. Wang, Y. Yu, Z. Zhang, B. S. Zou, Y. Q. Wang, H. P. Sun, D. Y. Zhao, Y. Wei, *J. Am. Chem. Soc.* **2001,** *123,* 5014-5021.

[16] K. Egeblad, C. H. Christensen, M. Kustova, C. H. Christensen, *Chem. Mater.* **2008,** *20,* 946-960.

[17] M. Choi, H. S. Cho, R. Srivastava, C. Venkatesan, D. H. Choi, R. Ryoo, *Nature Mater.* **2006,** *5,* 718-723.

[18] M. Ballauff, *Prog. Polym. Sci.* **2007,** *32,* 1135-1151.

[19] Y. Lu, Y. Mei, M. Schrinner, M. Ballauff, M. W. Moller, *J. Phys. Chem. C* **2007,** *111,* 7676-7681.

[20] Y. Mei, Y. Lu, F. Polzer, M. Ballauff, M. Drechsler, *Chem. Mater.* **2007,** *19,* 1062-1069.

[21] M. Fröba, O. Muth, A. Reller, *Solid State Ionics* **1997,** *101,* 249-253.

[22] F. Schüth, W. Schmidt, *Adv. Mater.* **2002,** *14,* 629-638.

[23] P. D. Yang, D. Y. Zhao, D. I. Margolese, B. F. Chmelka, G. D. Stucky, *Nature* **1998,** *396,* 152-155.

[24] P. D. Yang, T. Deng, D. Y. Zhao, P. Y. Feng, D. Pine, B. F. Chmelka, G. M. Whitesides, G. D. Stucky, *Science* **1998,** *282,* 2244-2246.

[25] J. Y. Ying, C. P. Mehnert, M. S. Wong, *Angew. Chem. Int. Ed.* **1999,** *38,* 56-77; *Angew. Chem.* **1999,** *111,* 58-82.

[26] J. Y. Ying, *Synthesis and applications of nanoporous materials*, Elsevier Science Publ. B V, Amsterdam **1998,** pp. 85-87.

[27] X. Chen, S. S. Mao, *Chem. Rev.* **2007,** *107,* 2891-2959.

[28] M. Gratzel, *Nature* **2001,** *414,* 338-344.

[29] M. Durr, A. Schmid, M. Obermaier, S. Rosselli, A. Yasuda, G. Nelles, *Nature Mater.* **2005,** *4,* 607-611.

[30] C. S. Karthikeyan, M. Thelakkat, *Inorganica Chimica Acta* **2008,** *361,* 635-655.

[31] K. Drew, G. Girishkumar, K. Vinodgopal, P. V. Kamat, *J. Phys. Chem. B* **2005,** *109,* 11851-11857.

[32] A. Testino, I. R. Bellobono, V. Buscaglia, C. Canevali, M. D'Arienzo, S. Polizzi, R. Scotti, F. Morazzoni, *J. Am. Chem. Soc.* **2007,** *129,* 3564-3575.

[33] X. C. Jiang, T. Herricks, Y. N. Xia, *Adv. Mater.* **2003,** *15,* 1205-1209.

[34] D. V. Bavykin, J. M. Friedrich, F. C. Walsh, *Adv. Mater.* **2006,** *18,* 2807-2824.

[35] A. Chemseddine, T. Moritz, *Eur. J. Inorg. Chem.* **1999,** 235-245.

[36] C. W. Wu, T. Ohsuna, M. Kuwabara, K. Kuroda, *J. Am. Chem. Soc.* **2006,** *128,* 4544-4545.

[37] J. J. Wu, C. C. Yu, *J. Phys. Chem. B* **2004,** *108,* 3377-3379.

[38] H. Strohm, P. Lobmann, *Chem. Mater.* **2005,** *17,* 6772-6780.

[39] D. M. Antonelli, J. Y. Ying, *Angew. Chem. Int. Ed* **1995,** *34,* 2014-2017; *Angew. Chem.* **1995,** *107,* 2202-2206.

[40] J. Yang, S. Mei, J. M. F. Ferreira, *J. Colloid Interface Sci.* **2003,** *260,* 82-88.

[41] B. Smarsly, D. Grosso, T. Brezesinski, N. Pinna, C. Boissiere, M. Antonietti, C. Sanchez, *Chem. Mater.* **2004,** *16,* 2948-2952.

[42] K. Yoo, H. Choi, D. D. Dionysiou, *Chem. Commun.* **2004,** 2000-2001.

[43] E. Hosono, S. Fujihara, H. Lmai, I. Honma, I. Masaki, H. S. Zhou, *Acs Nano* **2007,** *1,* 273-278.

[44] T. I. Yang, P. Kofinas, *Polymer* **2007,** *48,* 791-798.

[45] S. J. Han, S. H. Choi, S. S. Kim, M. Cho, B. Jang, D. Y. Kim, J. Yoon, T. Hyeon, *Small* **2005,** *1,* 812-816.

[46] H. Kaper, F. Endres, I. Djerdj, M. Antonietti, B. M. Smarsly, J. Maier, Y. S. Hu, *Small* **2007,** *3,* 1753-1763.

[47] Y. W. Wang, L. Z. Zhang, K. J. Deng, X. Y. Chen, Z. G. Zou, *J. Phys. Chem. C* **2007,** *111,* 2709-2714.

[48] M. Niederberger, M. H. Bard, G. D. Stucky, *J. Am. Chem. Soc.* **2002,** *124,* 13642-13643.

[49] M. Niederberger, M. H. Bartl, G. D. Stucky, *Chem. Mater.* **2002,** *14,* 4364-4370.

[50] P. D. Cozzoli, A. Kornowski, H. Weller, *J. Am. Chem. Soc.* **2003,** *125,* 14539-14548.

[51] M. N. Tahir, P. Theato, P. Oberle, G. Melnyk, S. Faiss, U. Kolb, A. Janshoff, M. Stepputat, W. Tremel, *Langmuir* **2006,** *22,* 5209-5212.

[52] S. T. Aruna, S. Tirosh, A. Zaban, *J. Mater. Chem.* **2000,** *10,* 2388-2391.

[53] J. Y. Li, W. H. Ma, C. C. Chen, J. C. Zhao, H. Y. Zhu, X. P. Gao, *J. Mol. Catal. A* **2007,** *261,* 131-138.

[54] Z. B. Li, E. Kesselman, Y. Talmon, M. A. Hillmyer, T. P. Lodge, *Science* **2004,** *306,* 98-101.

Received: ((will be filled in by the editorial staff))
Revised: ((will be filled in by the editorial staff))
Published online on ((will be filled in by the editorial staff))

Supporting Information

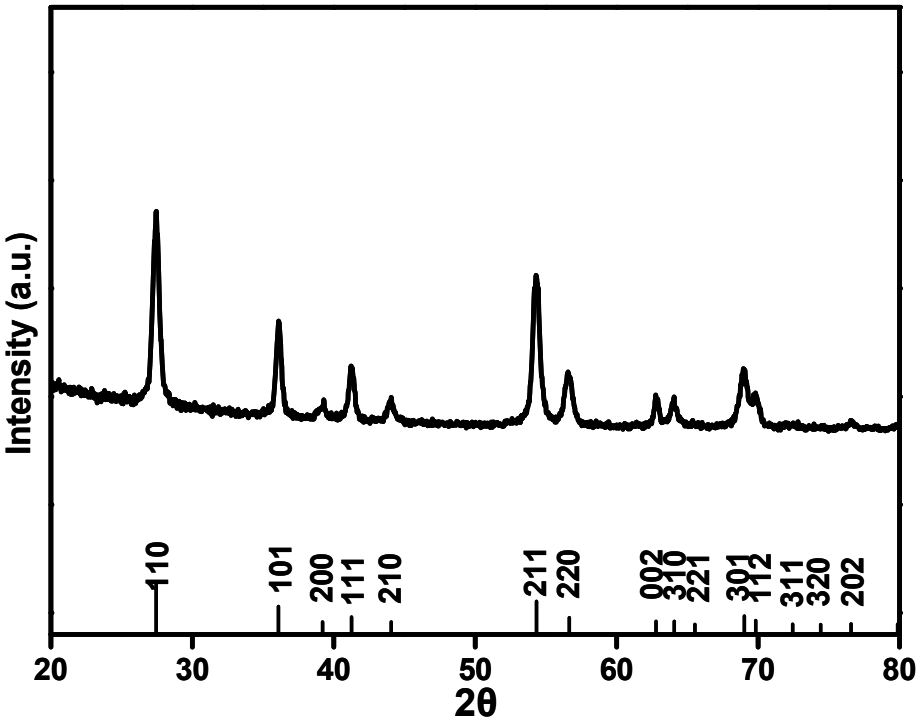

Figure S1. PXRD pattern of the rutile nanocrystals synthesized in absence of polymer brush. For comparison standard rutile (bottom) peaks were given.

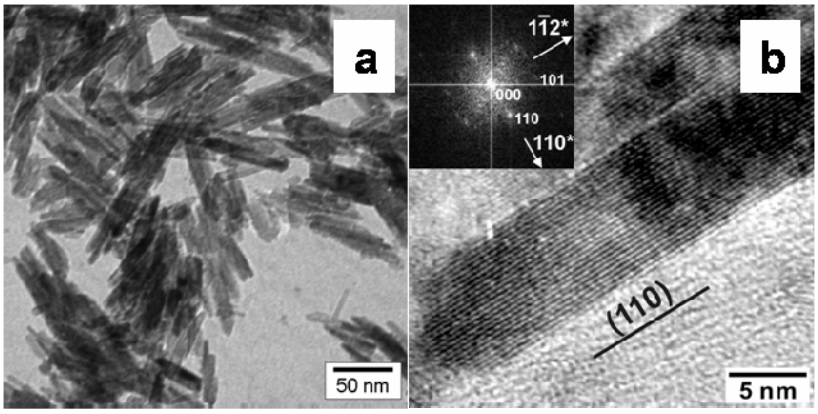

Figure S2. HRTEM images of rutile nanocrystals synthesized in absence of polymer brush at different magnifications.

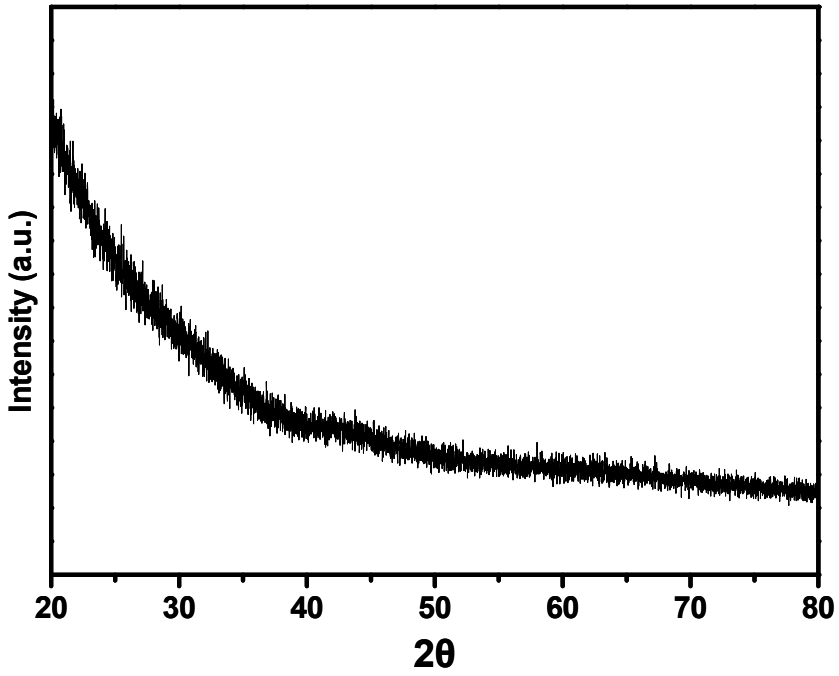

Figure S3. PXRD pattern of the PS-NaSS polyelectrolyte brush particles.

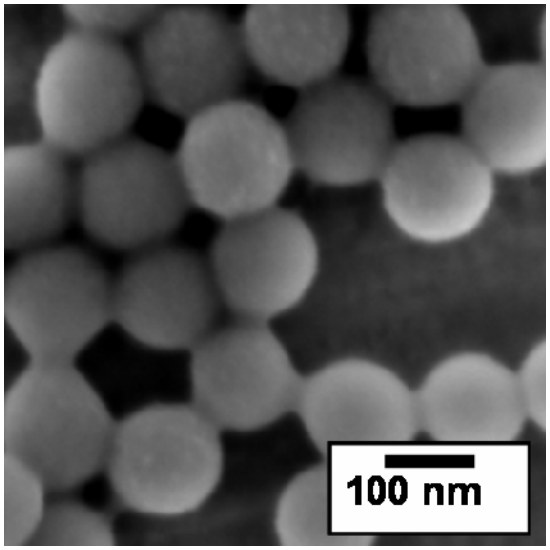

Figure S4. FESEM image of the PS-NaSS polyelectrolyte brush particles.

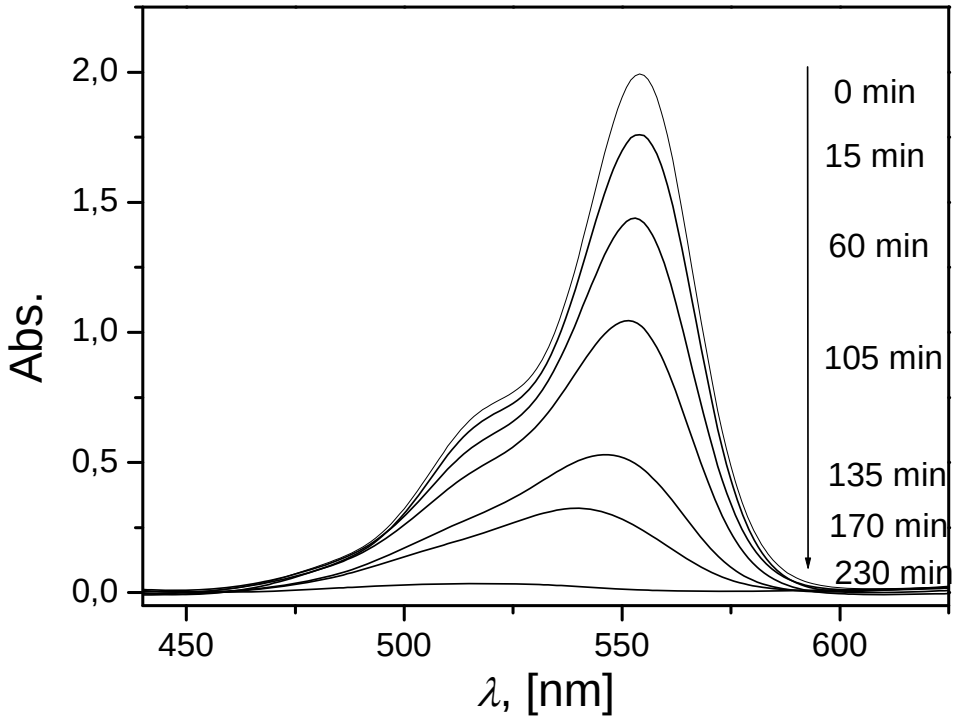

Figure S5. Successive UV-vis spectra of RhB photocatalytic degradation in the presence of porous rutile balls (1g/l) under UV irradiation.